Characterizing Strength Loss in High Plasticity Clays Along Alabama Highways

by

Mengwei Xuan

A dissertation submitted to the Graduate Faculty of
Auburn University
in partial fulfillment of the
requirements for the Degree of
Doctor of Philosophy

Auburn, Alabama
August 3, 2024

Keywords: Torsional ring shear; High plasticity clay; Drained shear strength; Slope stability; Embankments; Nonlinear strength envelopes; Suction

Copyright 2024 by Mengwei Xuan

Approved by

Jack Montgomery, Ph.D., Chair, Associate Professor, Department of Civil and Environmental Engineering
J. Brian Anderson, Ph.D., P.E., Professor, Department of Civil and Environmental Engineering
David Timm, Ph.D., Elton & Lois G. Huff Eminent Scholar Chair, Department of Civil and Environmental Engineering
Lorraine W. Wolf, Ph.D., Professor Emerita, Department of Geosciences
Xinyu Zhang, Alumni Professor, Chemical Engineering

ABSTRACT

Strength loss in high plasticity clay soils is a common occurrence along roadways in western and central Alabama and has considerable impact on pavement distress and slope failures. Approximately $16 million was spent to repair slope failures in western and central Alabama between 2005 and 2015 with many of these failures occurring in areas with high plasticity Prairie clays. Selecting strengths for these soils to use in slope stability analyses is often a key source of uncertainty and the selected strengths must account for effects of loading conditions and any potential changes in strength over time. For high plasticity clay, such as the Prairie clays in Alabama, repeated cycles of wetting and drying can reduce the available drained shear strength to the fully softened condition before large movements occur. This reduction in strength can lead to failure without any change in loading and accounting for this potential strength loss when analyzing the stability of these slopes is critical to obtain accurate results. The torsional ring shear test can measure both the fully softened strength (used for first time failures) and the residual strength (used for ongoing or reactivated failures) of high plasticity clays. For this study, clay samples were collected at six landslide sites around Alabama. Samples were tested to determine the index properties, electrical resistivity, mineralogy, and fully softened and residual strengths. The results from these tests were compared with existing correlations to determine which correlations were the most appropriate for use in Alabama. For two of the sites, slope stability analyses were performed to compare with observed performance at the site. The results show that the strength envelopes from ring shear testing are consistent with the observations at both sites,

although nonlinear envelopes are needed. Recommendations are provided for correlations that can be used to estimate strengths when ring shear testing is not available and for cases where existing correlations do not provide good estimates.

ACKNOWLEDGMENTS

I would like to take this opportunity to express my sincere gratitude to all those who have contributed to the completion of this dissertation.

Many people contributed to this research by providing previous background, data, and their individual experiences. First of all, I would like to express my deepest appreciation to my supervisor, Dr. Jack Montgomery, for his invaluable guidance, mentorship, and unwavering support and expert knowledge throughout the research process and my study at Auburn University. I would also like to extend my sincere gratitude to my committee members, Dr. J. Brian Anderson, Dr. David Timm, and Dr. Lorraine Wolf, and Dr. Xinyu Zhang for their insightful feedback, and the thoughful suggestions and continuous encouragement have been instrumental in shaping the direction and quality of this dissertation and pushed me to strive for excellence.

I am grateful to my colleagues and friends, Lydia Kennedy, Michael Kiernan, Patricia Carcamo, and all my other friends who have been part of this journey, for their friendship and support and have made this journey both enjoyable and fulfilling, and the funding support, ALDOT. I value my friends developed at Auburn who offered friendly caring and encouragement during my time at Auburn. I would also like to express my appreciation to my family for their constant encouragement and support, understanding, and encouragement throughout this academic journey. Their love, belief in my abilities, and motivation have been my pillars of strength during challenging times.

Furthermore, I extend my thanks to the research community and colleagues who have provided valuable discussions and insights, both in person and through academic forums. Their

contributions have stimulated my thinking and have broadened my perspective on the subject matter.

Completing this dissertation would not have been possible without the support and encouragement of all the individuals mentioned above. I am sincerely grateful for their contributions, and their impact on my academic and personal growth will forever be cherished.

TABLE OF CONTENTS

ABSTRACT ii

ACKNOWLEDGMENTS iv

TABLE OF CONTENTS vi

LIST OF TABLES x

LIST OF FIGURES xi

LIST OF ABBREVIATIONS xvi

Chapter 1 : INTRODUCTION 1

1.1 Background 1

1.2 Objectives 4

1.3 Summary of findings 6

1.4 Organization 7

Chapter 2 : LITERATURE REVIEW 10

2.1 Introduction 10

2.2 Clays 11

2.2.1 Clay mineralogy 11

2.3 Engineering index properties of clays 16

2.3.1 Moisture content (ASTM D2216 2019) 16

2.3.2 Clay fraction (ASTM D7928 2021) 17

2.3.3 Atterberg limits (ASTM D4318 2018) 17

2.3.4 Activity (ASTM D2487 2020) 19

2.4 X-Ray diffraction 20

2.4.1 Measurement of clay minerology 20

2.4.2 Data presentation and interpretation 22

2.5 Drained shear strength of clays 23

2.5.1 Selecting strengths for slope stability analyses 25

2.5.2 Measuring fully softened and residual strengths 26

2.5.3 Shear strength envelopes 28

2.5.4 Correlations for fully softened strength and residual strength 32

Chapter 3 : METHODOLOGY 35

3.1 Sample collection 35

3.2 Index testing 36

3.2.1 Moisture content 36

3.2.2 Clay fraction and Atterberg limits 37

3.3 X-Ray diffraction 41

3.3.1 Specimen preparation 41

3.3.2 Identification of clay minerals 44

3.4 Torsional ring shear testing 46

3.4.1 Specimen preparation 46

3.4.2 Preconsolidation 49

3.4.3 Consolidation 50

3.4.4 Shearing 51

3.5 Statistics of laboratory data 55

3.5.1 Statistics 55

3.5.2 Statistical of torsional ring shear 57

3.5.3 Goodness of fit 58

3.5.4 Outlier detection 59

3.5.5 Comparison with existing models 60

Chapter 4 : SOIL CHARACTERIZATION RESULTS 62

4.1 Introduction 62

4.2 Engineering index properties results 62

4.2.1 Moisture content 62

4.2.2 Grain size distribution and clay fraction 63

4.2.3 Atterberg limits 65

4.2.4 Activity and soil classification 67

4.3 X-Ray diffraction results 69

4.4 Torsional ring shear results 75

4.4.1 Statistical analysis of torsional ring shear results 81

4.4.2 Comparison with existing correlations 83

Chapter 5 : APPLICATION OF STRENGTH RESULTS TO SLOPE STABILITY ANALYSES 93

5.1 Introduction 93

5.2 Slope stability for SR-5 site 94

5.3 Stability analyses for US-231 site 100

Chapter 6 : CONCLUSION AND RECOMMENDATIONS 106

6.1 Summary and conclusions 106

6.2 Discussion on practical benefits of research 111

6.3 Limitation 114

6.4 Future research 114

REFERENCE 117

APPENDIX A 126

LIST OF TABLES

Table 3-1. Locations selected for laboratory testing. 36

Table 3-2. Target moisture contents for torsional ring shear testing 48

Table 4-1. Averaged Moisture Content for the Collected Samples. 63

Table 4-2. Grain Size Parameters for the Collected Samples. 65

Table 4-3. Liquid Limit Values for the Collected Samples 66

Table 4-4. Plastic Limit Values for the Collected Samples 67

Table 4-5. A Summary of Engineering Index Results for the Collected Samples 68

Table 4-6. Clay mineralogy results. 73

Table 4-7. Clay mineralogy and Atterberg limits results of US-231 in this study and soil mineral types with the similar range of liquid limit and plasticity limit from other studies. 74

Table 4-8. Comparisons between the fully softened shear strength data and models. 86

Table 4-9. Comparisons between the residual shear strength data and models. 87

Table 5-1. Saturated shear strength envelopes for SR-5. 97

Table 5-2. Summary of minimum factors of safety for the different strength envelopes. 98

Table 5-3. Saturated Shear Strength Envelopes for US-231 103

Table 5-4. Summary of Minimum Factors of Safety for Southbound Failure for the Different Strength Envelopes. 105

LIST OF FIGURES

Figure 1-1. Locations of sites and key geologic units (after Szabo et al. 1988). 3

Figure 1-2. Repaired slope failure in an embankment section of AL-5 in Perry County near the interchange with US-80. 4

Figure 2-1. Molecular structure of kaolinite crystal (USGS, accessed August 2022). 13

Figure 2-2. Molecular structure of montmorillonite crystal (USGS accessed August 2022). 14

Figure 2-3. Molecular structure of illite crystal (USGS accessed August 2022)..... 15

Figure 2-4. Molecular structure of chlorite crystal (USGS accessed August 2022 after Grim 1962). 16

Figure 2-5. Plasticity chart of USCS system (CL: Lean Clay/Low Plasticity Clay; OL: Low Plasticity Organic Clay or Silt; CH: Fat Clay/High Plasticity Clay; OH: High Plasticity Organic Clay or Silt; ML: Low Plasticity Silt; MH: High Plasticity Silt) (Holtz et al. 2011). 18

Figure 2-6. Common Clay minerals on Casagrande's plasticity chart (developed from Casagrande 1948, and data in Mitchell and Soga 2005) (Holtz et al. 2011). 19

Figure 2-7. Bragg's law (Rigak.com accessed 2022). 21

Figure 2-8. Bruker D2 PHASER benchtop diffractometer (Bruker, 2015). 23

Figure 2-9. Schematic illustration of stress strain curves for softening clays showing the intact peak, fully softened, and residual strengths (Duncan et al. 2014). 25

Figure 2-10. Bromhead torsional ring shear apparatus (after Controls Group accessed on Aug 2022). 27

Figure 2-11. Bromhead torsional ring shear soil specimen container with porous stone (after Controls Group accessed on Aug 2022). 28

Figure 2-12. Effect of air entry value on unsaturated shear strength envelopes (after Fredlund 2006). 31

Figure 2-13. Definition of secant friction angle for a nonlinear strength envelope (Stark et al. 2005). 32

Figure 3-1. (a) Equipment used for hydrometer analysis testing; (b) reference solution (left) and soil sample sedimentation suspension (right). 38

Figure 3-2. (a) liquid limit tools (left) and Casagrande cup with groove used for measuring liquid limit (right), and (b) plastic limit tools (left) and the rolled strip showing inconsistency of soil samples (right). 39

Figure 3-3. Soil preparation for XRD (a) mix soil powder and distilled water by Orbital shaker (b) shake soil solution by conic device (c) settle soil solution for 1 hours until the top 1/3 of the solution appears clear (d) centrifuge soil solution to remove silt (e) straw 1/3 clear solution into a clean centrifuge tube and settle for 24 hours (f) spread the soil solution on the glass slide (g) dry glass slide for 24 hours. 43

Figure 3-4. XRD results of illite clay subjected to different treatment methods prior to testing (Poppe et al. 2001). 44

Figure 3-5. Torsional ring shear apparatus (a) Controls Group ring shear apparatus; (b) modified porous stones used in this study. 46

Figure 3-6. Specimen preparation within container. 49

Figure 3-7. Specimen container assembled with datum indicated 54

Figure 4-1. Grain Size Distribution Curves for the Twelve Collected Samples 64

Figure 4-2. Atterberg limits results for the collected samples along with boundaries for different classifications and common ranges for different minerals (after Holtz et al. 2011). 69

Figure 4-3. XRD results for the sample collected from SR-5 (B-5.5A, 1-7 feet). 70

Figure 4-4. XRD results for the sample collected from SR-22 (B-3, 9-10.5 feet). 70

Figure 4-5. XRD results for sample collected from I-59 (B-1, 33.5-35 feet). 71

Figure 4-6. XRD results for sample collected from US-231 (SB4-1, 35.5-36 feet). 71

Figure 4-7. XRD results for sample collected from I-65 (B-7, 4.5-6 feet). 72

Figure 4-8. Shear stress versus displacement curves for three ring shear tests performed on samples from SR-5 at normal stresses of 455, 1,580 and 3,050 psf, respectively. 75

Figure 4-9. Saturated residual and fully softened shear strengths from ring shear tests performed on clay samples collected for this study over the full range of normal stresses. 77

Figure 4-10. Saturated residual and fully softened shear strengths from ring shear tests performed on clay samples collected for this study for stresses less than 3,200 psf (approximately 153 kPa). 78

Figure 4-11. Saturated residual and fully softened shear strengths from ring shear tests performed on clay samples from US-231 compared with strength results from Okagbue (1986). Okagbue (1986) performed direct shear (DS) tests on two intact samples of red shale collected from a landslide site in West Virginia. The strength envelope used by Okagbue (1986) for back-analysis is also shown for comparison. 80

Figure 4-12. Repeatable tests on SR-5 soil of three normal stresses with the power fitted strength envelope and 95% CI and 95% PI 82

Figure 4-13. Residuals (data – model) for fully softened and residual secant friction angles predicted by the lower bound relationship from Mesri and Shahein (2003). 89

Figure 4-14. Residuals (data – model) for fully softened and residual secant friction angles predicted by the relationships from Wright (2005), which include equations from Stark (2005).89

Figure 4-15. Residuals (data – model) for fully softened and residual secant friction angles predicted by the spreadsheet provided by Stark (2022). 90

Figure 4-16. Comparison of fully softened and residual strength envelopes measured at US-231 with envelopes predicted by the spreadsheet provided by Stark (2022) and used by Okagbue (1986) for back analysis of a slope failure in similar soils. Direct shear results by Wu et al. (1987) from slickensides found within red shale deposits in western Ohio are shown for comparison. 92

Figure 5-1. Locations of geologic units containing the high plasticity Prairie clays (after Szabo et al. 1988) and the location of the research site and borings examined in the current study. 95

Figure 5-2. Cross-section of SR-5 at borehole B5.5. The dashed line shows the depth of the water table in the analysis. 96

Figure 5-3. Fully softened (FSS) and residual strength (RS) envelopes for SR-5 at borehole B5.5 using both linear fits to data with a normal stress less than 1,000 psf and power fits. 97

Figure 5-4. Critical failure surfaces for the linear and power fit residual strength envelopes. Similar surfaces were found for the fully softened strengths. 98

Figure 5-5. View of the slide area along US-231 after removal of the pavement. The geophysical survey team can be seen along the SB shoulder on the left side of the figure. 101

Figure 5-6. Map of the US-231 landslide showing approximate geophysical survey locations along with cracks mapped from UAV images and borings completed by ALDOT. A shaded relief map derived from UAV-based LiDAR collected after the landslide occurred is shown in the background. 102

Figure 5-7. Analysis cross-section for US-231. 103

Figure 5-8. Key failure surfaces for US-231. 105

LIST OF ABBREVIATIONS

A	Activity
AL	Alabama
ALDOT	Alabama Department of Transportation
CF	Clay Fraction
deg	degrees
ER	Electrical Resistivity
ft	Feet
FSS	Fully Softened Strength
MC	Moisture Content
in	Inches
LL	Liquid Limit
PL	Plastic Limit
PI	Plastic Index
kg	Kilograms
kN	Kilonewtons
kPa	Kilopascals
mm	Millimeters
RS	Residual Strength
VMC	Volumetric Moisture Content
SD	Standard Deviation

TRS	Torsional Ring Shear
XRD	X-Ray Diffraction
^{o}	Degree

CHAPTER 1: INTRODUCTION

1.1 Background

Shallow slope failures are a common occurrence in both fill and cut slopes in western Alabama. In this area and others, expansive clays in the Selma, Tuscaloosa, and Midway Groups (Figure 1-1), sometimes referred to as Prairie clays, exhibit very low strengths causing repeated failures of even relatively flat slopes. Failures in geologic units with Prairie clays cost the state of Alabama a significant amount of money each year. The Alabama landslide database (Knights et al. 2020) found that almost $16 million was spent to repair slope failures in the Selma, Tuscaloosa and Midway Groups between 2005 and 2015. This figure only includes landslides for which federal emergency relief funds were requested, so the repair cost for all landslides in these units is likely much higher. This figure also does not include maintenance costs due to the need to repave and regrade shoulders failures (Stallings 2016). It is believed that these failures can be partially explained through strength loss due to repeated cycles of wetting and drying in the high plasticity clays that are ubiquitous in these regions. This reduction in strength can lead to failure without any change in loading (Khan et al. 2017). Understanding the strength of these soils is critical to be able to design effective repairs and avoid repeated failures.

Soil strengths for slope stability studies are commonly estimated using triaxial tests on undisturbed or remolded samples, but while these tests can be used to measure the fully softened strength (i.e., the peak drained shear strength of a clay soil under normally consolidated conditions), they cannot reach large enough shear strains to accurately determine the residual strength (Skempton 1970). In overconsolidated clays, softening tends to occur quickly after reaching the

peak strength (Holtz et al. 2011), therefore, residual strengths can be an important factor in assessing the stability of overconsolidated clay slopes (Skempton 1970, 1984, 1985). The ring shear test (Bromhead 1979, ASTM D6467 2021, Stark and Vettel 1992) can be used to measure residual strengths of clays, but its use in practice is still limited due to limited availability of the equipment in commercial labs and the difficulty in preparing high quality specimens. To overcome some of the difficulties in both the laboratory and field measurements of fully softened strengths, correlations have been developed which relate the long-term strength of the clay to an index properties such as the Atterberg limits (e.g., Stark and Eid 1994, 1997, Mesri and Shahien 2003, Stark and Hussain 2013, Eid and Rabie 2017, Stark and Fernandez 2020), which are commonly measured during routine geotechnical investigations. These correlations depend on the properties and mineralogy of the clay deposit, so correlations must be developed or verified for use in regions where these materials are found. Previous authors have also highlighted the importance of considering nonlinear strength envelopes for both fully softened and residual strengths (Stark and Eid 1997, Mesri and Shahien 2003, and Lade 2010), although the use of these envelopes is still limited in practice.

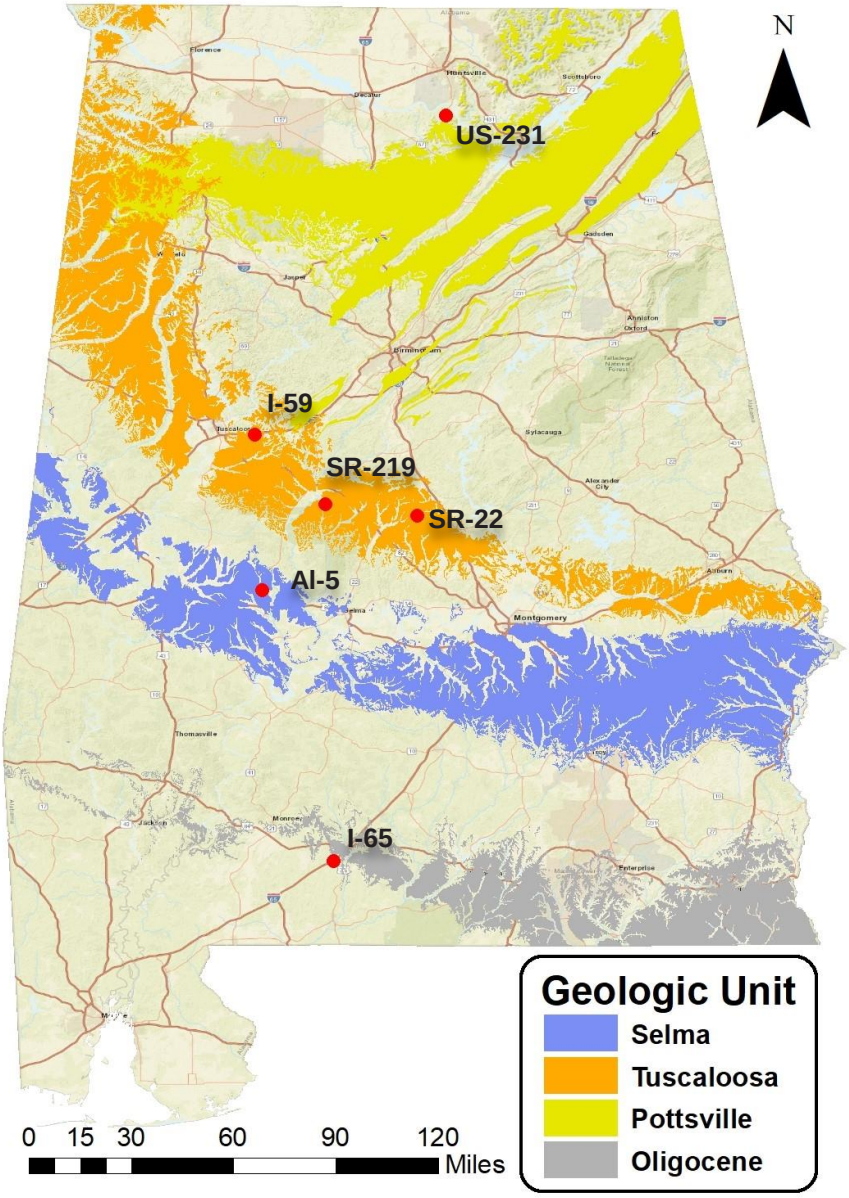

Figure 1-1. Locations of sites and key geologic units (after Szabo et al. 1988).

Six locations where high plasticity clays are believed to have led to slope instabilities are shown in Figure 1-1. An example of a repaired slope failure in a high plasticity clay deposit along Alabama Highway 5 (SR-5) in Perry County is shown in Figure 1-2. Understanding the soil strength is critical for designing repairs like this and preventing future failures. Twelve clay samples were collected for this study to characterize the strength loss and their characteristics.

Previous researchers have developed correlations to estimate the strength of high-plasticity clays, but these correlations have not been evaluated for soils in Alabama. In addition, previous studies have demonstrated that clay properties will be affected by mineralogy, but very little data exist on the mineralogy of high plasticity clays in Alabama. This study marks a first step in filling these gaps.

Figure 1-2. Repaired slope failure in an embankment section of AL-5 in Perry County near the interchange with US-80.

1.2 Objectives

The objective of this study was to develop approaches to estimate the potential for strength loss in Clays in Alabama and provide guidance on the use of these strengths in slope stability analyses. Strength envelopes needed to be developed for clay samples collected at six landslide sites (Figure 1-1) and compare those strength envelopes to existing correlations for fully softened

and residual strengths. The samples were characterized to determine index properties (Atterberg limits and clay fraction) and mineralogy through X-ray diffraction. Ring shear testing was performed on each of the samples to measure the fully softened and residual strength envelopes over a wide range of stresses. These strength results were then compared with predictions from existing correlations for both fully softened and residual strengths (Mesri and Shahien 2003, Wright 2005, Stark and Hussain 2013, Eid et al. 2016, Eid and Rabie 2017, and Stark and Fermandez 2020) to determine how well existing correlations fit the measured data. The developed strength envelopes were also used to perform slope stability analyses for two of the sites, which demonstrated that the measured strength envelopes can match the observed performance. The importance of using nonlinear envelopes and identifying the sources and structure of the identified clay for these sites were also explored.

In order to accomplish the above-mentioned objectives, the study involved the following major tasks:

(1) Collected detailed information on laboratory test procedures and existing correlations for the fully softened and residual strengths of clays.

(2) Characterized the collected samples from each site and conduct ring shear tests on the clay specimens in the laboratory.

(3) Evaluated correlations between the fully softened strength and index properties for clays in Alabama.

(4) Developed guidance for ALDOT engineers on the measurement and use of fully softened and residual strengths in geotechnical design.

The project was divided into the following tasks to satisfy the defined research objectives as follows:

(1) The first task was to perform torsional ring shear testing on the twelve collected clay samples to measure the fully softened and residual strengths of high-plasticity clays.

(2) The second task was to perform geotechnical laboratory index property testing on soil samples.

(3) The third task involved X-ray diffraction testing in order to identify the dominant clay minerals in each of the selected samples.

(4) The final task focused on integrating the results from the four tasks above to provide recommendations on how to predict strength values in the field for high-plasticity clays in Alabama.

1.3 Summary of findings

The findings from this work highlight the importance of considering potential for strength loss when analyzing landslides in high plasticity clays. Ring shear testing is a good way to measure these strengths, but the tests are rather slow and the equipment is not commonly available in commercial laboratories. The correlations developed by Mesri and Shahien (2003) and Stark and Hussain (2013) show reasonable agreement with the measured strengths from most of the sites and can be used to estimate strengths when ring shear testing is not available. The exception to this is the residual strengths measured for the clay at the Lacey Springs landslide on US-231. This soil shows a very nonlinear residual strength envelope that cannot be easily fit with any of the existing correlations. The findings from this study can be used to help improve current procedures to estimate strengths of clayey soils for use in slope stability analyses and provide more reliable estimates of stability and more effective designs for repairs. Recommendations for implementing

this research and for topics related to this study that could benefit from future research are discussed in Chapter 6.

1.4 Organization

This dissertation is divided into six chapters that organize, illustrate, and describe the steps taken to meet the research objectives. Portions of these chapters have been published in Montgomery et al. (2019), Xuan et al. (2021), Kiernan et al. (2022), and Xuan et al (2023).

Chapter 1 introduces the background, objective and tasks of this study, along with the structure of each chapter.

Chapter 2 presents a review of existing literature on the index characterization, shear characteristics of clays and the implication of these characteristics on slope analysis and design. Experimental methods used to determine the drained shear strengths and to identify clay mineralogy of clay are reviewed.

Chapter 3 begins with an introduction of the depth and location of each collected soil sample of the study. Methodologies of the testing are then outlined for evaluating soil engineering behaviors through a combination of index testing, X-ray diffraction (XRD), and torsional ring shear testing. Each method is introduced with detailed procedures, required equipment or apparatus, and relevant equations for interpreting test results, providing a theoretical explanation. Index Testing serves as a preliminary assessment tool, utilizing ASTM standard tests such as Atterberg limits and grain size analysis to classify soil behavior. XRD is conducted to characterize mineralogical composition, investigating presence of clay minerals and their impact on soil properties. Torsional Ring Shear Testing is introduced for assessing shear strength parameters under targeted moisture condition and normal stresses and it is crucial for understanding the

drained shear strengths of the soil for stability analysis. Statistical analysis of laboratory data is also emphasized, focusing on methods such as goodness-of-fit tests, outlier detection, and comparisons with existing models. These statistical techniques enhance the confidence for interpretating the measured data and the conclusions drawn from the tests. By integrating these methodologies, this chapter provides a framework for characterizing soil engineering properties and the drained shear strengths.

Chapter 4 presents the results of experimental study of the engineering index, drained fully softened and residual shear strengths, and mineralogy of the clay samples. These laboratory data were used to develop slope stability analysis for the proposed sites with fully softened and residual shear strengths, to compare fully softened and residual shear strengths measured using ring shear of this study to the existing correlations, and to understand the strength loss with identified minerals. This comparison provides an understanding of the evaluation on the measured shear strength and the effect of drained repeated shear stresses on the accumulation of shear displacement, and the effect of mineralogy on the resulting shear strength reduction of high plasticity clays.

Chapter 5 provides practical application of the shear strength results on two case histories of Alabama state: SR-5 and US-231, focusing on slope stability assessments. The SR-5 site investigates the impact of fully softened and residual strength parameters on slope stability analysis. It emphasizes the effects of both linear and nonlinear strength envelopes, highlighting suction influences on stability outcomes. Through this analysis, the chapter demonstrates the importance of selecting appropriate strength parameters in slope stability evaluations. In the US-231 site, the focus shifts to the nonlinear shear strengths observed under high and low groundwater conditions. This analysis illustrates the interactions between groundwater levels and shear strength.

Chapter 6 summarizes the research work conducted in this study, concludes with the results obtained from the series of laboratory tests for high plasticity clays collected in Alabama, and provides design recommendations for the shear strength of high plasticity clay involved in first-time and reactivated slides using the slope stability analysis of the field cases. Chapter 6 also discusses the comparison of the measured shear strength results and existing shear strength models, and emphasizes the practical benefits of this research with the integration of these laboratory test results. Future research will focus on advancing more test results to develop any reasonable correlations of the similar type of soils, involving electrical resistivity measurements, and expanding slope stability studies upon the two site case histories.

CHAPTER 2: LITERATURE REVIEW

2.1 Introduction

The potential for strength loss in fine-grained soils poses a significant hazard for many geotechnical projects, e.g., instability and failure of foundations, embankments, and retaining structures (Roy and Bhalla 2017; Das 2016; Terzaghi et al. 1996; Lambe and Whitman 1969; Casagrande 1936). Damage to infrastructure attributed to strain-softening of clayey soils has been documented in many case histories involving both static (e.g., Gregersen 1981, Locat et al. 2017) and cyclic loading (e.g., Shannon and Wilson 1964, Heritage 2013, Nakamura et al. 2014). Fine-grained soils that exhibit a post-peak reduction in strength include overconsolidated clays, high plasticity clays, and marine clays that have experienced salt-water leaching (L'Heureux et al. 2014). Strength loss in high-plasticity clay soils is a common condition of the roadways in western and central Alabama and brings considerable impact including cracking of pavement and slope failures (Figure 1-2).

This chapter reviews important literature concerning strengths of high plasticity clays and tools that can be used to investigate landslides in high plasticity clays. Section 2.2 discusses clay soils and typical crystal structure mineral types. Following this section, engineering index properties that are used to characterize clay soils are presented in Section 2.3. Advanced experimental methods for characterizing mineralogy of clay soils are discussed in Section 2.4. The definition of strengths (fully softened and residual strengths) along with strength selection and measurement in high plasticity clays are discussed in Section 2.5. Both linear and nonlinear strength envelopes and the effects of suction on soil strength are covered in this section.

Additionally, this section reviews previously developed correlations for fully softened and residual strengths based on index properties of clays.

2.2 Clays

Clay is commonly found in various geological formations around the world and is often defined based on fine particles with diameters smaller than 0.002 mm. Clayey soils are known for their plasticity, high water-retaining capacity and a group of microcrystalline structure minerals. Clay particles carry a net negative charge due to isomorphous substitution of ions and imperfections in the crystal lattice. To neutralize this charge, water dipoles are attracted to clay crystals in the presence of moisture and get adsorbed (Mitchell and Soga 2005). The characteristics of a clay, such as particle size, negative charge, and plasticity, give clays their unique properties and play a crucial role in geotechnical engineering, including foundation design, slope stability analysis, and embankment construction (Mitchell and Soga 2005). The behavior of clays in engineering aspects is significantly influenced by the presence of electrochemically active particles and their affinity to moisture. Different clay minerals will respond differently to changes in moisture conditions or the chemistry of the groundwater.

2.2.1 Clay mineralogy

This section describes four common types of clay minerals: kaolinite, montmorillonite, illite, and chlorite. These four were selected due to their common presence in clayey soils within Alabama, as shown in the results in Chapter 4. This section describes the formation, crystalline structure, and relative size of the clay minerals. These descriptions are summarized from work by

USGS (2002), Cullity (1956), Douglas (1989), Folk (1974), Poppe et al. (1988), Commeau et al (1985), Biscaye (1965), and Mitchell and Soga (2005).

2.2.1.1 Kaolinite

Kaolinite is a 1:1 layered aluminum silicate mineral with the chemical formula $Al_2Si_2O_5(OH)_4$. It is formed by the weathering of feldspar-rich rocks under tropical and temperate climatic conditions. The occurrence of kaolinite is widespread in different geological settings, including sedimentary, residual, and hydrothermal deposits (USGS 2022). Figure 2-1 shows a molecular structure of kaolinite mineral with its crystal structure connected by the chemical elements.

Kaolinite minerals exhibit a surface morphology consisting of six-sided hexagonal plates. The crystal structure of kaolinite is characterized by sheets of alumina octahedra and silica tetrahedra stacked on top of each other. The sheets are held together by hydrogen bonding and van der Waals forces. The morphology of kaolinite particles can vary from platy to lath-like, and their size and shape influence the engineering properties and behavior of the material that contains this type of clay mineral. These plates have lateral dimensions ranging from 0.1 – 0.4 μm and thicknesses varying between 0.05 – 2 μm. Due to its unique crystal structure and morphology, the typical specific surface area of kaolinite falls within the range of 10 to 20 m^2/g (Holtz 1981). The hydrogen bond within kaolinite crystal structure is strong enough to resist hydration and therefore kaolinite is not known for large swelling potential with increasing moisture content.

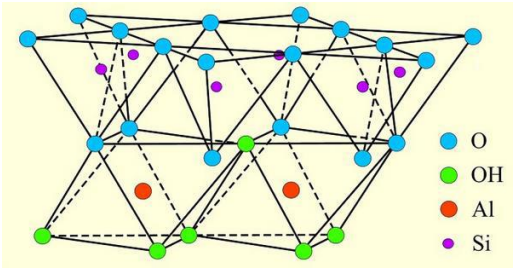

Figure 2-1. Molecular structure of kaolinite crystal (USGS, accessed August 2022).

2.2.1.2 Montmorillonite

Montmorillonite is a type of clay mineral with diverse applications in various fields. It is represented by a 2:1 layered crystal structure, consisting of two tetrahedral sheets sandwiching one octahedral sheet. Figure 2-2 shows a molecular structure of a montmorillonite mineral with its crystal structure connected by the aluminum, iron, magnesium, silicon, oxygen, and hydroxyl groups.

The layers of montmorillonite are held together by weak van der Waals forces. These layer characteristics make montmorillonite susceptible to cation exchange and the surface morphology of montmorillonite mineral is marked by thin-film equidimensional flakes. A substantial substitution of Fe^{3+} and/or Mg^{2+} for Al^{4+} can lead to directional strain, resulting in a needle-shaped fabric structure in montmorillonite. Owing to its inherent configuration and significant surface activity, the specific surface area of montmorillonite can range from 50 to 120 m^2/gm (Helmy 1999).

Montmorillonite is also characterized by its surface reactivity prominent characteristics that tend to have high swelling capacity due to its large interlayer. The swelling behavior in response to water absorption plays a crucial role in the behavior of clay soils with montmorillonite.

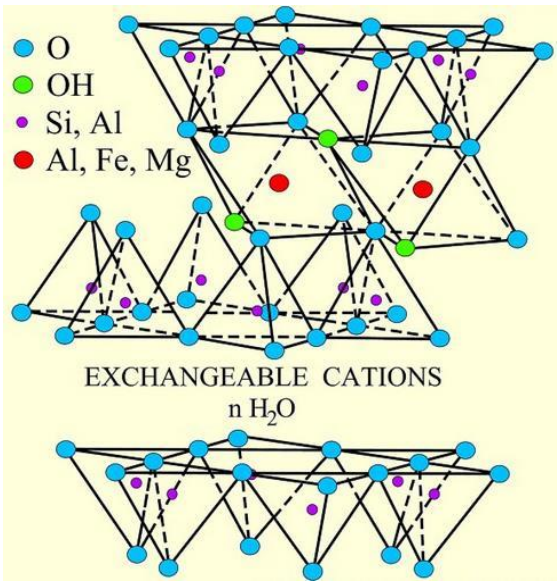

Figure 2-2. Molecular structure of montmorillonite crystal (USGS accessed August 2022).

2.2.1.3 Illite

Illite is another type of 2:1 layered crystal structure that has a layered crystal structure consisting of two tetrahedral sheets sandwiching one central octahedral sheet similar to montmorillonite, while its layer is bonded by ionic bound of potassium (K+). Figure 2-3 shows a molecular structure of illite mineral with its crystal structure connected by the aluminum, iron, magnesium, silicon, oxygen, and hydroxyl groups. The presence of Potassium (K+) makes the bond between the layers very strong. This strong bond means that illitic clays often have low swell potential, but it also means that loss of this potassium ion through cation exchange or chemical weathering or leaching can cause significant changes in the properties of the soil (Van Schouwenburg and Schuffelen 1963).

Illite is a product of the weathering process of potassium-rich minerals, such as feldspars, and is commonly found in shale, mudstone and other sedimentary rocks. It often occurs in association with other clay minerals, such as kaolinite, smectite, and chlorite. The morphology of

illite is characterized by hexagonal small flaky particles when well crystallized, and its surface area of this mineral ranges from 65 to 100 m2/gm (Holtz 1981).

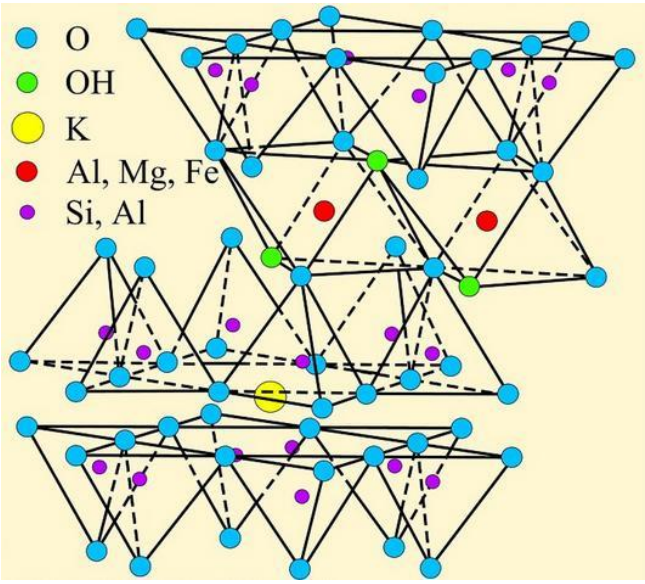

Figure 2-3. Molecular structure of illite crystal (USGS accessed August 2022).

2.2.1.4 Chlorite

Chlorite has negatively charged mica-like (2:1) layers alternating with positively charged brucite-like (octahedral) sheets (Grim 1962). The chlorite minerals are frequently found in low-grade greenschist facies metamorphic rocks and can occur in igneous rocks as hydrothermal alteration products of ferromanganese minerals (Deer et al. 1975). Additionally, chlorites are common components of argillaceous sedimentary rocks. chlorite's chemical composition typically includes magnesium (Mg), aluminum (Al), silicon (Si), oxygen (O), and hydroxyl (OH) groups. Figure 2-4 shows a molecular structure of illite mineral with its crystal structure connected by aluminum, iron, magnesium, silicon, oxygen, and hydroxyl groups.

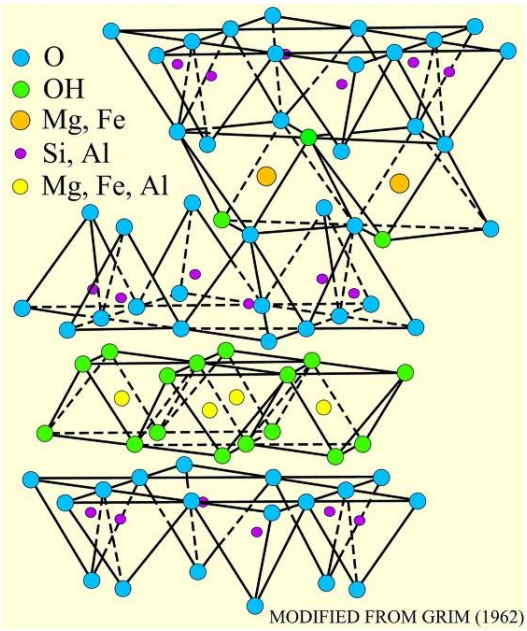

Figure 2-4. Molecular structure of chlorite crystal (USGS accessed August 2022 after Grim 1962).

2.3 Engineering index properties of clays

Index properties (e.g., grain size characteristics, moisture content, Atterberg limits) are commonly used to characterize soils in geotechnical engineering practice because the tests are inexpensive, easy to perform, and widely available in geotechnical labs across the world. Index tests do not provide direct information on the engineering properties of the soil or its mineralogy but can be used to develop correlations to these and other properties. For this study, the moisture content, clay fraction, and Atterberg limits are considered as these are commonly used in the characterization of clayey soils.

2.3.1 Moisture content (ASTM D2216 2019)

The moisture content of soils is typically determined using two approaches: gravimetric and volumetric. Gravimetric moisture content is defined as the ratio of the mass of water present

in the voids to the mass of the soil solids. On the other hand, volumetric moisture content measures moisture in terms of the volume of water relative to the total volume of the soil. Both methods are important for assessing and managing the behavior of clayey soils in engineering applications, but this study will focus on gravimetric as it is more commonly used in geotechnical engineering practice.

2.3.2 Clay fraction (ASTM D7928 2021)

Clay fraction refers to the portion of soil particles that falls within the size range of clay particles. Specifically, it includes soil particles that are smaller than 2 micrometers in diameter. Clay fraction is also indicative of the presence of surface charge of a soil specimen (Holtz 1981). The surface activity and affinity to water increases with the increase in the clay fraction. The clay fraction influences the microstructure of clay soils, affecting factors such as pore size distribution, surface area, and water retention. Due to their small size and large surface area, clay particles have a higher capacity to attract and retain water molecules. This influences the soil's moisture content, swelling potential, and overall volume change behavior.

2.3.3 Atterberg limits (ASTM D4318 2018)

Atterberg limits are threshold moisture contents that describe transition between different physical states of a fine-grained soil. In geotechnical engineering, the plastic limit and liquid limit are the two most commonly used. These limits provide the behavior of clays under varying moisture conditions and are applicable to understand soil stability, and engineering properties. The plastic limit defines the boundary between the plastic and non-plastic by defining the consistency of the soil. The liquid limit defines the boundary between low plasticity and high plasticity. The

plastic limit is measured using the glass plate with a reference soil thread tool, and the liquid limit is measured using Casagrande cup as described in the Section 3.2.

Atterberg limits are used in the Unified Soil Classification System (USCS) (ASTM 2487 2020) and the AASHTO soil classification system, which categorize soils based on their plasticity and moisture content. Figure 2-5 shows the plasticity chart of USCS system used for this study with boundaries.

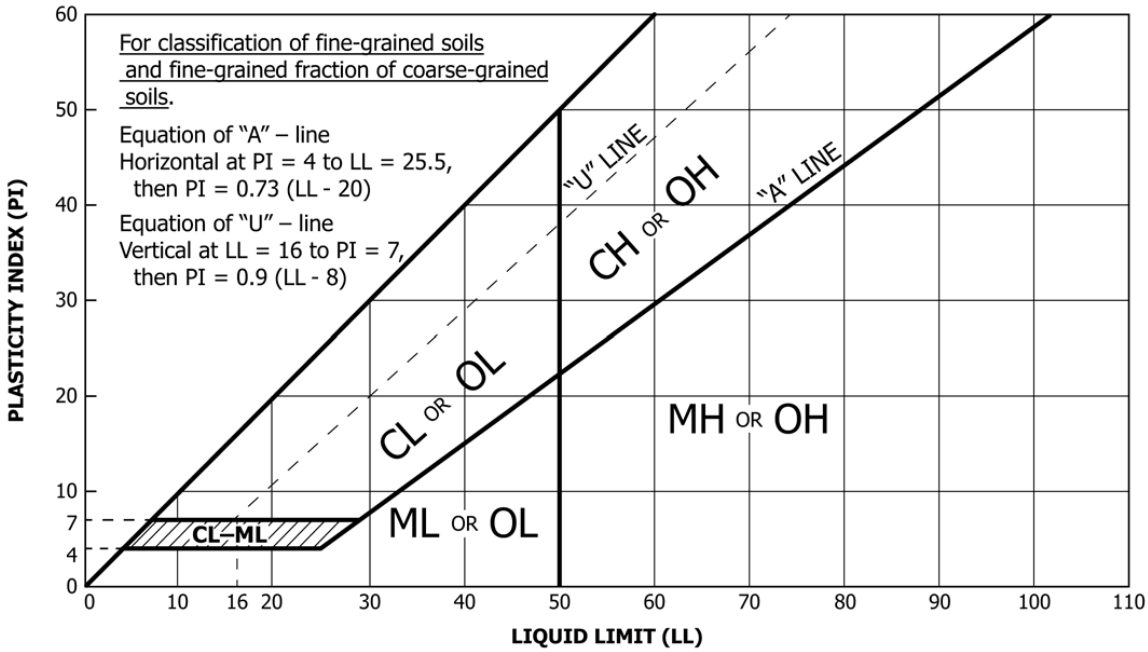

Figure 2-5. Plasticity chart of USCS system (CL: Lean Clay/Low Plasticity Clay; OL: Low Plasticity Organic Clay or Silt; CH: Fat Clay/High Plasticity Clay; OH: High Plasticity Organic Clay or Silt; ML: Low Plasticity Silt; MH: High Plasticity Silt) (Holtz et al. 2011).

The Atterberg limits are usually used with other index properties for characterization of clay minerals and identify the engineering and physico-chemical behavior of fine-grained soils. It is also essential in the design of stabilizers for these soils. Casagrande (1948) utilized Atterberg limits to determine the qualitative mineralogical content of soils. Mitchell and Soga (2005) further

expanded this approach, showing that different clay minerals tend to fall within different regions of the Casagrande plasticity chart and this can provide an indication of the dominant mineral in a soil sample. Figure 2-6 shows the plasticity chart of USCS system used for this study with boundaries.

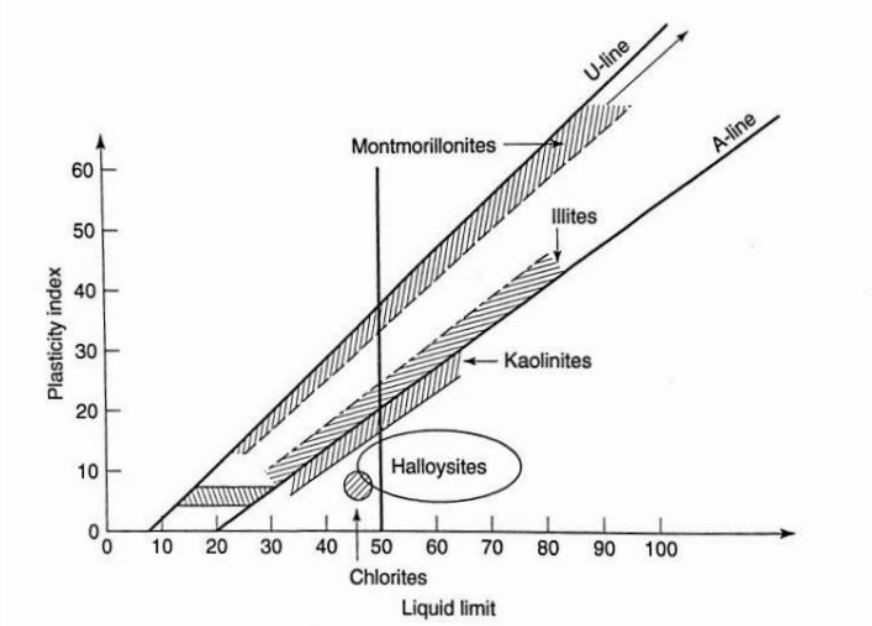

Figure 2-6. Common Clay minerals on Casagrande's plasticity chart (developed from Casagrande 1948, and data in Mitchell and Soga 2005) (Holtz et al. 2011).

2.3.4 Activity (ASTM D2487 2020)

Soil activity is a parameter in geotechnical engineering commonly used for reflecting the plasticity and swelling potential of clay soils, defined as the ratio of the plasticity index to the percentage of clay fraction. The plasticity index is typically measured through Atterberg limits tests, while the clay fraction is determined using sedimentation methods such as the hydrometer analysis (ASTM D7928 2021). Soil activity serves as a valuable indicator of soil behavior under varying moisture conditions.

2.4 X-Ray diffraction

2.4.1 Measurement of clay minerology

X-ray diffraction (XRD) is a powerful analytical technique widely used in the identification and characterization of clay minerals. It plays a crucial role in determining the mineralogical composition of clay-rich samples and provides valuable information about their crystal structure. By analyzing the intensity of diffraction peaks, XRD can also be used to quantify the relative abundance of different clay minerals in a sample. XRD distinguishes clay minerals and their structure based on their distinct diffraction patterns, providing a more accurate characterization. Diffraction takes place when x-ray photons from the source or beam interact with adjacent scattering centers in consecutive layers of the crystal structure of the target material. A scattering center refers to an atom or a cluster of atoms and can be visualized as a distinct lattice point in the crystal. The x-ray photon beam predominantly interacts with the electrons surrounding atomic nuclei, and the resulting reflected beam is the combined effect of interactions with all electrons at each atom or scattering center (Moore and Reynolds 1989).

When reflected waves from different scattering centers are in phase or close to it, their wavelets combine to form a combined wave of greater amplitude. This occurrence is diffraction, the result of constructive interference between scattered x-ray wavelets. This may occur when the component of x-ray wavelength normal to the crystal lattice plane is approximately equal to unit cell thickness of the crystal. This satisfies the Bragg condition, where λ is wavelength, d is vertical lattice spacing in the crystal unit cell, and Θ is diffractometer beam angle to the lattice plane. An illustration of X-ray radiations and their dependency on the crystal spacing is presented in the figure below. The present minerals can be identified using Bragg's law ((1) during XRD tests.

$$N\lambda = 2d\sin\Theta \quad (1)$$

Where N = an integer, referred to as the order of diffraction, and is often unity

λ = the wavelength of the radiation used

d = the inter-planar spacing involved

Θ = T=the angle between the incident (or diffracted) ray and the relevant crystal planes

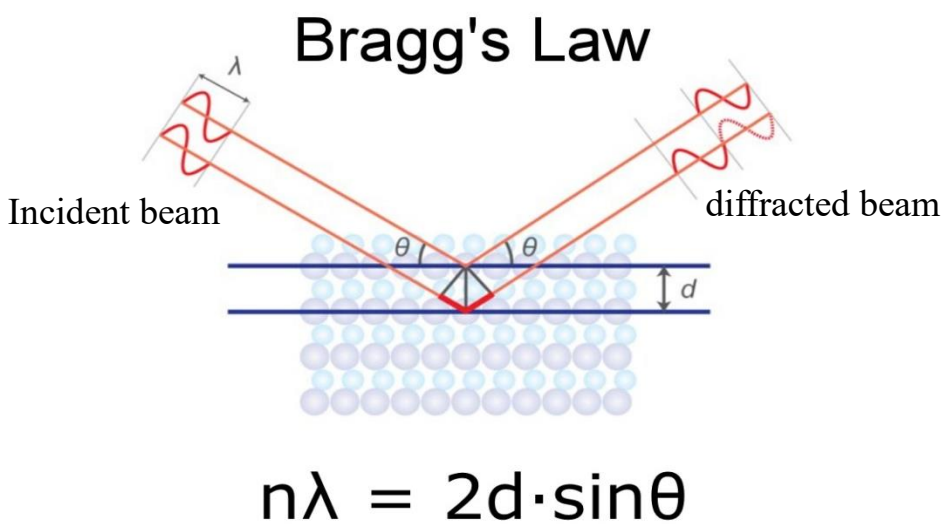

Figure 2-7. Bragg's law (Rigak.com accessed 2022).

The Structure Factor accounts for differences in electron distribution, atomic positioning, and thermal motion of different kinds of atoms in a crystal – and how those differences affect scattering intensity of a material (Jenkins and Snyder 1996). For instance, crystals with larger atoms of relatively low electron density tend to scatter x-rays less efficiently than those with smaller atoms of higher electron density.

2.4.2 Data presentation and interpretation

To quantitively identify the mineral, a reference-intensity-ratio (RIR) method can be used for result analysis. Mineral quantities in soils and geologic samples can be determined using various methods from x-ray diffraction data. One such method is the Reference-Intensity-Ratio (RIR) approach, which involves employing an internal standard of known mass, typically corundum or zincite. By comparing the ratios of diffraction peak intensities for a 50%-50% mass mixture of standard reference minerals, the unknown quantities of real minerals in the samples can be calculated using Xi = Xc/ki*Ii/Ic (2 (Snyder and Bish 1989). Ic is the diffraction intensity of the internal standard in the sample. RIR was in use before the advent of personal computers, and one advantage to this method is its simplicity as it can be performed with a ruler and pencil if necessary. However, major limitations of RIR are its focus on primary diffraction peaks and the lack of entirely quantitative tools for resolving peak overlap effects.

$$X_i = X_c/k_i*I_i/I_c \qquad (2)$$

Where X_i = weight fraction of the mineral of interest,

Xc = known weight fraction of the internal standard,

ki = diffraction intensity ratio of a 50 %-50 % mixture of the internal standard and mineral of interest,

Ii = diffraction intensity of the mineral of interest in the sample,

Ic = diffraction intensity of the internal standard in the sample.

A Bruker x-ray diffractometer in Figure 2-8 was used for collecting X-ray patterns consisting of a series of reflection of different intensities and values of diffraction angles. The type of clay mineral can be identified based on the X-ray patterns with the comparison with patterns for known materials using a clay mineral identification flow diagram (Poppe et al. 2001).

Figure 2-8. Bruker D2 PHASER benchtop diffractometer (Bruker, 2015).

2.5 Drained shear strength of clays

Selecting strengths for use in slope stability analyses is often a key source of uncertainty and selected strengths must account for effects of loading conditions and any potential changes in strength over time. For slopes along highways, long-term drained strengths are often used to analyze failures that occur without significant changes in loading (Vandenberge et al. 2013, Duncan 2014), such as those observed in sites underlain by Prairie Clays. This is especially true for expansive clays, such as the Prairie clays considered in this study, where the strengths can be

reduced as repeated cycles of wetting and drying occur (Hou et al., 2013). Groundwater fluctuations have also been shown to be an important factor in landslide development along highways where the roadway is underlain by expansive clays (Khan and Hossain 2017, Yilmaz and Karacan 2002). Accounting for this potential strength loss when analyzing the stability of these slopes is therefore important to obtain accurate results.

Clays tend to show a significant reduction in shearing resistance when sheared to large displacements (Figure 2-9). As the clay is sheared, the shear stress usually reaches a peak value at a relatively small shear displacement. When displacement is increased to larger values, the clay undergoes a post-peak strength loss, until a constant minimum or residual value is reached. Overconsolidated (OC) clays tend to have a higher peak strength than normally consolidated (NC) clays.

Skempton (1970) defined the fully softened shear strength as the peak strength of drained strength of a normally consolidated clay (Figure 2-9), which has been found to be equivalent to the long-term drained strength of stiff fissured clay soils (Skempton 1970). This definition is also used by the US Army Corps of Engineers (Stephens and Branch 2013). The fully softened strength is distinct from the critical state strength (Duncan et al. 2014, VandenBerge 2013), which represents the shear strength of the soil when no further dilation or contraction occurs (Schofield and Wroth 1968). The critical state strength is usually lower than and occurs at a larger displacement than the fully softened strength (Duncan et al. 2014), but at smaller displacements than the residual strength (Duncan 2014, Crabb and Atkinson 1991, Lupini 1981).

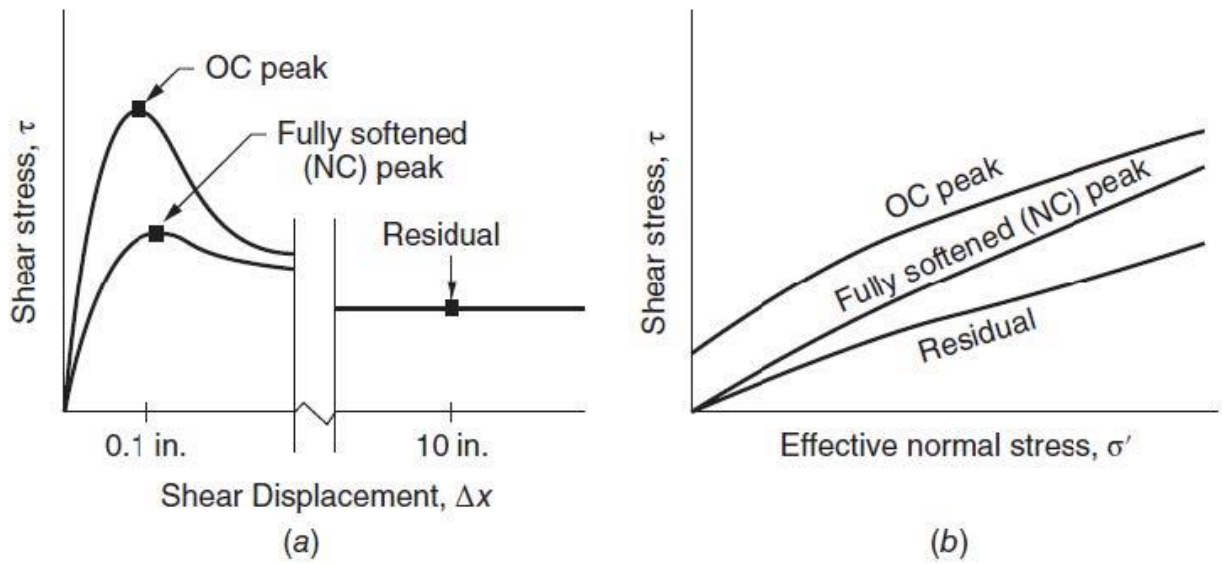

Figure 2-9. Schematic illustration of stress strain curves for softening clays showing the intact peak, fully softened, and residual strengths (Duncan et al. 2014).

2.5.1 Selecting strengths for slope stability analyses

Several authors have examined landslide case histories to determine the appropriate strength to use in analyzing failures in clay slopes. Stark and Eid (1997) found that the fully softened shear strength was appropriate to use when analyzing first-time failures in natural cut slopes and compacted embankments. Mesri and Shahien (2003) reanalyzed a large database of slope failures in soft clays, stiff clays and clay shales to assess the mobilized shear strength. They found that first-time failures were primarily controlled by the fully softened strength, while residual strengths controlled reactivated landslides. Reactivated landslides are landslides that resume movement after a period of inactivity and the shearing resistance is commonly reduced to the residual condition along the entire failure surface (Mesri and Shahien 2003). Both of these studies highlighted the importance of considering the stress-dependent nature of the strength envelopes through either nonlinear envelope or use of secant friction angles. A study of long-term slope stability of slopes in shale regions in the Sydney Basin found that both landslide occurrence

and long-term slope stability were governed by the residual shear strengths (Dunkerley 1976). Residual strengths have also been recommended for being used for the long-term slope stability of clay soils by Skempton (1970, 1984, 1985, 1964), Tiedemann (1937) and Haefeli (1951). Correlations for both fully softened and residual shear strengths with index properties, such as the liquid limit and plasticity index, have been developed by multiple authors (Stark and Eid 1994, 1997, Mesri and Shahien 2003, Stark and Hussain 2013, Eid and Rabie 2017, Stark and Fernandez 2020).

2.5.2 Measuring fully softened and residual strengths

Stark and Eid (1992) found that the torsional ring shear test was an accurate and timesaving method to obtain both fully softened and residual strengths compared with triaxial tests. The testing method has also been used to characterize fully softened and residual strength parameters of the landslides consisting of expansive clay minerals (Bhandary et al. 2007) This test is performed by placing a remolded soil specimen in a steel ring between two porous stones. The upper stone is then rotated relative to the bottom stone to shear the specimen (Figure 2-10). The specimen and porous stone interface are important as the porous stone should not slide across the surface of the soil (Stark 2017). Brass porous elements assembled with sample container are shown in Figure 2-11. These porous stones have been machined as recommended by Stark (2017) to ensure that the torsional loading was properly transferred to the soil specimen. Details on the machining of the porous stones used in this study are discussed by Kennedy (2019).

Ring shear testing for drained strengths is conducted on saturated specimens following the procedures discussed in ASTM D6467 (2021). A constant normal stress is applied using a counter balanced lever loading system. The shear loading is applied at a slow rate to assure drainage of

any excess pore pressures. The tests for this study were performed using the “flush” procedure, which ensures the top porous stone remains approximately flush with the surface of the specimen container. Details on the testing procedure used for this study are discussed in the next chapter. The test can be conducted as a single stage test or multiple stage test. The single stage test procedure includes loading the remolded specimen to the desired normal stress and then shearing the specimen. The multistage procedure reduces test duration by allowing all stages of testing to be performed on one specimen.

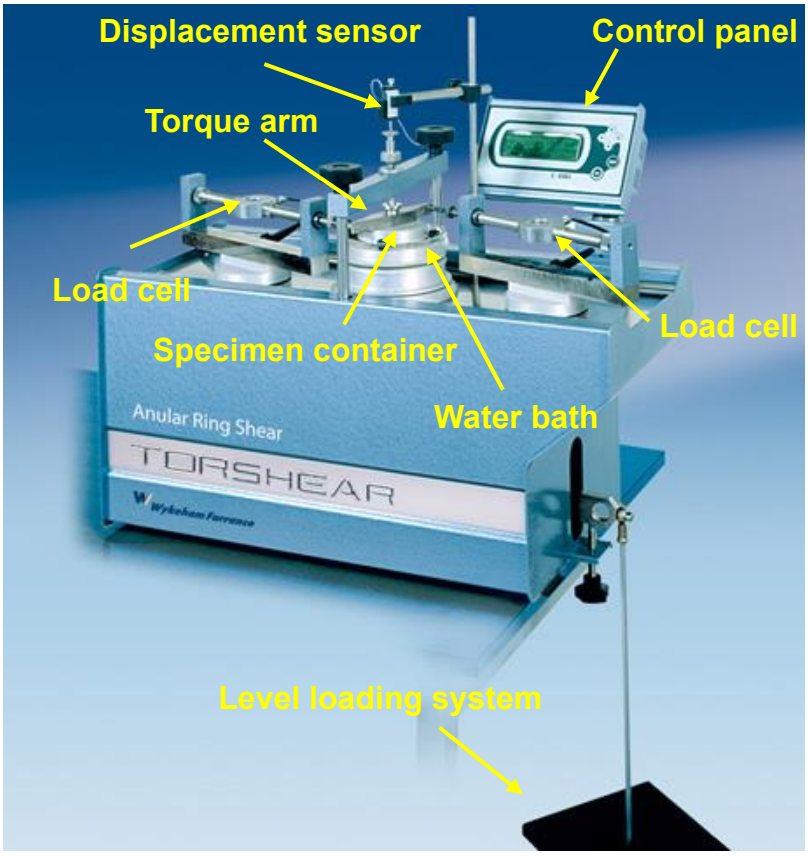

Figure 2-10. Bromhead torsional ring shear apparatus (after Controls Group accessed on Aug 2022).

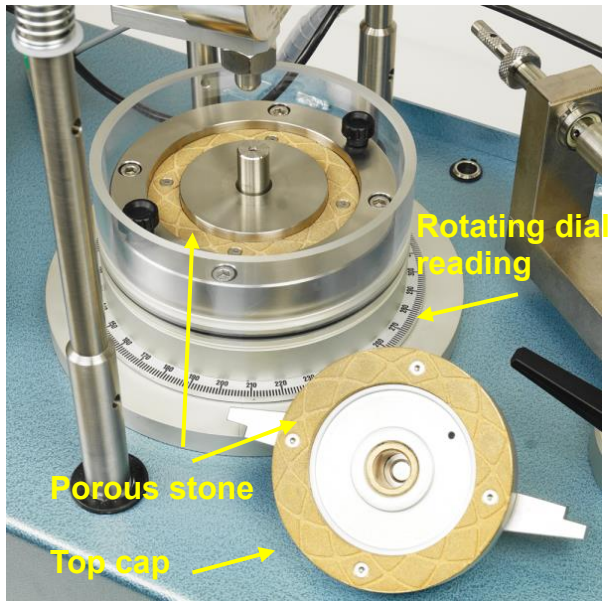

Figure 2-11. Bromhead torsional ring shear soil specimen container with porous stone (after Controls Group accessed on Aug 2022).

2.5.3 Shear strength envelopes

Drained (or effective stress) strength envelopes are commonly used to evaluate slope failures that occur due to long-term loading as opposed to loads that are applied rapidly relative to the permeability of the soil (Duncan et al. 2014). Long-term drained shear strengths of saturated soils are commonly represented in slope stability analyses using an effective stress Mohr-Coulomb failure envelope as shown in (3, where the effective cohesion is typically zero for uncemented soils.

$$\tau = c' + \sigma' \cdot tan\,\phi' \tag{3}$$

Where τ = shear strength (psf or kPa)

c' = effective cohesive intercept (psf or kPa)

σ' = $\sigma - u$ = effective normal stress (psf or kPa)

σ = total stress (psf or kPa)

u = pore water pressure (psf or kPa)

ϕ' = effective angle of internal friction (deg)

Nonlinear strength envelopes can be used when a linear fit does not match the data for a particular soil. Multiple authors have highlighted the importance of considering nonlinear strength envelopes for both fully softened and residual strengths (Stark and Eid 1997, Mesri and Shahien 2003, Lade 2010) of fine-grained soils. This can be done through a stress-dependent secant friction angle or a strength envelope with a nonlinear functional form. An example of a nonlinear strength envelope is the power curve shown in Equation (4), which has been shown to work well for analyzing surficial shallow slope failures (Lade 2010).

$$\tau = a \cdot P_a \left(\frac{\sigma'}{P_a}\right)^b \tag{4}$$

Where a, b = dimensionless fitting parameters describing curvature and slope

P_a = atmospheric pressure (2116 psf or 101.3 kPa)

Correlations for the parameters a and b have been developed for fully softened strength (Stark and Fernandez 2020) and residual strengths (Stark and Idries 2021) and are available in spreadsheet form from Stark (2022).

This suction effect is crucial in determining the engineering properties and shear strength of clay soils. Suction of clay refers to the phenomenon where clay particles attract and retain water due to their fine size and high surface area. When clay becomes saturated, it creates a negative pressure or suction within the soil matrix as the water is drawn into the tiny spaces between the

particles. Soils above the groundwater table will have negative pore pressures (positive suction) that will increase the effective stress and therefore the strength of the soil. This increase in strength due to suction is important for many geotechnical problems, including landslides which may be triggered by reductions in suction during rain events (Taha 2000). The total suction in soils has two primary components. The first is the matric suction, which is defined as the difference between the pore water pressure (u_w) and the pore air pressure (u_a). The second component is the osmotic suction, which is associated with the salt content of the pore water. Osmotic suction is not considered in this study as it usually has a small effect on the shear strength of soils (Leong and Abuel-Naga 2018).

The effects of suction on the strength of the soil can be included through the use of an unsaturated strength envelope (Fredlund et al. 1978) as shown in Equation (5).

$$\tau = c' + (\sigma - u_a) \cdot tan\,\phi' + (u_a - u_w) \cdot tan\,\phi_b \tag{5}$$

Where: ϕ_b= unsaturated shear strength angle (kPa)

u_a= pore air pressure (kPa)

u_w = pore water pressure (kPa)

At suction values below the air entry value (AEV), and the unsaturated strength envelope reverts to the saturated strength envelope, but with a negative pore pressure. The AEV is defined as the matric suction value that is exceeded before air recedes into the soil pores (Fredlund and Rahardjo 1993). When matric suction exceeds the air entry value, the strength envelope for the soil can be described by Equation (3). This envelope is often assumed to be bilinear (Figure 2-13) but has also been shown to be dependent on the suction value resulting in a nonlinear envelope at

higher suction values (Fredlund 2006). Figure 2-12 illustrates the correlation of saturated and unsaturated condition with the air entry value (AEV).

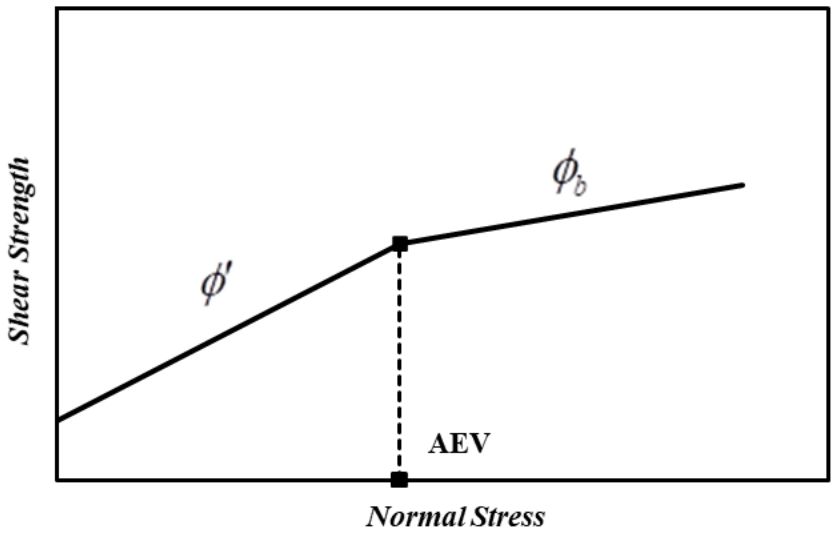

Figure 2-12. Effect of air entry value on unsaturated shear strength envelopes (after Fredlund 2006).

In a nonlinear strength envelope, the shear strength can be expressed in terms of a secant friction angle under varied effective stress. The secant friction angle is defined as the inclination of a failure envelope drawn from the origin to a point on the curved Mohr failure envelope for a particular effective normal stress as shown in Figure 2-13. A secant friction angle is commonly used to develop correlations relating shear strengths with liquid limit, clay fraction, and effective normal stress (i.e., Stark et al. 2005).

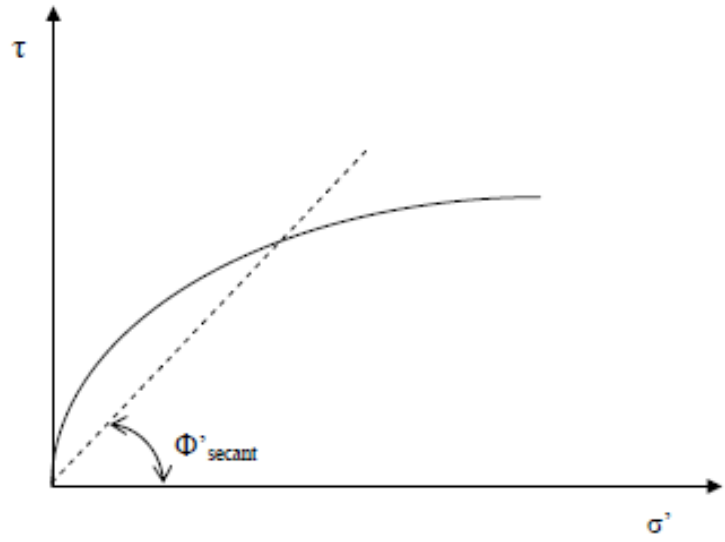

Figure 2-13. Definition of secant friction angle for a nonlinear strength envelope (Stark et al. 2005).

2.5.4 Correlations for fully softened strength and residual strength

Five fully softened strength correlations developed by Mesri and Shahien (2003), Stark and Hussain (2013), Eid and Rabie (2017), Stark and Fermandez (2020), and Stark (2022) and five residual strength correlations developed by Mesri and Shahien (2003), and Wright (2005)-Stark (2005), Stark and Hussain (2013), Eid et al. (2016), and Stark (2022) are summarized in this section.

Mesri and Shahien (2003) presented detailed analyses of 99 case histories of slope failures in 36 soft clays to stiff clays and clay shales. The study analyzed 107 sections using the observed actual slip surface and carries out analyses in terms of effective stress at failure using the reported porewater pressure condition. The paper provided empirical correlations between both the fully softened and residual friction angles and index properties (LL, and PL) under varied effective normal stresses of 50, 100, and 400 kPa and highlighted the significance of stratigraphic

discontinuities in first-time slope failures, and the causes of delayed first-time failure in stiff clays and clay shales under residual condition develops in response to excavation in excavated slopes.

Wright (2005) used data from Stark et al. (2005) to develop a correlation and equation for both fully softened and residual secant friction angles based on previous work by Duncan et al. (1989) that related the secant friction angle to the logarithm of the effective confining pressure.

Stark and Hussain (2013) measured both the fully softened shear strength and residual under effective normal stresses typically encountered in first-time slope failures and in failed slides. Remolded normally consolidated specimens were prepared and sheared at effective normal stresses of 50, 100, 400, and 700 kPa in a modified ring shear apparatus. The specimen preparation procedure detailed by Mesri and Cepeda-Diaz (1986) for direct shear test specimens was followed (Stark et al. 2005). A spreadsheet relating to FSS and RS to clay fraction (CF) and liquid limit (LL) was developed under various effective normal stresses.

Eid et al. (2016) developed correlations aimed to predict the residual shear strength of soils for slope stability analyses. These correlations take into account factors such as clay mineralogy, soil texture, sample preparation techniques, and effective normal stress. The study found that these correlations yielded the highest coefficient of determination (R^2), closest mean (μ) to 1.0, and the lowest standard deviation (S) and coefficient of variation (COV) compared to other existing correlations. The correlations were generated between residual friction angle and plasticity indexes (LL, PL, and PI) along with wide range of effective stresses of 10, 25, 50, 100, 200, and 400 kPa.

Eid and Rabie (2017) presented an empirical relationship used to predict the fully softened shear strength of soils, mudstones, and shales. It was based on the concept that the peak shear strength of these materials is controlled by the strength along fissures, which is close to the fully softened (critical) strength. The correlation takes into account the plasticity index (PI) of the soil,

which encapsulates the effect of both liquid limit (LL) and clay fraction (CF) along with varied effective normal stresses of 10, 25, 50, 100, 200, and 400 kPa. The correlation has been validated through comparisons with measured fully softened shear strength data available in the literature.

The correlation developed in Stark and Fermandez (2020) used liquid limit (LL), plasticity index (PI), and the ratio of plasticity index to void ratio (PI/e) as input parameters to estimate the fully softened shear strength and residual shear strength envelopes. The correlation is based on torsional ring shear testing with a 2.5-degree adjustment for the triaxial compression mode of shear. The authors compared this correlation with other existing correlations and found that it adequately predicts the FSS from CD- and CU-TX tests, even at high effective normal stresses and pIs. However, the accuracy and applicability of this correlation may vary depending on the specific soil conditions.

The mathematical expressions for a and b, as defined in Equation (4), were developed using data analysis methods, and both a and b adequately represent the variability of these coefficients as a function of plasticity index (PI). Overall, the correlations in this study show agreement between predicted and measured values of a and b coefficients, with most data falling within the range of two SDs of the b coefficient.

CHAPTER 3: METHODOLOGY

This chapter describes the testing methodologies used in this study. This includes a description of the samples that were collected and tested, along with the testing procedures used for the index testing on these samples. Procedures for X-ray diffraction (XRD) and ring shear testing are also described with a brief description of the statistical analysis approaches that were used to assess the ring shear data.

3.1 Sample collection

Samples for laboratory testing were collected from six sites (Figure 1-1) where landslides had either been observed or pavement cracking had been observed and previous studies had suggested a landslide may be occurring (Kennedy 2019). Electrical resistivity measurements were performed at five of the sites and MASW tests were performed at three. These geophysical results are discussed by Kiernan (2021) and Montgomery et al. (2020). Borings were performed at each of the sites to collect samples and the boring numbers and approximate coordinates of the site are listed in Table 3-1. The clay soils were located in Selma, Tuscaloosa, Pottsville, and Undifferentiated Oligocene geologic units, and came from the limestones of these geologic units. All these geologic units mainly consist of calcareous, micaceous, and carbonaceous clay and silty clay, and thin bed of shale and claystone.

Table 3-1. Locations selected for laboratory testing.

Route	Milepost	Approximate Coordinates	Observations	Boring
SR-5	53.1	32.51185, -87.37282	Pavement Cracking	B-5.5A
SR-22	62.0	32.83092, -86.71142	Landslide	B-3
SR-219	35.9	32.87873, -87.10227	Landslide	B-2, B-3
I-59	80.4	33.17520, -87.40238	Landslide	B-1
US-231	35.9	34.53320, -86.58983	Landslide	SB4-1
I-65	87.4	31.35989, -87.06662	Landslide	B-6, B-7

3.2 Index testing

3.2.1 Moisture content

The moisture contents (w%) of the soil samples were measured after the soil samples were delivered to the laboratory, and before and/or after each test. The testing followed the standard moisture content measurement procedure according to ASTM D2216 (2019). The same procedures described here were consistently followed in this project to ensure accuracy and reliability of the data. Equipment needed for this testing were moisture tins, a balance with an accuracy of 0.01 g, and a drying oven capable of maintaining a temperature of 100°C.

Moisture tins were thoroughly cleaned and dried. Empty tins were weighed using the weighting balance, and the weights were recorded as W_1. Approximately 10 to 30 grams wet soil was placed into a labeled moisture tin with clear site information, the weights were recorded as W_2. The tin containing the wet soil samples then was placed into the drying oven. The oven temperature was set to 100°C, and the samples were left to dry for 24 hours, ensuring that the oven door remained closed to maintain a consistent temperature. After 24 hours, the tin was carefully

removed from the oven using tongs or heat-resistant gloves. The tin was placed in a desiccator to cool down to room temperature, preventing moisture absorption from the air. The cooled tin with the dry soil was weighed again, and the weights were recorded as W_3.

$$w\% = \frac{(W_2 - W_3)}{(W_3 - W_1)} * 100 \quad (6)$$

Where W_1 = weight of the empty tin (g)

W_2 = weight of the tin with wet soil (g)

W_3 = weight of the tin with dry soil (g)

3.2.2 Clay fraction and Atterberg limits

Each of the collected samples was tested to determine both the Atterberg limits and clay fraction. These tests followed the procedures outlined in ASTM D7928 (2021) for hydrometer and ASTM D4318 (2018) for liquid limit and plastic limit.

Grain size distributions of the clay specimens were determined according to ASTM D7928 (2021). The soil samples were dried in an oven at 100°C for 24 hours. Soil passing through No. 40 sieve during wash sieving was utilized in the hydrometer test. The oven-dried soil sample was broken by mortar and rubber covered pestle, and approximately 50 g sample was considered for the sieve analysis after being passed through the No 40 sieve. The soil sample was transferred into a graduated cylinder or a dispersing container for mixing preparation. Distilled water and the dispersing agent were added to the container and mixed thoroughly with the soils to form a soil-water suspension. The soil particles must be completely dispersed in the water. After the soil suspension was transferred to the sedimentation cylinder, more distilled water was added to fill to 1000 mL. The suspension density was read by hydrometer in the sedimentation cylinder starting

at 30 s, 1 min, 2 mins, 4 mins, 16 mins, 30 mins, 1 hr, 2 hrs, 4 hrs, 16 hrs, and 24 hrs along with the temperature of the suspension. After the test was completed, the soil sample was washed through the #200 sieve until the leached water was completely clear. The retained samples were dried in the oven at 100 °C for 24 hours to determine the dry mass. Figure 3-1 (a) shows the equipment that was used for this grain size distribution test, and Figure 3-1 (b) are the reference solution for the hydrometer test on the left and the sedimentation cylinder with a hydrometer suspended on the right.

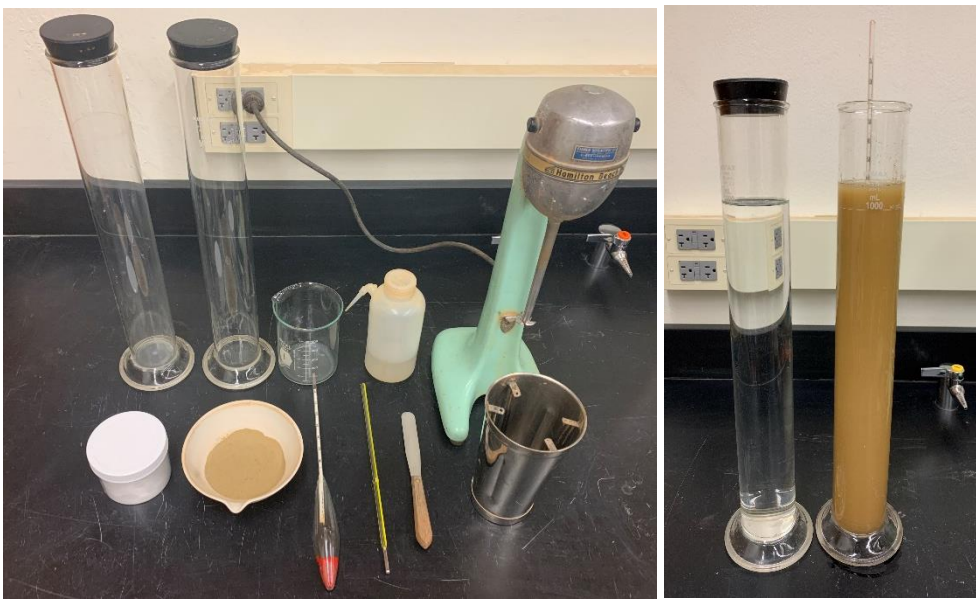

(a) (b)

Figure 3-1. (a) Equipment used for hydrometer analysis testing; (b) reference solution (left) and soil sample sedimentation suspension (right).

The Atterberg limits were determined for the soil specimens following ASTM D4318 (2018). Only the soils passing through the No. 40 sieve were used for the test. The soil was mixed with certain amount of water, and then the mixture was chopped, stirred, and kneaded repeatedly to achieve proper consistency. The wet soils for both tests were placed in a in humidity room for

24 hours to ensure uniform moisture distribution, reduce experimental errors, and adhere to standardized procedures. Figure 3-2 (a) shows the equipment for liquid limit test and the Cassagrande cup with a groove in the center, and Figure 3-2 (b) the tools for plastic limit and the rolled strip soil indicating an inconsistency of soil samples.

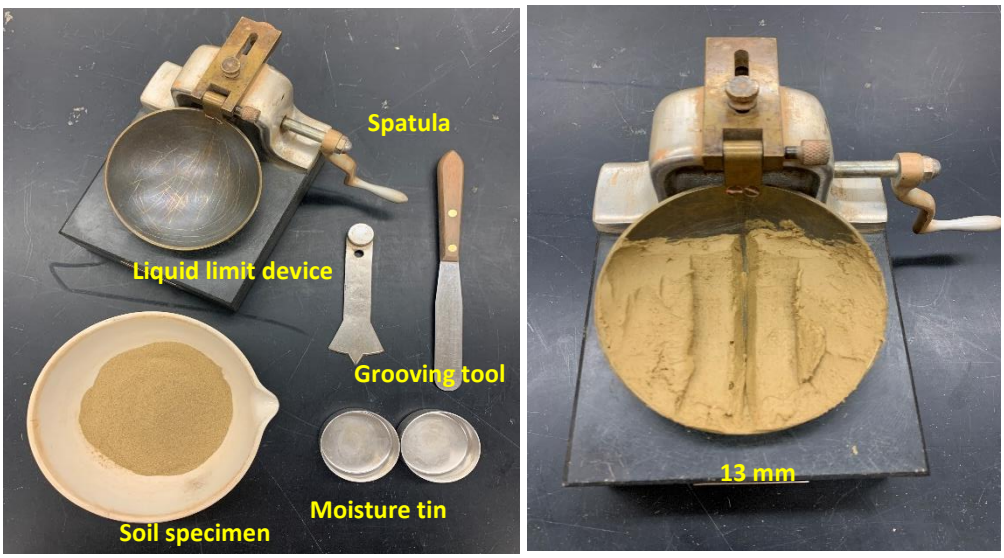

(a)

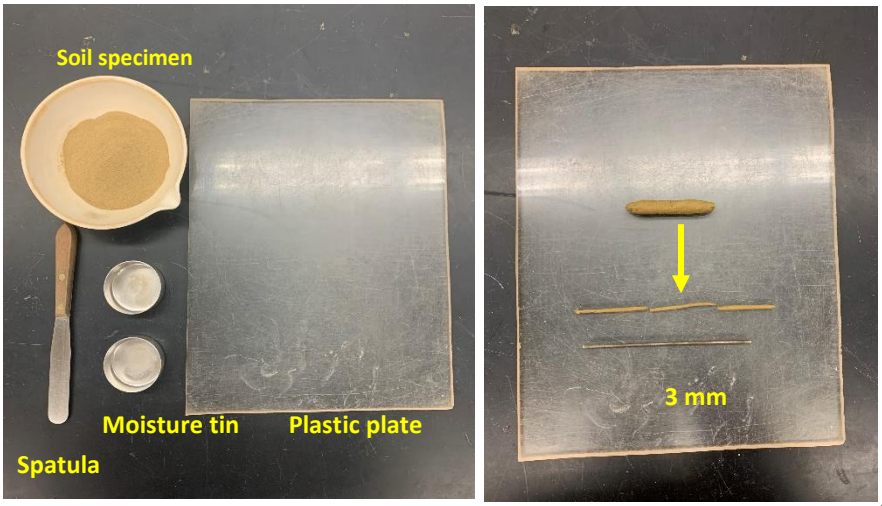

(b)

Figure 3-2. (a) liquid limit tools (left) and Casagrande cup with groove used for measuring liquid limit (right), and (b) plastic limit tools (left) and the rolled strip showing inconsistency of soil samples (right).

To begin to measure the liquid limit, wet soil was transferred to the Casagrande cup and smooth the specimen surface to cover ¾ of the cup, and a groove was cut at the center of the cup. The cup of the device was lifted and dropped at a constant rate of 2 drops per second until the groove closed to approximately 13 mm. Each lift and drop of the Casagrande cup constituted one blow, and the number of blows required for the groove closure was recorded at each attempt. Soil was collected at the closing part to measure its moisture content following steps in Section 3.2.1. The number of blows and the moisture content were recorded each time. More water was added to the wet soil and the test was repeated the steps described until 5 test points with blows varying between 35 to 15 were completed. Each was repeated three times to ensure results. A plot of the number of blows against the moisture content was created. The moisture content corresponding to 25 blows on the plot was identified as the liquid limit, and the plasticity index is defined in (7.

$$PI\ (\%) = LL - PL \tag{7}$$

Where PI = Plasticity index

LL = Liquid limit

PL = plastic limit

For the plastic limit, as defined in (8, approximately 15g wet soil was rolled out to threads on the glass plate to form a thread of uniform diameter. The rolling process continued until the soil thread crumbled when it reached a diameter of 3.2 mm. If the thread crumbles before reaching this diameter, the soil was considered too dry. A small amount of water was mixed thoroughly, and rolling process was repeated until 5 times. The soil threads were collected into

moisture cans to measure its moisture content following steps described in Section 3.2.1 each time. Each was tested three times for plastic limit to ensure results.

$$PL\ (\%) = \frac{\sum_1^n \omega\%}{n} \tag{8}$$

Where $\omega\%$ = moisture content of threads

n = number of measurements

3.3 X-Ray diffraction

3.3.1 Specimen preparation

The index testing provided information about the potential mineralogy of the samples, but a more quantitative analysis of mineralogy was achieved using X-ray diffraction (XRD) testing. X-ray diffraction is an important tool used to characterize crystalline substances (e.g., minerals). Crystalline substances consist of parallel layers of atoms and radiation entering the substance will be scattered (diffracted) by these layers. By measuring the diffraction pattern at different incident angles between the beam and the mineral surface, information on the crystal structure and the spacing between the crystalline sheets can be obtained. This process can be very useful for identifying clay minerals and a summary of using XRD for this purpose is provided by Mitchell and Soga (2005). The XRD testing performed for this study was conducted using equipment in the Geosciences department at Auburn University and generally followed the procedures described by Poppe et al. (2001) for clay mineral identification.

The sample preparation of XRD test followed the protocol from USGS Open-File Report 01-041 (accessed 2022). Clay samples were prepared by ball milling the dried clay to form a

powder and then mixing the powder with distilled water. The objective was to extract all clay-sized particles, including those interlocked within the matrix of limestones aggregates. To achieve this, cementing agents like carbonate minerals, along with manganese oxides and organic matter, were removed through a series of treatments using pH 5 buffer and 30% hydrogen peroxide solutions. After cementing agents were removed from specimens, the aggregates were treated with pH 10 sodium carbonate solution (Na_2CO3) to suspend silt (2 – 53 μm) and clay (< 2 μm) sized particles in solution. Samples were then placed in a centrifuge to settle the clay minerals. The clay solution was spread onto glass slides and air dried for 24 hours. The preparation of the slides after this depended on the test. Some slides were treated with ethylene glycol to expand swelling clays, while others were heated to either 400°C or 550 °C. This heating can reveal changes in the spacings of the crystal structure due to dehydration of the clay minerals. Different minerals will react differently to the various preparations and Poppe et al. (2014) provide flowcharts for identifying dominant clay minerals based on these changes. After preparing the slides, the samples were placed in a Bruker D2 PHASER benchtop diffractometer for analysis.

(a) (b) (c)

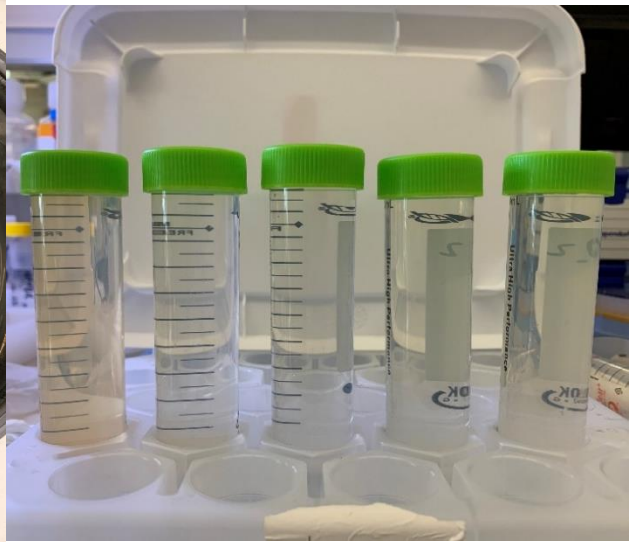

(d) (e)

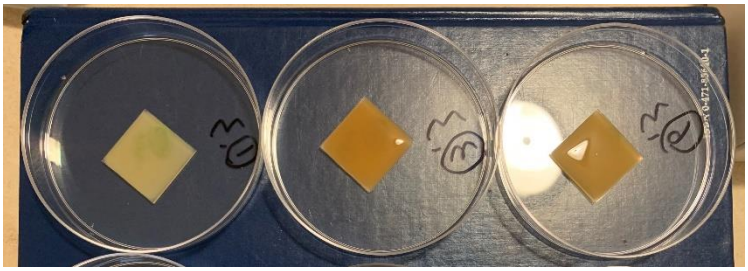

(f)

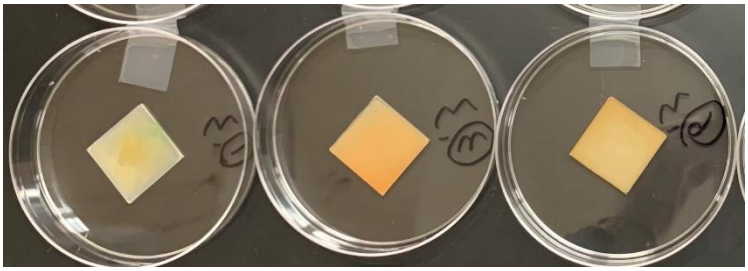

(g)

Figure 3-3. Soil preparation for XRD (a) mix soil powder and distilled water by Orbital shaker (b) shake soil solution by conic device (c) settle soil solution for 1 hours until the top 1/3 of the solution appears clear (d) centrifuge soil solution to remove silt (e) straw 1/3 clear solution into a clean centrifuge tube and settle for 24 hours (f) spread the soil solution on the glass slide (g) dry glass slide for 24 hours.

3.3.2 Identification of clay minerals

The XRD testing performed for this study was conducted using equipment in the Geosciences Department at Auburn University and generally followed the procedures described by Poppe et al. (2001) for clay mineral identification. Clay samples were prepared by ball milling the dried clay to form a powder and then mixing the powder with distilled water. Samples were then placed in a centrifuge to settle the clay minerals. The clay solution was spread onto glass slides and air dried for 24 hours. The preparation of the slides after this depended on the test. Some slides were treated with ethylene glycol to expand swelling clays, while others were heated to either 400°C or 550 °C. This heating can reveal changes in the spacings of the crystal structure due to dehydration of the clay minerals. Different minerals will react differently to the various preparations (e.g., Figure 4-3) and Poppe et al. (2001) provide flowcharts for identifying dominant clay minerals based on these changes. After preparing the slides, the samples were placed in a Bruker D2 PHASER benchtop diffractometer for analysis.

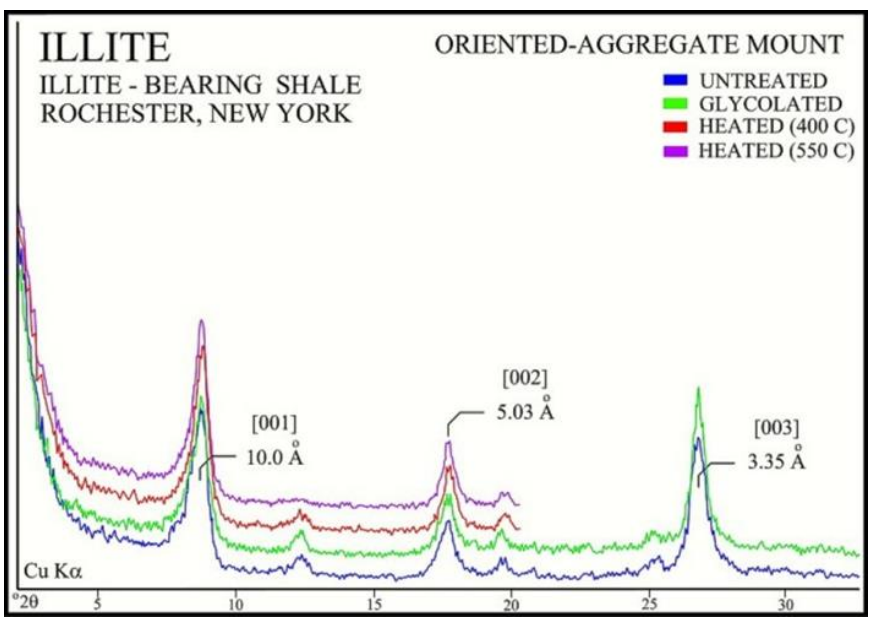

Figure 3-4. XRD results of illite clay subjected to different treatment methods prior to testing (Poppe et al. 2001).

The diffraction patterns were recorded using the Bruker D8 Advance X-ray diffractometer (Bruker accessed May 2022). The experimental setup included a Cu Kα source, with a beam energy of 35 kV and 45 mA. To identify the clay cristals, step size of 0.05° was chosen, with a dwell time of 3 seconds per step. The disc rotation occurred at 30 rpm, and the diffractometer was equipped with a SolX energy-dispersive, solid-state radiation detector.

Following the generation of diffraction patterns for all clay samples, an X-ray diffraction (XRD) analysis was conducted to identify and quantify the clay minerals present in the samples (Srodon 2006; Hughes et al. 1994). The procedure of XRD tests followed by the guidance (Poppe et al. 2014). Smectite is identifiable by layer thickness of 14 to 15 Å (Angstroms) in the magnesium saturation treatment that expands to approximately 18 Å in the magnesium glycerol treatment. Vermiculite is recognizable by its 14.4 Å peak in the glycerol treatment. Additionally, the layer thickness of vermiculite reduces to 10 Å upon water expulsion during the heating treatments to 550 °C. Consequently, through a process of elimination, the 14.4 Å peak observed in the potassium 550 °C treatment was attributed to chlorite minerals. Kaolinite can be identified by a distinct peak in the 7 Å region, which is visible in the lower four patterns but disappears upon undergoing the 550 °C treatment. On the other hand, illite is observed as a shoulder of the smectite peak at approximately 10 Å in both the magnesium and potassium treatments. To differentiate between smectite, vermiculite, and chlorite, all five treatments are necessary because they all exhibit peaks in the 14 Å region, with no specific saturation or magnesium treatment being sufficient for conclusive identification.

3.4 Torsional ring shear testing

The torsional ring shear tests followed the ASTM 6467 (2021) and ASTM 7608 (2018) with a separate specimen at each normal stress level to measure the drained fully softened and drained residual shear stresses of the twelve soil samples. Only one test was performed for each specimen as recommended from Stark and Vettel (1992). A separate test specimen was used for each normal stress to measure the fully softened strength, otherwise a post-peak or even drained residual strength will be measured because of the existence of a prior shear surface (ASTM 7608 2018). Residual strength was measured from the same sample used to determine the fully softened strength. Figure 3-3 shows the machine and the soil specimen container for testing strengths.

(a) (b)

Figure 3-5. Torsional ring shear apparatus (a) Controls Group ring shear apparatus; (b) modified porous stones used in this study.

3.4.1 Specimen preparation

The materials from the subsurface investigation were oven dried, ground and sieved to prepare the remolded specimens for torsional ring shear testing. The material passing through No.

40 Sieve or having a grain size less than 0.42 millimeters, was collected and separated for each borehole location and layer, removing any large particles to ensure the uniformity. Distilled water was added to the material until an average target moisture content was achieved. Table 3-2 lists the target moisture contents for the twelve soil samples. The soil specimens were supposed to be prepared to a moisture content near the liquid limit (ASTM 6467 2021), which corresponded to a saturated condition to minimize trapped air during placement of soil into the container. However, the soil was too wet to ensure sufficient specimens for shearing after consolidation (ASTM 7608 2018) in the torsional ring shear when this material was prepared at the liquid limit. For this study, samples were prepared at a moisture content as close to the liquid limit as possible, while still ensuring the settlement requirement during the strength testing was achieved. For most samples, this achieved moisture content was at least 75% of the liquid limit. This difference is preparation moisture content is not expected to significantly affect the drained shear strength results. Sensitivity examination of moisture contents was conducted carefully by Castellanos (2014), and no significant difference was found of fully softened strength at different remolded moisture contents, similar results were found by Bjerrum (1951, 1954. All tests were performed on saturated specimens.

Table 3-2. Target moisture contents for torsional ring shear testing

Site	Boring	Depth Range (ft)	Average Target Moisture Content (%)
SR-5	B-5.5A	1-7	41.3
SR-22	B-3	12-13.5	39.4
SR-22	B-3	9-10.5	39.3
SR-219	B-2	38.5-39.9	33.0
SR-219	B-3	19-20.5	35.1
I-59	B-1	33.5-35	46.8
US-231	SB4-1	35.5-36	31.1
US-231	SB4-1	36.4-37	28.1
I-65	B-6	4.5-6	74.2
I-65	B-7	4.5-6	68.1
I-65	B-7	7.5-9	74.2
I-65	B-7	13.5-15	79.6

Once the soil was prepared with the target moisture content, the material was kept in a humidity-controlled space to rehydrate for at least 24 hours, then transferred into the specimen container as shown in Figure 3-6. The soil specimen was prepared flush with the top of the container being trimmed with a flat and smooth surface using a spatula and a razor blade. The weights of the container was measured before and after the soil was filled to it to determine the weight of the soil in the container. The top platen with a moist porous stone was also weighed for determining the normal stress in the consolidation process. The specimen and porous stone interface are important as the porous stone should not slide across the surface of the soil (Stark 2017). The brass porous elements were machined to have a rough surface (as shown in Figure 3-6 left), as recommended by Stark (2017), to ensure that the torsional loading was properly transferred

to the soil specimen. Details on the machining of the porous stones are discussed by Kennedy (2019).

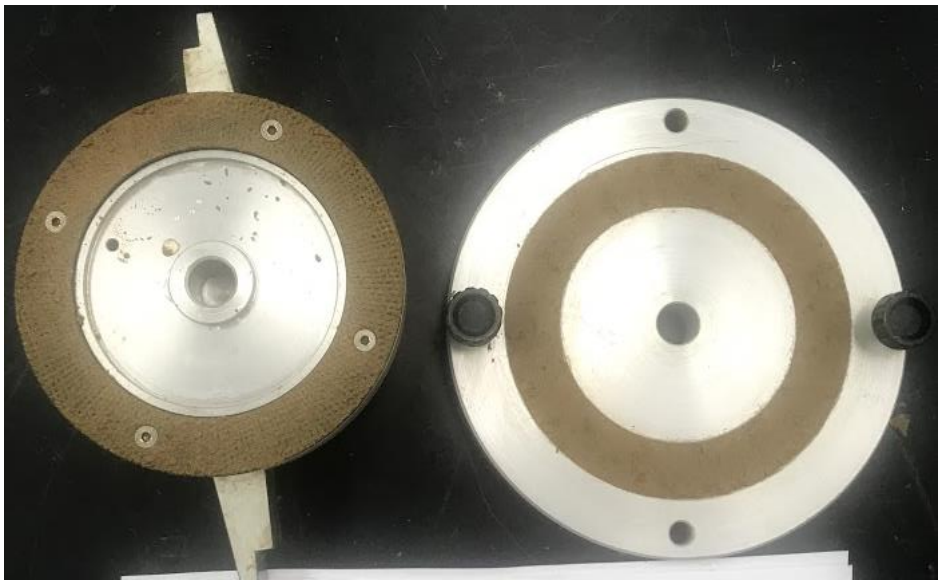

Figure 3-6. Specimen preparation within container.

3.4.2 Preconsolidation

After the specimen were placed and secured in the ring shear water bath of the apparatus, the top plate with a moist porous stone was placed on the top. The vertical displacement sensor was adjusted to contact the top plate. A small seating load of 0.1 kilograms was placed on the lever along with the weight of the top platen to achieve a normal stress of approximately 4.6 kPa. The vertical displacement sensor was read to obtain an initial vertical displacement. The specimen and container were then placed in the ring shear device and the water bath was filled to submerge the specimen in order to prevent the specimen from drying and to maintain saturation during testing. Preconsolidation loads of either 0.1, 0.7, or 1.0 kg were placed on the loading arm (corresponding to a normal stress of 5, 19, and 25 kPa on the specimen) and the vertical displacement was

monitored. The magnitude of the preconsolidation load was based on the available weights with the requirement that should be less than the consolidation load used for the shearing phase. The load was left in place for ten minutes or until vertical movements had stopped. Next, the water bath was filled with distilled water and water was added as needed to keep the soil saturated for the remaining tests.

3.4.3 Consolidation

The consolidation process applied the desired effective normal stresses to the specimen using a load increment ratio (LIR) of unity to obtain the shear strength envelope. Each soil sample in this study was consolidated under similar effective normal stresses with the same corresponding weights applied to the loading lever. For each load increment, primary consolidation was verified to be completed using ASTM D2435 (2011) before proceeding. To ensure sufficient specimen (3mm or 60% of the initial specimen height) remained in the container, no more than 15% of the initial specimen height (5 mm) was allowed to settle per ASTM D6467 (2021). The specification for 0.75 mm of settlement was used for accounting for the thickness of the two bronze sporous stones. If the soil specimens settled more than 0.75 mm, additional soil was added to the specimen container until the material was flush again with the top of the specimen container as mentioned in Section 3.4.1. The specimen was taken apart to add more soil to it and repeated the same precoslidation process to reconsolidate.

Consolidation continued for 24 hours or until the consolidation process was complete. A consolidation curve was used to determine if a well-defined normal deformation versus log time relationship which extended into secondary compression per ASTM D2435 (2011). The time to mobilize the peak shear resistance or failure should be computed using (9. Otherwise, the

relationship between the normal deformation versus square root time could be used if the curve was not well-defined for the relationship between the normal deformation versus log time. The time to failure should be computed using following (10 ASTM D2435 (ASTM 2011).

$$t_f = 50t_{50} \tag{9}$$

Where t_f = total estimated elapsed time to failure (min)

t_{50}= time required for the specimen to achieve 50 % consolidation under the specified effective normal stress (min)

$$t_f = 11.6t_{90} \tag{10}$$

Where t_f = total estimated elapsed time to failure (min)

t_{90}= time required for the specimen to achieve 90 % consolidation under the specified effective normal stress (min)

3.4.4 Shearing

The shear process was conducted by rotating the bottom stone of the specimen container relative to the upper stone. The shearing rate to apply the shear loading was firstly determined by (11 (ASTM D6467 2021). The displacement rate should be sufficiently slow to assure dissipation of any shear-induced pore excess water pressure (Stark et al. 2020). Rapid shearing of the remolded test specimen could cause partially drained shear results that differ from the drained strength of the material. As a guide from ASTM D6467 (2021) and ASTM D7608 (2018), a shear rate of 0.02 mm/min or 0.03 degree/min was usually required for a high plasticity clay for fully softened shear results and for residual shear results, respectively. The magnitude of the estimated

displacement at failure is dependent on many factors including the type of soil. As a guide, use d_f = 5 mm for an undisturbed or reconstituted fine-grained soil of high plasticity (CH), and use d_f = 2.5 mm for an undisturbed or reconstituted fine-grained soil of low plasticity (CL).

$$d_r = \frac{d_f}{t_f} \tag{11}$$

Where d_r = displacement rate (mm/min)

d_f = estimated shear displacement at failure (mm)

t_f = determined using Equation (9) or Equation (10)

Once the displacement rate was set, the two load cells were swung toward the torque arm with the two bearing adjustment rods create a right angle with the bearing stop then secured them and adjusted them to be just touching the torque arm. The load cell rods were then locked into place. The ring shear apparatus set up to shear the specimen with the load cell rods touching the torque arm are shown in Figure 3-3 (a). The initial time of the test was recorded along with the initial vertical and shear displacement readings. The dial readings of rotation angle were read in reference to the datum (Figure 3-7) on the container to record the initial location of the soil specimen. Before the specimen started shearing under the same desired normal stress level, the specimen was rested for sufficient time to allow the dissipation of any excess pore water pressure induced during the assembling. The specimen was sheared when the vertical displacement became almost negligible. Data was recorded using the data logger and computer software. Data was recorded for 24 hours or until a well-defined residual strength state was obtained. The final rotation angle was recorded after shearing was completed.

The actual average displacement rate was calculated by the average shear displacement over the testing time as expressed in (12. The degree that the specimen was sheared was read before and after the shearing process from the rotating dial reading disc attached to the specimen container as shown in Figure 3-7. The difference of the two readings was the rotation angle, and converted to shear displacement for the actual average shear displacement rate using (13.

$$d_r = \frac{d_h}{t_e} \tag{12}$$

$$d_h = (rotation\ angle)(\frac{\pi}{180°})(\frac{R_1+R_2}{2}) \tag{13}$$

Where d_r = actual average shear displacement rate (mm/min)

d_h = shear displacement (mm) or using Equation (13)

t_e = elapsed time of test (min)

R_1, R_2 = inner and outer specimen radii (mm)

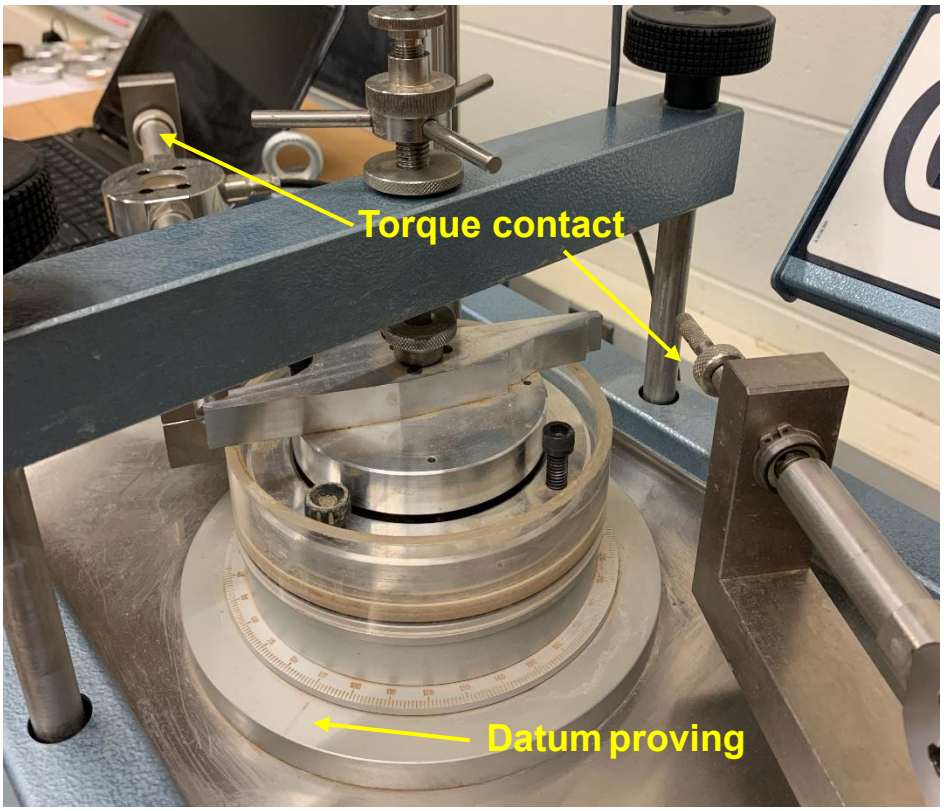

Figure 3-7. Specimen container assembled with datum indicated

As the shearing continued, the load cells measured forces applied to the torque arm on the Torque contact and data logger recorded the measured data. The effective normal stress and shear stress were calculated using (14 and (15, respectively. After the shearing process completed, the top plate was carefully separated from the specimen with a sliding motion in the same direction as the failure plane to ensure minimal damage to the specimen. Plots of shear stress verses shear displacement and shear stress verses effective normal stress were used to identify the value of fully softened shear strength and residual shear strength for each effective normal stress. The values of each full softened shear strength and residual shear strength were plotted in both shear strength envelopes as a result in the next chapter.

$$\sigma_n' = \frac{P}{\pi(R_2^2 - R_1^2)} \tag{14}$$

Where σ_n' = effective normal stress (Pa)

P = normal vertical force acting on the specimen (N)

$$\tau = \frac{3(F_1 + F_2)L}{4\pi(R_2^3 - R_1^3)} \tag{15}$$

Where τ = shear stress (Pa)

F_1, F_2 = measured forces on the proving rings (N)

L = Torque length (mm)

R_1, R_2 = inner and outer specimen radii (mm)

3.5 Statistics of laboratory data

3.5.1 Statistics

Initial statistical analysis is a crucial step to examine laboratory measured raw data before further analysis. Descriptive statistical analysis of the measured raw data is indispensable for checking the precision and deriving further conclusions (Mandel 2012).

Statistical measures, such as number of tests, mean, standard deviation, and coefficient of variance (COV) play pivotal roles in this analytical process. The mean serves as a cornerstone metric, providing a central tendency that encapsulates the average value of measurements within a dataset (Cohen & Cohen, 1983). These measures are used for characterizing the typical response or quantity under study, offering a foundational reference point from which deviations and patterns can be discerned (Baecher and Christian 2003).

Standard deviation complements the mean by quantifying the dispersion or variability of data points around the mean value (Gelman et al., 2013). By calculating standard deviation, the spread of measurements can be quantized, thereby consistency and reliability of experimental outcomes are assessed. In laboratory settings, a low standard deviation indicates that measurements are tightly clustered around the mean, suggesting robust experimental protocols and reliable data collection methods. This statistical measure is essential for evaluating the precision of measurements and identifying potential sources of variability that may influence experimental results.

Coefficient of variance extends the statistical analysis by measuring the degree to which two variables co-vary, providing insights into their relationship and mutual influence (Hays, 1988). In laboratory research, covariance analysis is pivotal for exploring dependencies between experimental parameters or variables. For instance, in microbiological studies investigating the relationship between nutrient availability and bacterial growth rates, covariance analysis can reveal how changes in one variable impact variations in another. By elucidating these interrelationships, covariance analysis aids researchers in refining hypotheses, optimizing experimental designs, and drawing informed conclusions based on empirical data.

In summary, the meticulous application of statistical measures such as mean, standard deviation, and covariance in laboratory measurements is essential for enhancing the accuracy, reliability, and interpretability of scientific findings. These statistical tools not only quantify central tendencies and variability within datasets but also elucidate relationships between variables, thereby enabling researchers to make informed decisions and advance knowledge in diverse fields of scientific inquiry.

$$\bar{y} = \frac{\sum_1^n y_i}{n} \tag{16}$$

$$\sigma = \sqrt{\frac{\sum_1^n (y_i - \mu)^2}{n}} \tag{17}$$

Where y_i= values of each data

n = number of tests

p = number of laboratories

$\bar{y}$ = average

σ = standard deviation

3.5.2 Statistical of torsional ring shear

The torsional ring shear method has been recommended by many authors (Bromheaed 1979, Stark and Vettel 1992, Duong and Van 2022, Stark and Eid 1997, 2013, 2020), but there is no established method for assessing variability in this measured shear strength and identifying outliers of the measured data. Ring shear results are likely to be affected by both inherent variability in the samples obtained for testing as well as variability in the measurement procedures. The term variability is used in this study to represent the consistency of measured drained shear strength, and the data analysis methods of this study are specific quantitative measures for representing variability with a nonlinear (power) regression model and predicting an acceptable range of measured data. In the following subsections, regression statistical analysis, t-test statistical analysis and the quantitative statistics are defined for applying to the measured shear strength in this study.

3.5.3 Goodness of fit

The coefficient of determination, denoted as R-squared (R^2), is used to assess the adequacy of fit models of this study. R^2 values, which evaluate the goodness of fit for the best fit lines by the least square method (Nagelkerke 1991, Baecher and Christian 2005). It quantifies the proportion of the total variation in the dependent variable that is explained by the independent variables in a fit model, as defined in Equation (21) (Miller 2006).

By using R^2 values, a statistical measure of fit can be achieved to appropriately find the best fit model in representing the measurements, as well as the accuracy of the fit. It is noted that a larger value of R^2 generally signal a better model performance or a high goodness of fit. R^2 value of 1 represents a perfect fit and the fitted model closely follow the measurements, indicating that all variability of dependent variable can be explained by the fit model in the independent values. Conversely, value of 0 represents the model explain none of the variability of the variables, implying poor fit accuracy that the fit may not accurately reflect the measurements, therefore, no relationship between the dependent and independent variables (Baecher and Christian 2005). It is possible to have negative R^2 indicating the model is worse than a simple mean-based model, meaning the predictions from the model are less accurate than predicting the mean of the observed values.

This study uses R^2 values to evaluate the goodness of fit for the shear strength failure envelope between the measured shear stresses and the normal stresses, thereby determining the accuracy of the fitted shear strength failure envelope equations capture the relationships. R^2 was transformed from the exponential model and calculated using Equation (18). The sum of square of residuals and sum of square of total are calculated using Equation (19) – (20). A R^2 value above 0.70 or 0.80 (Cohen 2013) is considered indicative of a strong fit for this study, such that enhance

confidence in the derived shear strength failure envelope. A negative R^2 highlights the model may not be suitable for the data, it can be a signal that a different model or approach should be considered.

$$R^2 = 1 - \frac{SSR}{SST} \tag{18}$$

$$\text{SSR} = \sum_1^n (y_i - \hat{y}_i)^2 \tag{19}$$

$$\text{SST} = \sum_1^n (y_i - \bar{y})^2 \tag{20}$$

Where R^2 = coefficient of determination

SSR = sum of square of residuals

SST =sum of square of total

y_i = dependent variable, which is the measured data

$\hat{y}_i$ = estimated dependent variable from regression model

$\bar{y}$ = mean of dependent variable

3.5.4 Outlier detection

Statistical t-tests are used to compare the means of two groups. t-statistics are used to find the confidence interval defined as Equation (21) that is defined as the likely range of values associated with of the data with a certain confidence level. A prediction interval defines a range of values within which a response is likely to fall given a specified value of a predictor by Equation (22), which is used cooperates with the t-test to predict likely variance and outliers in this study.

$$\mathrm{CI} = \hat{y} \pm t_{\alpha/2}\frac{\sigma}{\sqrt{n}} = \hat{y} \pm t_{\alpha/2}\sqrt{\frac{1}{n} + \frac{(x-\bar{x})^2}{SS_{xx}}} \tag{21}$$

$$\mathrm{PI} = \hat{y} \pm t_{\alpha/2}\frac{\sigma}{\sqrt{n}} = \hat{y} \pm t_{\alpha/2}\sqrt{1 + \frac{1}{n} + \frac{(x-\bar{x})^2}{SS_{xx}}} \tag{22}$$

Where CI = confidence interval

PI = prediction interval

$\hat{y}$ = estimated dependent variable by the regression model

α = significance level of 5%

$t_{\alpha/2}$ = t statistics for confident level or prediction level of 95%

s = standard deviation of estimated dependent variable by the regression model

SS_{xx} = standard deviation of the independent variable

n = number of the measurements

3.5.5 Comparison with existing models

As the drained shear strength models mentioned in Section 2.5.4 were used to estimate the secant friction angles, the statistical values were calculated for the secant friction angles of both the estimated and measured drained shear strengths of the twelve soil samples. The objective in this process is to evaluate how well the listed drained shear strength models (estimated data) can estimate the measured data (measured data of this study).

The statistical parameters that provide insight on data fit were used for this part, these include residual, average of residual, and root mean square (RMS) to compare the estimated data

and the measured data. The residual and the average residual (Weiss et al 2012, Chatterjee and Ali 2015) are to determine the difference between the estimated data and measured data, as defined in Equations (23) and (25). To further validate the difference of the listed shear strength models and the measurements of the study, RMS is used to statistically reflects the average of the squared difference between the listed models and the measurements of the study, which is defined in Equation (25).

$$\text{Residual} = \phi'_{\text{sec}} - \widehat{\phi'_{\text{sec}}} \tag{23}$$

$$\text{Average Residual} = \frac{\sum_1^n (\phi'_{\text{sec}} - \widehat{\phi'_{\text{sec}}})}{n} \tag{24}$$

$$\text{RMS} = \sqrt{\frac{\sum_1^{\text{n}} (\phi'_{\text{sec}} - \widehat{\phi'_{\text{sec}}})^2}{\text{n}}} \tag{25}$$

Where ϕ'_{sec} = secant friction angle of measured drained shear strengths (Duncan 2014)

$\widehat{\phi'_{\text{sec}}}$ = secant friction angle of drained shear strengths estimated from correlations

n = number of the determination

CHAPTER 4: SOIL CHARACTERIZATION RESULTS

4.1 Introduction

This chapter presents the results of the experimental testing and the results of the investigation into the comprehensive characterization of soil properties at the selected six sites in Alabama. The chapter includes the engineering index properties of moisture content, soil gradation and clay fraction, Atterberg limits, Activity and soil classification, clay minerology results from XRD testing, and the drained fully softened and residual results.

4.2 Engineering index properties results

Understanding the physical properties of high plasticity clay is essential for comprehending its behavior under various conditions. This section presents the results of physical property tests conducted on the twelve clay samples collected from the sites in Alabama. These tests included grain size distribution, Atterberg limits, and activity to provide a foundational understanding of the soil's composition and characteristics. Tests were conducted on soil samples listed in Section 3.1.

4.2.1 Moisture content

The moisture contents of soils were measured three times for the twelve sites samples to reduce any of the repeatable variability of the results. Soil sample of various depths were tested to understand its distribution and variability across the study area. The test followed ASTM D2216

(2019), ensuring accuracy and consistency in data collection. The average moisture contents and the corresponding standard deviations are shown in Table 4-1.

Table 4-1. Averaged Moisture Content for the Collected Samples.

Site	Boring	Depth Range (ft)	Number of Tests	Average Moisture Content (%)	Standard Deviation
SR-5	B-5.5A	1-7	3	41.3	0.2
SR-22	B-3	12-13.5	3	39.4	0.0
SR-22	B-3	9-10.5	3	39.3	0.1
SR-219	B-2	38.5-39.9	3	33.0	0.2
SR-219	B-3	19-20.5	3	35.1	0.2
I-59	B-1	33.5-35	3	46.8	0.1
US-231	SB4-1	35.5-36	3	31.1	0.2
US-231	SB4-1	36.4-37	3	28.1	0.2
I-65	B-6	4.5-6	3	74.2	0.1
I-65	B-7	4.5-6	3	68.1	0.1
I-65	B-7	7.5-9	3	74.2	0.1
I-65	B-7	13.5-15	3	79.6	0.1

4.2.2 Grain size distribution and clay fraction

Figure 4-1 shows the grain size distribution curves of the twelve soil samples, and Table 4-2 provides a summary of the key grain size parameters. To examine the precision of the grain size distribution results, two tests was performed for soil sample, and the averaged percentage of passing on each sieve size was calculated. Figure 4-1 below shows the averaged percentage of passing for the grain size distribution curve. As suggested in ASTM D6913 (2022), the acceptability of test results for grain size distribution within laboratory should fall below 2%. Table 4-2 also shows the difference of clay fraction and percentage of the fines of the two tests' results,

and all of the test results are lower than 2%, which are within the acceptability criteria (ASTM D6913). It was observed that the percent passing through No. 200 sieve ranged from 35.6% to 94.4% in the soil samples. Clay fraction of SR-22, SR-219, and US-231 (clay fractions less than 55%) was low compared to the other soils samples. Analysis of the grain size distribution curves reveals the predominance of fine particles, consistent with the clayey nature of the soil.

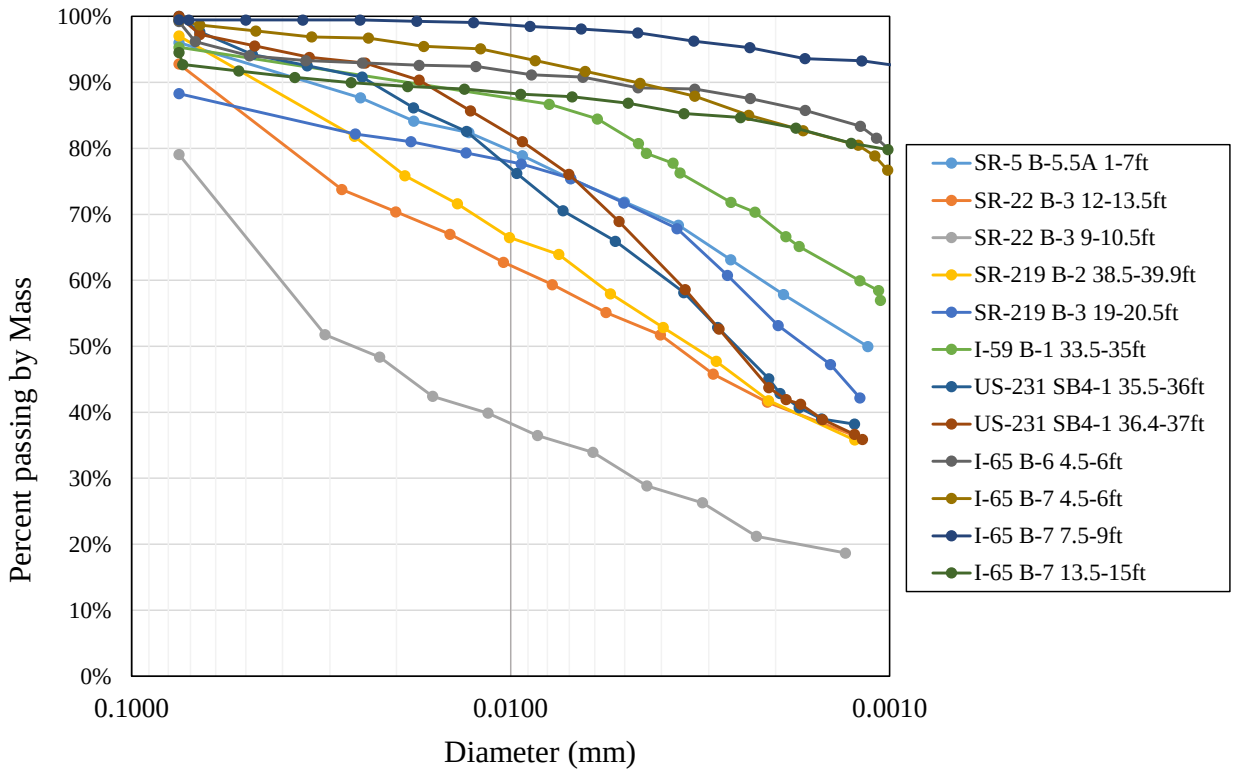

Figure 4-1. Grain Size Distribution Curves for the Twelve Collected Samples

Table 4-2. Grain Size Parameters for the Collected Samples.

Site	Boring	Depth Range (ft)	Number of Tests	Average Clay Fraction (%)	Average Fines Content (%)	Clay Fraction Difference of Two Tests (%)	Fines Content Difference of Two Tests (%)
SR-5	B-5.5A	1-7	2	58.5	96.0	0.9	0.9
SR-22	B-3	12-13.5	2	40.9	92.8	0.8	0.7
SR-22	B-3	9-10.5	2	35.6	79.1	0.7	0.8
SR-219	B-2	38.5-39.9	2	41.2	97.0	0.6	0.7
SR-219	B-3	19-20.5	2	53.5	88.3	0.5	0.6
I-59	B-1	33.5-35	2	67.8	95.3	0.6	0.4
US-231	SB4-1	35.5-36	2	40.9	100.0	0.6	0.2
US-231	SB4-1	36.4-37	2	40.7	100.0	0.4	0.2
I-65	B-6	4.5-6	2	86.7	99.2	0.8	0.3
I-65	B-7	4.5-6	2	83.8	99.4	0.7	0.3
I-65	B-7	7.5-9	2	94.4	94.5	0.8	0.3
I-65	B-7	13.5-15	2	83.6	99.5	0.7	0.3

4.2.3 Atterberg limits

The Atterberg limits, including the liquid limit and plastic limit results are summarized in Table 4-2 and Table 4-3 respectively along with the standard deviation for determining acceptability of the test results. Each soil sample were repeatedly tested three times, and a liquid limit with standard deviation less than 0.7 and plastic limit with standard deviation less than 0.5 are considered acceptable Atterberg limits results (ASTM D4318 2022). Six of the twelve soil samples stand out due to their high plasticity. Samples from sites on SR-5, I-59, and I-65 classify as high plasticity clay or silt, while the samples from US-231, SR-22, and SR-219 classify

primarily as low plasticity clays. Plasticity indices are summarized in Table 4-4 for use in soil classification and screening common range of clay minerals in the following sections. These results shed light on the soil's propensity to undergo changes in consistency and strength in response to moisture variations.

Table 4-3. Liquid Limit Values for the Collected Samples

Site	Boring	Depth Range (ft)	Number of Tests	Average Liquid Limit (LL)	Standard Deviation
SR-5	B-5.5A	1-7	3	86	0.3
SR-22	B-3	12-13.5	3	48	0.5
SR-22	B-3	9-10.5	3	51	0.5
SR-219	B-2	38.5-39.9	3	46	0.5
SR-219	B-3	19-20.5	3	50	0.5
I-59	B-1	33.5-35	3	65	0.5
US-231	SB4-1	35.5-36	3	45	1.0
US-231	SB4-1	36.4-37	3	46	1.0
I-65	B-6	4.5-6	3	116	0.5
I-65	B-7	4.5-6	3	102	0.5
I-65	B-7	7.5-9	3	115	0.5
I-65	B-7	13.5-15	3	105	0.5

W

Table 4-4. Plastic Limit Values for the Collected Samples

Site	Boring	Depth Range (ft)	Number of Tests	Average Plastic Limit (PL)	Standard Deviation
SR-5	B-5.5A	1-7	3	26	0.3
SR-22	B-3	12-13.5	3	27	0.5
SR-22	B-3	9-10.5	3	25	0.5
SR-219	B-2	38.5-39.9	3	23	0.5
SR-219	B-3	19-20.5	3	26	0.5
I-59	B-1	33.5-35	3	35	0.5
US-231	SB4-1	35.5-36	3	28	0.5
US-231	SB4-1	36.4-37	3	25	0.5
I-65	B-6	4.5-6	3	53	0.3
I-65	B-7	4.5-6	3	42	0.3
I-65	B-7	7.5-9	3	50	0.3
I-65	B-7	13.5-15	3	56	0.3

4.2.4 Activity and soil classification

The clay fraction and activity (PI / Clay Fraction) of the samples is also shown in Table 4-4. Activity can be useful for assessing the influence of the clay fraction are on the overall properties of the clay and can be correlated with engineering behavior (e.g., swelling potential) and mineralogy (Mitchell and Soga 2005). The activities for the sites considered in this study fall into three main categories. SR-5 has the highest activity and falls on the lower end of range normally seen for smectite clays, such as montmorillonite (Mitchell and Soga 2005). Samples from I-65 and the shallower sample from SR-22 all show activities between 0.6 and 0.75, which would be more typical of illite clays (Mitchell and Soga 2005). This range would also be typical for attapulgite and allophane clays, but these are not expected to occur in the study area. The other samples (US-231, I-59, SR-219, and the lower depth from SR-22) have activities ranging from 0.44 to 0.56,

which would be more typical of kaolinite clays (Mitchell and Soga 2005) or mixtures of kaolinite and illite. These correlated mineralogy results are consistent with the approximate ranges for the various clay minerals shown in Figure 4-2. With a typical range of the plasticity index, Atterberg limits are useful to indicate and inference the type of minerals in the soil, and its behavior (Holtz et al. 2011).

Table 4-5. A Summary of Engineering Index Results for the Collected Samples

Site	**Boring**	**Depth Range (ft)**	**Liquid Limit (LL)**	**Plasticity Index (PI)**	**Clay Fraction (%)**	**Activity**
SR-5	B-5.5A	1-7	86	60	58.5%	1.02
SR-22	B-3	12-13.5	48	21	40.9%	0.51
SR-22	B-3	9-10.5	51	26	35.6%	0.73
SR-219	B-2	38.5-39.9	46	23	41.2%	0.56
SR-219	B-3	19-20.5	50	24	53.5%	0.45
I-59	B-1	33.5-35	65	30	67.8%	0.44
US-231	SB4-1	35.5-36	45	20	40.9%	0.49
US-231	SB4-1	36.4-37	46	18	40.7%	0.44
I-65	B-6	4.5-6	116	63	86.7%	0.73
I-65	B-7	4.5-6	102	60	83.8%	0.72
I-65	B-7	7.5-9	115	59	94.4%	0.62
I-65	B-7	13.5-15	105	55	83.6%	0.66

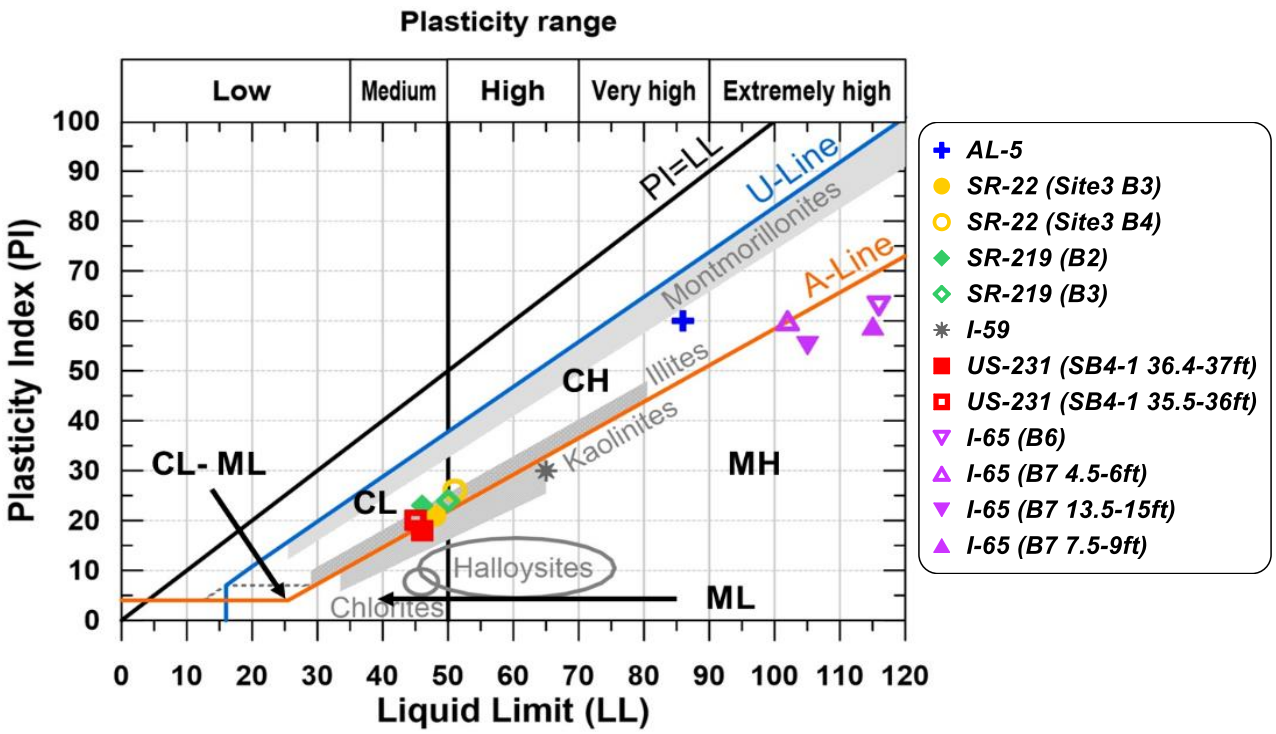

Figure 4-2. Atterberg limits results for the collected samples along with boundaries for different classifications and common ranges for different minerals (after Holtz et al. 2011).

4.3 X-Ray diffraction results

XRD testing was performed on five of the samples (Figures 4-4 – 4-8) to confirm the correlated mineralogical results based on the Atterberg limits and activity discussed in the previous section. The mineralogical results from the XRD testing are summarized in Table 4-6. The XRD results largely agree with the correlations based on activity, especially when considering that many of the samples showed more than one constituent. Montmorillonite-illite is one of the most common mixed-layer clays (Mitchell and Soga 2005) and is seen in the XRD results at both I-65 and SR-22. The Atterberg limits of these two sites are very different with the samples from I-65 showing much higher LLs, likely indicating these samples have a larger proportion of montmorillonite. The samples from US-231 standout as the XRD indicates the presence of chlorite,

while the Atterberg limits (Figure 4-3) do not. The results for US-231 are discussed in more detail below.

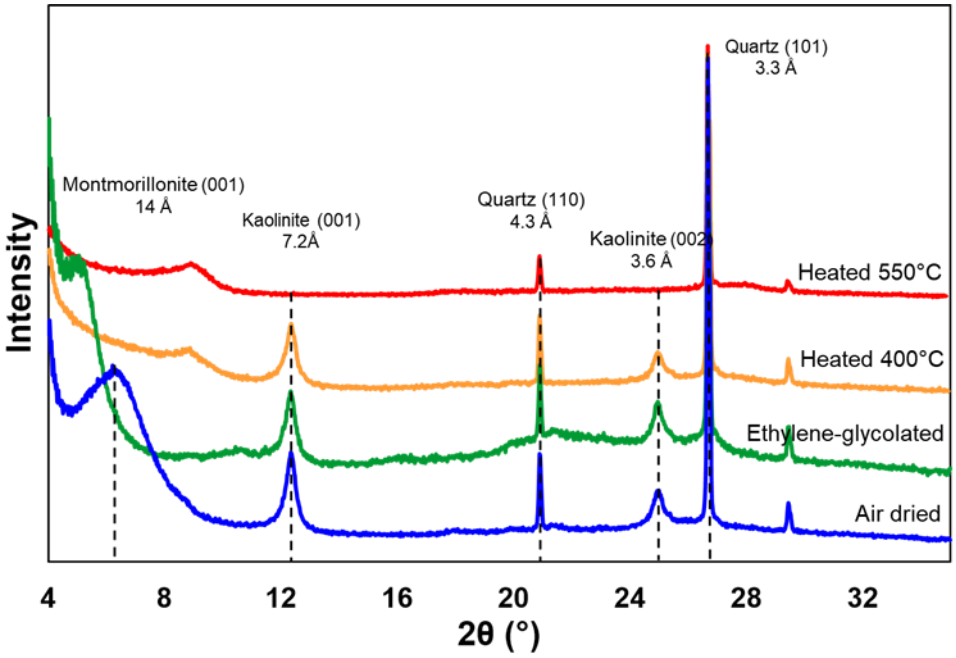

Figure 4-3. XRD results for the sample collected from SR-5 (B-5.5A, 1-7 feet).

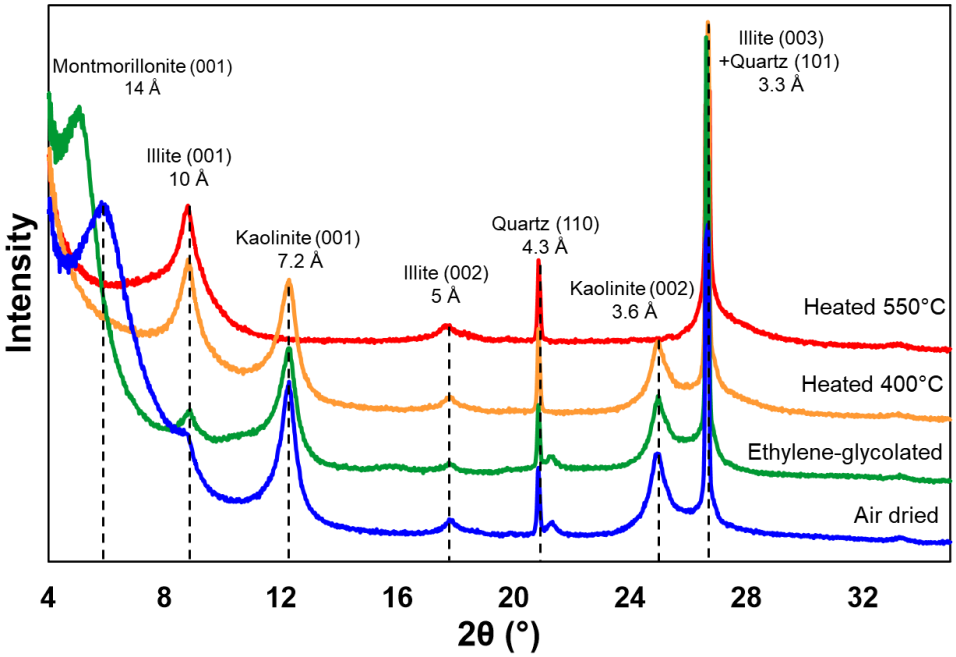

Figure 4-4. XRD results for the sample collected from SR-22 (B-3, 9-10.5 feet).

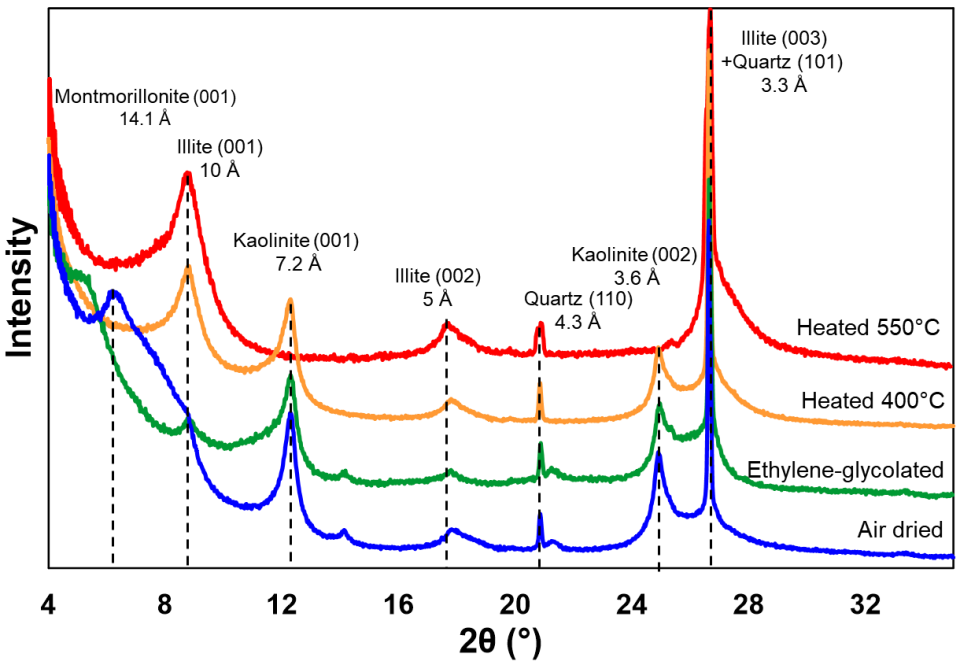

Figure 4-5. XRD results for sample collected from I-59 (B-1, 33.5-35 feet).

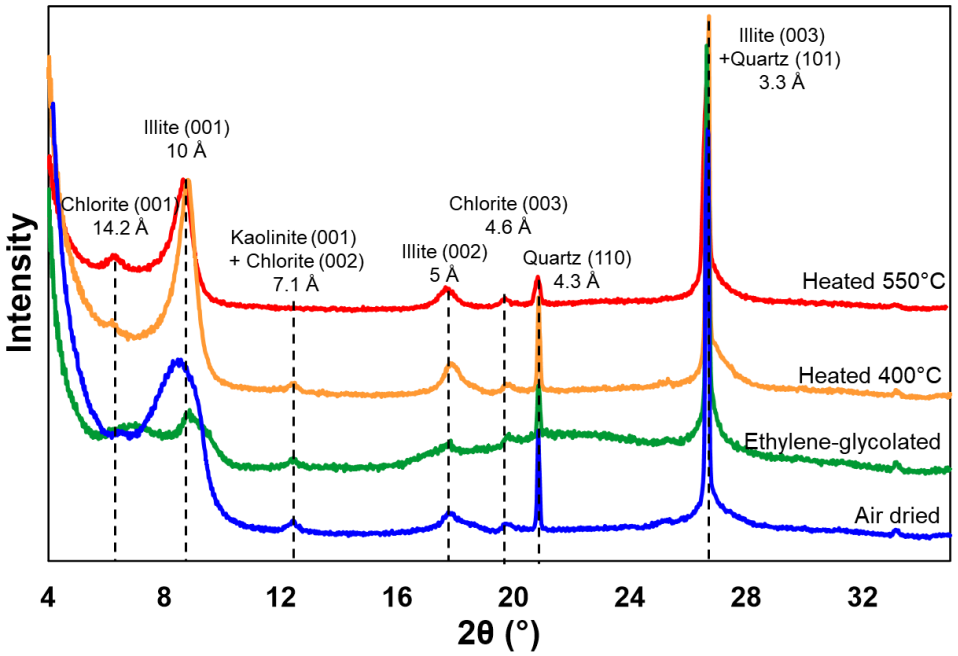

Figure 4-6. XRD results for sample collected from US-231 (SB4-1, 35.5-36 feet).

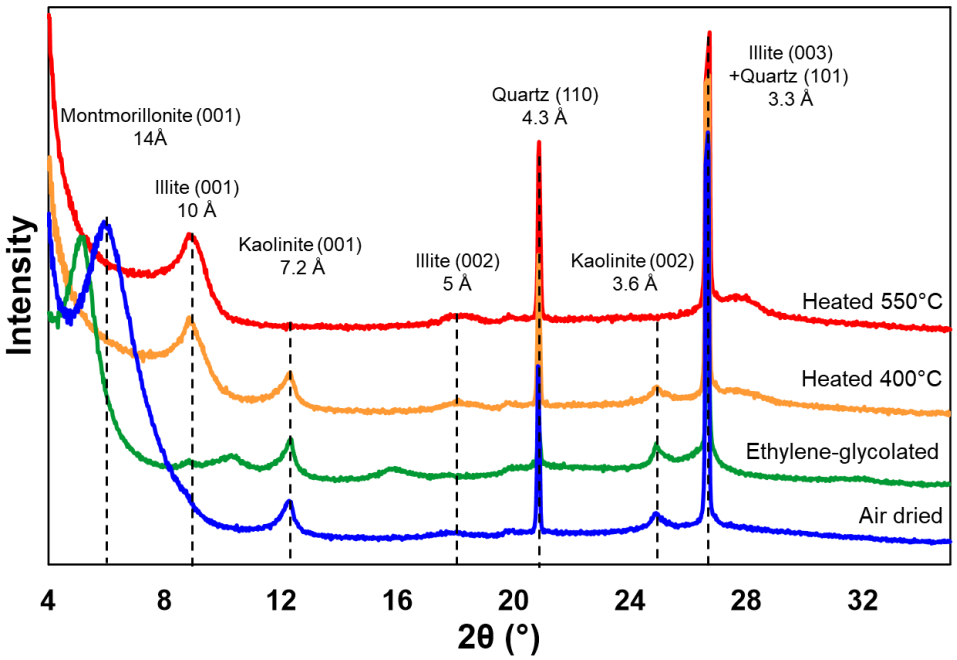

Figure 4-7. XRD results for sample collected from I-65 (B-7, 4.5-6 feet).

Table 4-6. Clay mineralogy results.

Site	Boring (Depth)	Depth Range (ft)	Correlations Based on Activity	XRD Results		
				Mineral 1	Mineral 2	Mineral 3
SR-5	B-5.5A	1-7	montmorillonite	montmorillonite	kaolinite	chlorite
SR-22	B-3	12-13.5	kaolinite or illite	Not tested		
SR-22	B-3	9-10.5	illite	montmorillonite	illite-montmorillonite or illite-vermiculite	kaolinite
SR-219	B-2	38.5-39.9	kaolinite or illite	Not tested		
SR-219	B-3	19-20.5	kaolinite or illite	Not tested		
I-59	B-1	33.5-35	kaolinite or illite	illite-vermiculite	kaolinite	chlorite
US-231	SB4-1	35.5-36	kaolinite or illite	illite-montmorillonite or illite-vermiculite	chlorite	kaolinite
US-231	SB4-1	36.4-37	kaolinite or illite	Not tested		
I-65	B-6	4.5-6	illite	Not tested		
I-65	B-7	4.5-6	illite	montmorillonite	illite-montmorillonite or illite-vermiculite	kaolinite
I-65	B-7	7.5-9	illite	Not tested		
I-65	B-7	13.5-15	illite	Not tested		

The XRD results for US-231 were interesting as this was the only sample that showed a significant amount of chlorite. The samples of soil from US-231 were taken from a weathered shale or mudstone layer that was consistent with the depth of the sliding plane. This zone is within the Pennington formation, which is a Mississippian age formation and consists of primarily shale with interbedded limestone, dolomite, sandstone, mudstone, and minor coal (Szabo et al. 1988). The upper sample used in this study had a purple color, while the lower sample was grey. Both samples had similar Atterberg limits and similar strengths as discussed later. The Atterberg limits and activity fall within the ranges usually associated with kaolinite or illite, while the XRD for the purple sample shows primarily mixed illite layers and chlorite. Illite and chlorite have similar

structures, but chlorite has an extra octahedral sheet making it a 2:1:1 clay mineral (Mitchell and Soga 2005). This extra octahedral sheet reduces the cation exchange capacity relative to illite and vermiculite and the liquid limit of chlorite is lower than illite. The plasticity index of chlorite is also usually low with some samples being non-plastic. The LL for the US-231 samples is within the range expected for chlorite, but the PI is quite a bit higher (Table 4-7) and more consistent with that expected for illite.

Table 4-7. Clay mineralogy and Atterberg limits results of US-231 in this study and soil mineral types with the similar range of liquid limit and plasticity limit from other studies.

Soil/Mineral Type	**Liquid Limit (LL)**	**Plasticity Limit (PL)**	**Source**
US-231 (SB-4, 35.5-36)	45	20	This study
Illite	60 - 120	35 - 60	Mitchell and Soga (2005)
Chlorite	44 - 47	36 - 40	Mitchell and Soga (2005)
Vinton County, OH	47 - 62	23 - 33	Webb and Collins (1967)
Lewis County, WV	38 - 54	29 - 39	Okagbue (1986)

The Atterberg limits and XRD results for the US-231 sample are consistent with similar soils found at landslide sites in Ohio (Webb and Collins 1967, Fisher et al. 1968, Wu et al. 1993) and West Virginia (Okagbue 1986). All three of these studies investigated landslides occurring within shale and/or mudstone layers within Mississippian or Pennsylvanian age formations. Illite and chlorite were also found to be the main mineral constituents, but the illite was found to be degraded due to the loss of potassium and abundance of ferric iron. A intensity ratio (003/001) is used for to quantify the abundance of any elements in the clay mineral. The (003)/(001) peaks ratio from the XRD results (Table 4-7) shows the illite mineral of this study is less than one indicating that the illite is deficient in potassium Pomeroy and Thomas (1985) performed XRD testing on

samples collected from the Pennington Formation in northern Alabama and determined that this deposit also contained degraded illite, which were likely to be unstable.

4.4 Torsional ring shear results

One of the key objectives of this study was to measure the fully softened and residual drained strength envelopes for the clays. This was completed using ring shear testing as discussed in previous sections. The response of three of the tested specimens is shown in Figure 4-8. The remolded samples quickly reach a peak followed by a large drop in strength. This peak is defined as the fully softened strength of the soil. After a certain amount of shear displacement (approximately 0.5 – 2.0 inches for the tests in this study), the shear stress is approximately constant, and the sample is assumed to have reached a residual strength. This process is repeated for multiple stress levels to define a strength envelope (Figure 4-9). All specimens were saturated.

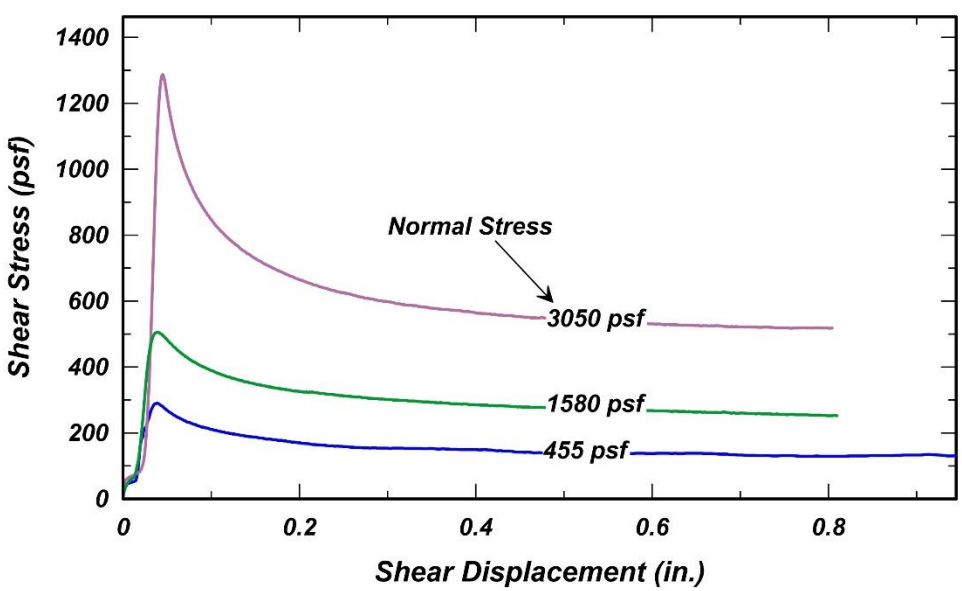

Figure 4-8. Shear stress versus displacement curves for three ring shear tests performed on samples from SR-5 at normal stresses of 455, 1,580 and 3,050 psf, respectively.

The fully softened and residual strengths from the six sites tested in this study are shown in Figure 4-9 for the full range of stresses considered, while results for stresses less than 3,200 psf in Figure 4-10. The individual test results are shown along with a power fit envelope. Table 1 in Appendix A summarizes the nonlinear fully softened and residual strength envelopes of the twelve collected samples.

There is scatter within each of the data sets, but some trends are visible. The data from I-65 has the lowest fully softened strength and residual strengths, followed by SR-5 and I-59. SR-22 and SR-219 have similar fully softened strengths to SR-5, but do not experience the same level of softening. The samples from US-231 stands out again as unique. At low stresses, (below 1,000 psf) US-231 has the highest fully softened and residual strengths. At higher stresses, the residual strength envelope becomes very curved as the soil undergoes significant softening and the residual strength becomes similar to the soils tested from I-59. This significant level of softening may explain some of the stability problems observed in similar soils in other regions.

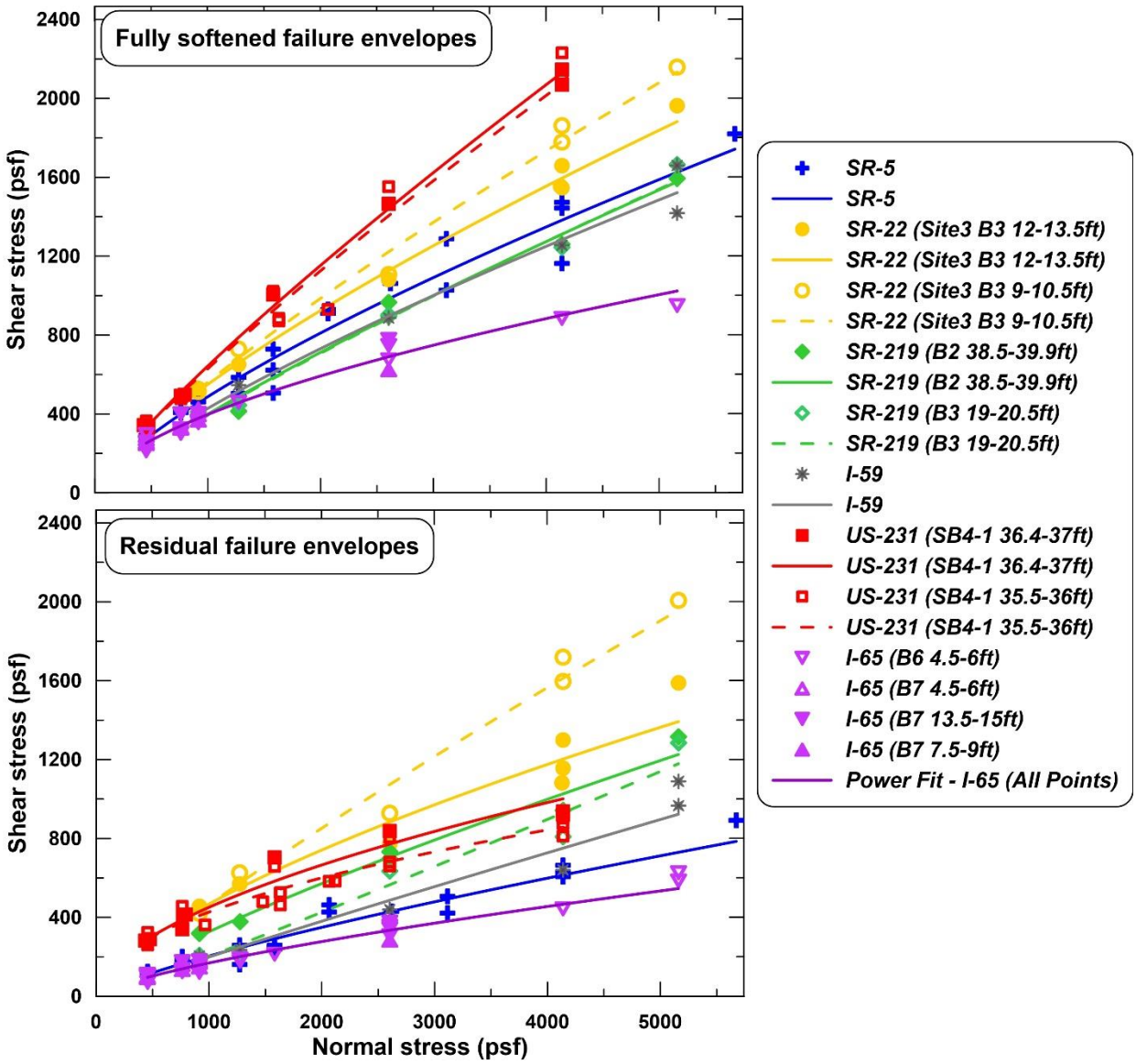

Figure 4-9. Saturated residual and fully softened shear strengths from ring shear tests performed on clay samples collected for this study over the full range of normal stresses.

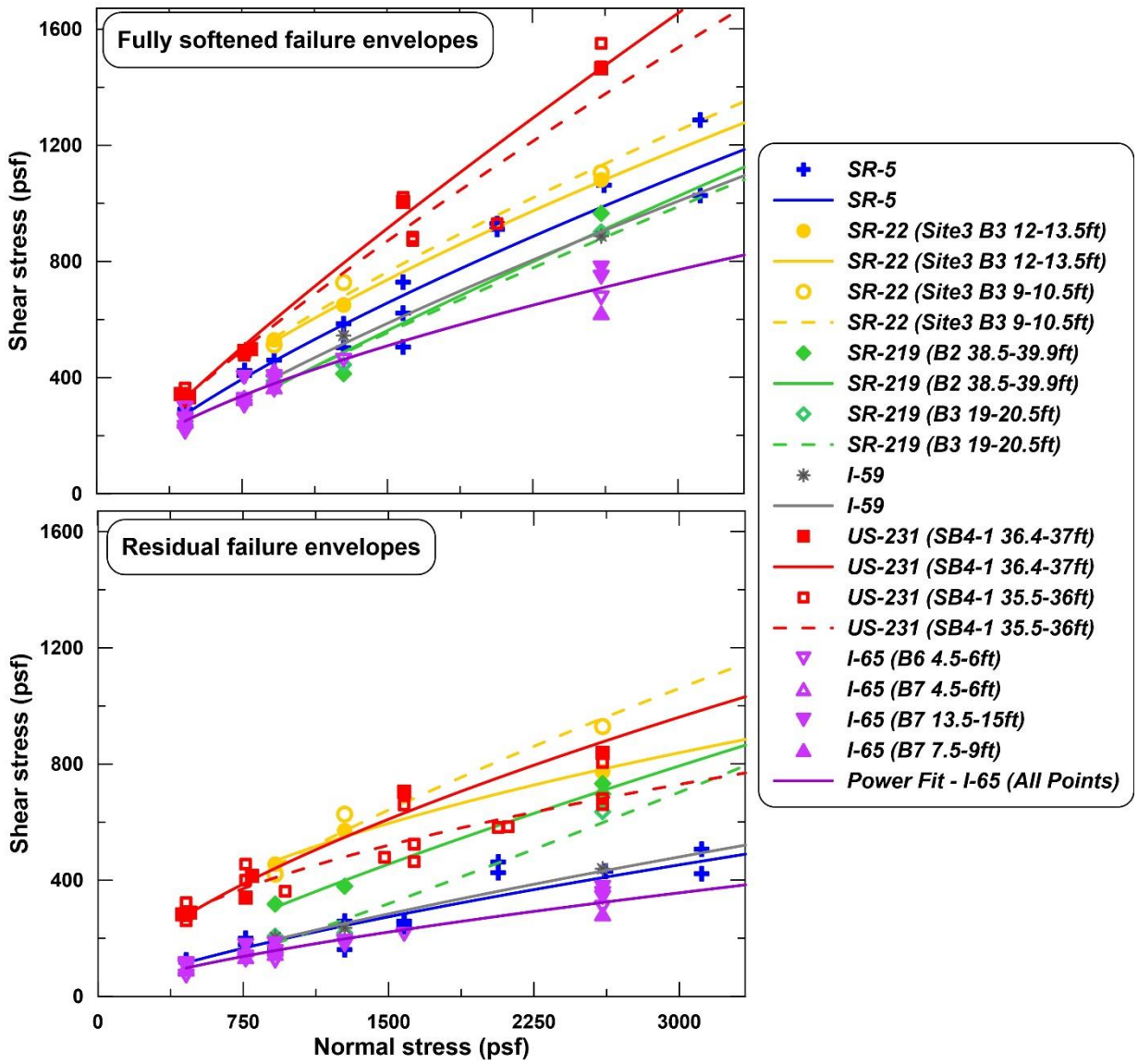

Figure 4-10. Saturated residual and fully softened shear strengths from ring shear tests performed on clay samples collected for this study for stresses less than 3,200 psf (approximately 153 kPa).

The strength envelopes for US-231 were quite different from the other samples, so a comparison was made with strength tests performed by Okagbue (1986) on a similar red shale from West Virginia (Figure 4-11). The index properties and XRD results of the soil tested by Okagbue (1986) is similar to the soils from US-231. Okagbue (1986) performed direct shear tests on intact samples of the shale collected from the interface between a spoil pile and natural ground.

The effective stresses used in the direct shear tests are not reported in the paper, but the slide plane was located at a depth of 15 – 30 feet in the central portion of the slide. The water table depth was also located at depth of approximately 15 feet in the analysis. This would suggest effective stresses between 1,000 and 2,500 psf would be a reasonable range for testing. The peak strength envelopes measured by Okagbue (1986) were higher than the fully softened envelope measured in this study, but this is expected as Okagbue (1986) tested intact instead of remolded specimens. The residual strength envelopes are also higher than those measured in this study, but the difference is not significant at stresses below 1,500 psf. It is interesting that the envelope used in the back-analysis of the landslide is in good agreement with the ring shear tests between 1,000 and 2,000 psf.

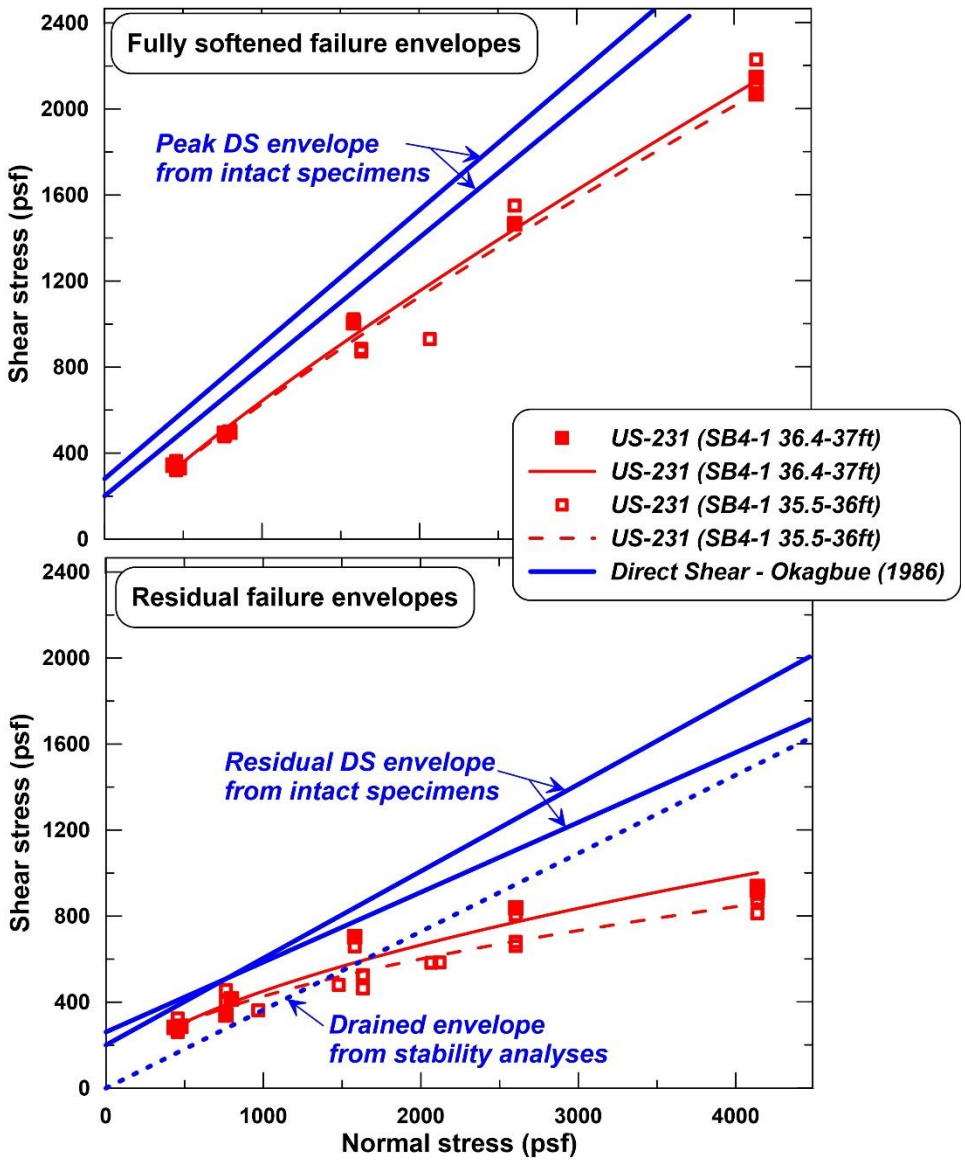

Figure 4-11. Saturated residual and fully softened shear strengths from ring shear tests performed on clay samples from US-231 compared with strength results from Okagbue (1986). Okagbue (1986) performed direct shear (DS) tests on two intact samples of red shale collected from a landslide site in West Virginia. The strength envelope used by Okagbue (1986) for back-analysis is also shown for comparison.

The comparison between the ring shear results and the strength envelopes from Okagbue (1986) highlight the need to consider stress-dependent strength envelopes for these soils. The true strength envelope is curved with a decreasing slope (i.e., friction angle) as effective stress

increases. Over a limited stress range this can be reasonably approximated as a straight line, but care must be taken to ensure that the strength tests are performed at similar effective stresses to those used in the analyses. The comparison of the strength envelopes in Figure 4-11 clearly demonstrates this. The linear envelope used for back-analysis by Okagbue (1986) would be a good match to the strength data measured in this study between 1,000 and 2,000 psf but would underestimate strengths at lower stresses and overestimate strengths at higher stresses. Using a nonlinear envelope like the power function shown in Figure 4-11 or a secant friction angle relationship would allow a single envelope to be used over a much wider range of stresses.

4.4.1 Statistical analysis of torsional ring shear results

A statistical analysis was performed to examine the variability of the test results obtained from repeated tests on the same soil sample and whether any test results were largely offset from the majority of the results. To ensure the reliability of the statistical results, repeated tests were conducted on SR-5 soil samples at ten normal stresses considering the constraints of time and economics. Statistics including mean, standard deviation, and 95% confidence interval and 95% prediction interval were calculated to examine the variability of the test results. To find any possible outlier results (Schoenemann and Pyles 1985), 95% confident interval and 95% prediction interval were determined as defined in Section 3.5. Figure 4-12 shows the 95% CI and 95 PI plotted along with SR-5 strength envelope.

The upper- and lower-lines region of the 95% CI indicates that 95% probability of the test results fall around the strength envelope, while any beyond it and within the 95% PI region were acceptable as variability of the tests. Any test results locate beyond the 95% PI are considered as outliers (as highlighted in Figure 4-12) due to the skewed measurement. The same outlier removal

process is conducted on the test results of each soil samples, the test results after removing any outliers are plotted with their fitted strength envelopes in Figure 4-9 and Figure 4-10.

R^2 were determined to evaluate the goodness of fit of each power fitted strength envelope. R^2 was transformed from the exponential model into a linear model by natural logarithm transformation and calculated using Equation (18). The power fitted strength in Figure 4-12 shows a good fit of the test results on SR-5 soil samples because its R^2 value of 0.9541 is above 0.80 (Cohen 2013). The equation of the power-fitted shear strength envelopes and their R^2 values of the other soil samples are summarized Table 1 in Appendix A. They all show a good fit of the test results due to high R^2 values obtained.

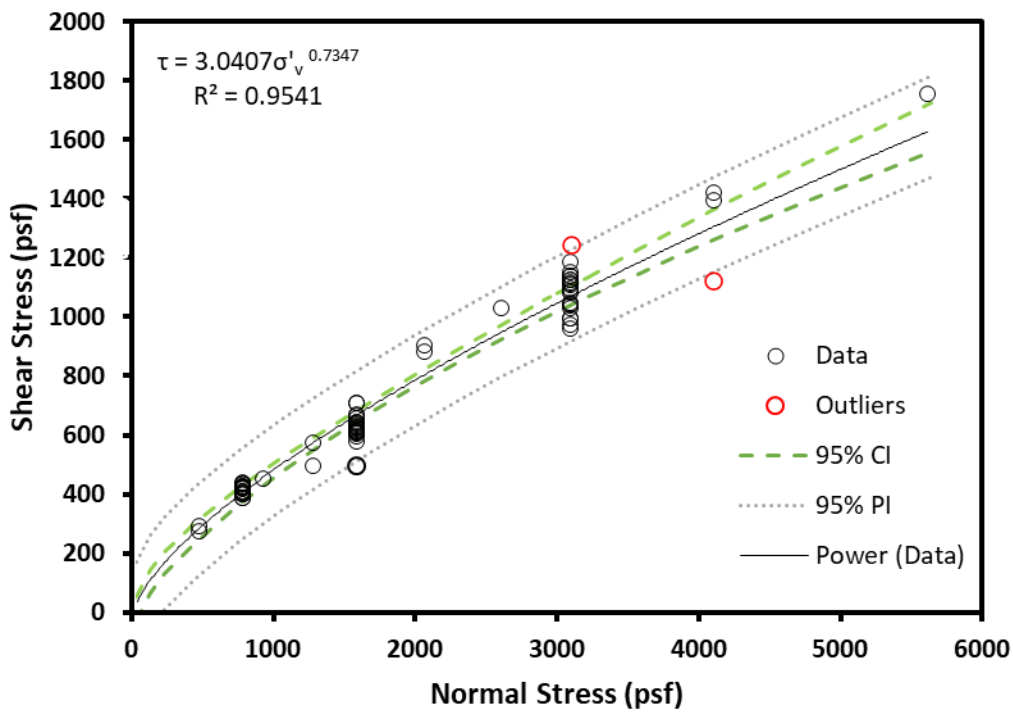

Figure 4-12. Repeatable tests on SR-5 soil of three normal stresses with the power fitted strength envelope and 95% CI and 95% PI

4.4.2 Comparison with existing correlations

The data presented in Figure 4-9 are only applicable to the sites and depths where measurements were conducted. To be applicable to other sites, correlations must be developed based on the properties of the samples. The database developed in this study is too limited to develop new correlations, but it is sufficient to examine previously developed correlations and to identify which would be most applicable to clays in Alabama.

As part of this study, a thorough literature review was performed to identify correlations for both fully softened and residual shear strengths that properly accounted for the curved strength envelopes observed in Figure 4-9. The data are compared separately with five correlations that relate the shear strength to soil index properties. Eight fully softened strength (FSS) correlations from Mesri and Shahien (2003) (upper, middle, and lower bound relationships), Wright (2005), Stark and Hussain (2013), Eid and Rabie (2017), Stark and Fernandez (2020), and Stark (2022) were selected for comparison. These are referred to as "FSS models" in the comparison figures (Figure 4-13 – Figure 4-15) between the data and models are made in terms of the secant friction angle at each stress level. Eight residual strength (RS) correlations from Mesri and Shahien (2003) (upper, middle, and lower bound relationships), Wright (2005), Stark and Hussain (2013), Eid et al. (2016) (CF and LL, and PI relationships), and Stark and Idries (2021) as implemented by Stark (2022) were selected and will be referred to as "RS models". Wright (2005), Eid et al. (2016), Eid and Rabie (2017), and Stark and Fernandez (2020) provided equations that correlated the strength of the soil to the clay fraction, LL, and/or PI as a function of effective stress. Wright (2005) uses equations developed by Stark (2005) for clay fractions less than 50% and so is listed as Wright/Stark (2005) in the comparisons. These equations were used to compute the model strength for each test considering the index properties and the stress level of the test. Stark (2022) provides

a spreadsheet that correlates the power function parameters to the liquid limit and clay fraction of the soil and these parameters were used to calculate strengths at each stress level. Stark and Hussain (2013) and Mesri and Shahien (2003) provide relationships that estimate the strength at discrete stress levels, so a power function was fit to the individual points from each of these correlations in order to develop strength estimates over the full range of stresses tested in this study. A separate power function was fit for each correlation and each soil sample due to differences in the index properties.

The data and models were compared by calculating residuals based on the measured and predicted secant friction angles (Residual = $[\phi'_{sec}]_{data} - [\phi'_{sec}]_{model}$). The secant friction angle was computed by taking the inverse tangent of the shear strength divided by the normal stress for each test. Using this definition, a negative residual indicates that the model (correlation) is overpredicting the strength relative to the measurements. Summaries of the root mean square (RMS) residual and average residual for the FSS models are shown in Table 4-8 and for the RS models in Table 4-9. Based on the overall results, thresholds of 3.0 degrees for the RMS residual and $\pm$1.5 degrees for the average residual were selected to define good agreement. The models meeting both of these criteria are highlighted in the tables. The residuals are computed as the difference between the secant friction angle measured in the experiment and the secant friction angle predicted by the model. The root mean square (RMS) residual and average residual are computed for each model. A negative average residual indicates the model is overpredicting the strength. Models with an RMS residual less than 3.5 degrees and an average residual less than $\pm$1.5 degrees are highlighted.

For the FSS strengths, almost all of the models are overpredicting strengths for SR-22, SR-219, and I-59. Stark and Idries (2021) is the closest fit for these sites, but still overpredicts by an

average of 3 – 9 degrees except for the shallower SR-22 sample, which is well fit. For the other sites, Stark (2022), Stark and Hussain (2013), Wright/Stark (2005), and the lower bound of Mesri and Shahien (2003) also provide the best agreement with the average difference being less than two degrees for most of the sites. This level of agreement is well within the scatter of the data.

For the residual strengths, most of the models are also overpredicting the measured strengths for SR-219, I-59, and US-231. Wright/Stark (2005) is the closest for these three sites, but there is significant scatter. For the other sites, Stark (2022), the LL-based relationship from Eid et al. (2016), Stark and Hussain (2013) and Wright/Stark (2005) provided the best fit, but the level of agreement is a little worse than it was for the FSS strengths. The lower bound relationship from Mesri and Shahien (2003) is also in reasonable agreement, but tends to underestimate RS.

Table 4-8. Comparisons between the fully softened shear strength data and models.

Site	Boring	Depth Range (ft)	Mesri and Shahien (2003) - Upper		Mesri and Shahien (2003) - Middle		Mesri and Shahien (2003) - Lower		Wright/Stark (2005)	
			RMS Residual	Average Residual	RMS Residual	Average Residual	RMS Residual	Average Residual	RMS Residual	Average Residual
SR-5	B-5.5A	1-7	6.28	-5.21	3.98	-2.52	2.78	-0.53	3.06	-0.34
SR-22	B-3	12-13.5	10.91	-10.42	6.75	-6.32	4.43	-3.87	5.36	-5.04
SR-22	B-3	9-10.5	7.89	-7.49	4.22	-3.77	1.95	-1.09	3.29	-2.91
SR-219	B-2	38.5-39.9	14.43	-14.25	10.61	-10.46	6.83	-6.42	9.81	-9.67
SR-219	B-3	19-20.5	13.52	-13.43	9.84	-9.78	7.40	-7.32	7.60	-7.53
I-59	B-1	33.5-35	13.16	-12.95	9.24	-9.08	6.86	-6.71	5.49	-5.33
US-231	SB4-1	35.5-36	4.47	-2.80	2.47	0.22	4.15	2.59	1.97	1.17
US-231	SB4-1	36.4-37	4.48	-2.49	2.78	0.28	4.37	2.83	2.60	1.00
I-65	B-6	4.5-6	10.05	-9.27	7.42	-6.62	5.62	-4.94	4.28	-2.87
I-65	B-7	4.5-6	4.88	-4.41	2.95	-2.25	1.88	-0.74	2.06	0.81
I-65	B-7	7.5-9	7.18	-6.03	5.10	-3.83	3.63	-2.02	3.28	0.06
I-65	B-7	13.5-15	11.43	-10.94	8.82	-8.32	6.86	-6.38	4.95	-4.06

Site	Boring	Depth Range (ft)	Stark and Hussein (2013)		Eid and Rabie (2017)		Stark and Fernandez (2020)		Stark (2022) - LL	
			RMS Residual	Average Residual	RMS Residual	RMS Residual	Average Residual	Average Residual	RMS Residual	Average Residual
SR-5	B-5.5A	1-7	2.61	-0.16	3.67	-1.73	3.18	-0.97	3.26	1.41
SR-22	B-3	12-13.5	5.24	-4.92	7.05	-6.54	5.29	-4.73	4.99	-4.37
SR-22	B-3	9-10.5	3.20	-2.83	4.26	-3.71	2.57	-1.79	1.92	0.54
SR-219	B-2	38.5-39.9	9.73	-9.59	10.64	-10.46	8.82	-8.64	9.07	-8.89
SR-219	B-3	19-20.5	6.37	-6.27	10.47	-10.38	8.63	-8.54	5.34	-5.23
I-59	B-1	33.5-35	4.62	-4.50	9.38	-9.19	7.43	-7.25	3.55	-3.29
US-231	SB4-1	35.5-36	2.00	1.24	2.66	0.35	2.83	1.65	3.44	2.57
US-231	SB4-1	36.4-37	2.40	0.74	3.06	0.44	3.30	1.81	3.56	2.19
I-65	B-6	4.5-6	3.96	-3.08	6.93	-6.01	6.32	-5.49	3.44	-1.50
I-65	B-7	4.5-6	1.60	0.08	2.45	-1.49	2.14	-1.10	2.85	2.22
I-65	B-7	7.5-9	2.73	-0.36	4.70	-3.13	4.05	-2.41	3.49	1.51
I-65	B-7	13.5-15	5.23	-4.65	8.19	-7.60	7.40	-6.84	3.80	-2.58

Table 4-9. Comparisons between the residual shear strength data and models.

Site	Boring	Depth Range (ft)	Mesri and Shahien (2003) - Upper		Mesri and Shahien (2003) - Middle		Mesri and Shahien (2003) - Lower		Wright/Stark (2005)	
			RMS Residual	Average Residual	RMS Residual	Average Residual	RMS Residual	Average Residual	RMS Residual	Average Residual
SR-5	B-5.5A	1-7	4.24	-3.83	1.76	-0.51	2.07	0.99	2.14	-1.06
SR-22	B-3	12-13.5	8.59	-7.52	4.06	-1.80	4.15	1.62	2.91	-1.42
SR-22	B-3	9-10.5	2.64	-1.70	4.36	4.03	7.53	7.30	3.13	2.73
SR-219	B-2	38.5-39.9	11.68	-11.65	4.49	-4.30	1.71	-0.88	5.64	-5.59
SR-219	B-3	19-20.5	11.59	-11.38	6.40	-5.85	3.67	-2.80	3.31	2.98
I-59	B-1	33.5-35	11.95	-11.89	7.70	-7.55	4.58	-4.39	3.20	-2.94
US-231	SB4-1	35.5-36	8.11	-5.32	6.65	0.17	8.01	3.92	4.73	-0.17
US-231	SB4-1	36.4-37	9.00	-5.69	7.03	-0.55	7.87	3.07	5.36	0.52
I-65	B-6	4.5-6	3.18	-5.38	2.78	-2.50	1.60	-0.63	1.51	-0.56
I-65	B-7	4.5-6	4.26	-4.22	1.37	-1.23	1.25	1.07	0.63	0.07
I-65	B-7	7.5-9	5.45	-5.29	5.45	-5.29	1.49	0.34	1.44	0.29
I-65	B-7	13.5-15	6.98	-6.94	3.60	-3.57	2.01	-1.84	1.54	-1.33

Site	Boring	Depth Range (ft)	Stark and Hussein (2013)		Eid et al. (2016) - LL		Eid et al. (2016) - PI		Stark (2022) - LL	
			RMS Residual	Average Residual	RMS Residual	RMS Residual	Average Residual	Average Residual	RMS Residual	Average Residual
SR-5	B-5.5A	1-7	1.99	-1.21	1.98	-1.10	1.90	-0.83	1.97	-1.18
SR-22	B-3	12-13.5	4.57	-3.74	4.93	-3.18	4.77	-3.00	4.03	-2.96
SR-22	B-3	9-10.5	1.58	0.44	2.20	1.12	3.31	2.78	1.96	1.26
SR-219	B-2	38.5-39.9	7.89	-7.85	7.13	-6.96	5.70	-5.51	7.09	-7.05
SR-219	B-3	19-20.5	6.29	-5.76	2.82	2.13	8.67	-8.45	6.24	-5.71
I-59	B-1	33.5-35	3.99	-3.63	8.99	8.90	7.65	-7.55	3.98	-3.62
US-231	SB4-1	35.5-36	5.41	-2.30	6.70	-0.13	6.78	-0.91	5.25	-1.38
US-231	SB4-1	36.4-37	6.93	-4.08	7.48	-1.98	7.35	-1.69	6.57	-3.17
I-65	B-6	4.5-6	1.50	-0.90	1.54	-0.86	3.02	-2.75	1.48	-0.86
I-65	B-7	4.5-6	0.89	-0.65	0.69	-0.35	1.77	-1.67	0.84	-0.57
I-65	B-7	7.5-9	1.04	-0.08	1.17	0.05	2.71	-2.43	1.05	-0.01
I-65	B-7	13.5-15	2.09	-2.06	1.64	-1.51	3.99	-3.95	1.52	-1.44

From the results shown in Table 4-8 and Table 4-9, the lower bound relationships from Mesri and Shahein (2003), the relationships from Wright (2005) with the additional equations from Stark (2005) and the LL-based relationship from Stark (2022) were selected for further examination. These relationships were selected as they provide both fully softened and residual strength estimates and had some of the lowest residuals across the range of sites. To examine potential bias in the results, residuals from the three best correlations were plotted versus effective stress and liquid limit, which serves as an input for all three models. The results are shown in Figure 4-13 – Figure 4-15. These figures show that all three models overestimate the fully softened strengths for SR-219, SR-22, and I-59 regardless of stress level. This does create a bias within the residuals with respect to the liquid limit. The residuals also show a bias with respect to effective stress with the models tending to underpredict the strength at low effective stresses and overpredict strength at higher stresses. This is more apparent for the fully softened strengths than for the residual strengths. It is worth noting that the databases used to develope the above correlation models for soil strengths were primarily created based on results from west of the Mississippi regions. These databases include a variety of soil types and conditions, but it may not fully represent the characteristics of soils from other areas, particularly those tested clay soils with distinct geological histories such as Alabama.

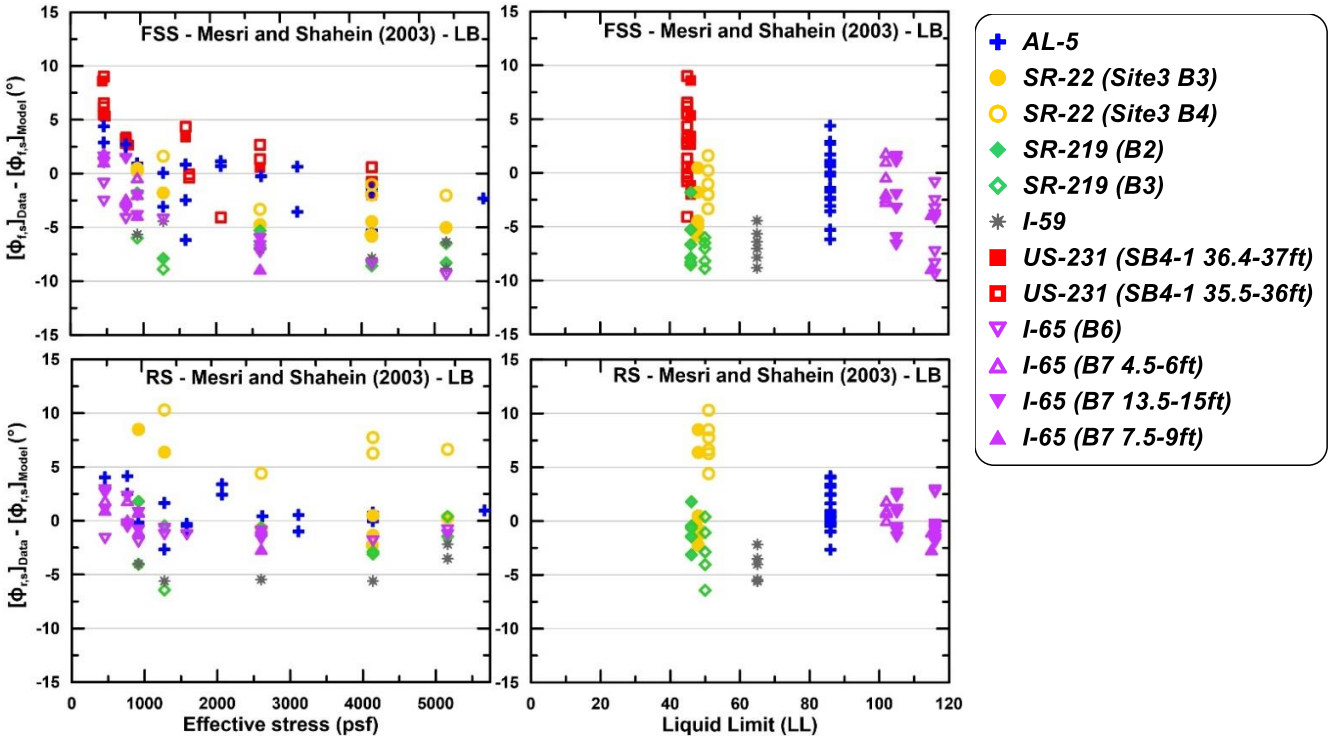

Figure 4-13. Residuals (data – model) for fully softened and residual secant friction angles predicted by the lower bound relationship from Mesri and Shahein (2003).

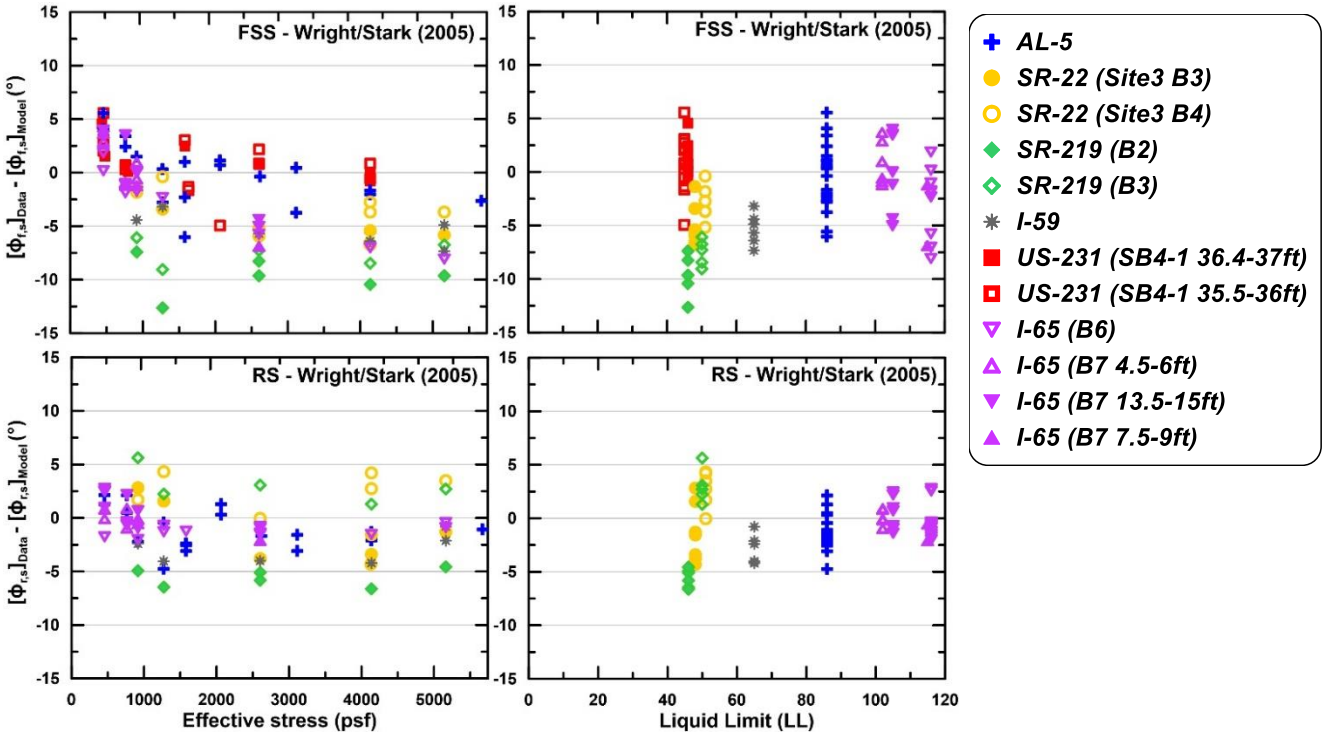

Figure 4-14. Residuals (data – model) for fully softened and residual secant friction angles predicted by the relationships from Wright (2005), which include equations from Stark (2005).

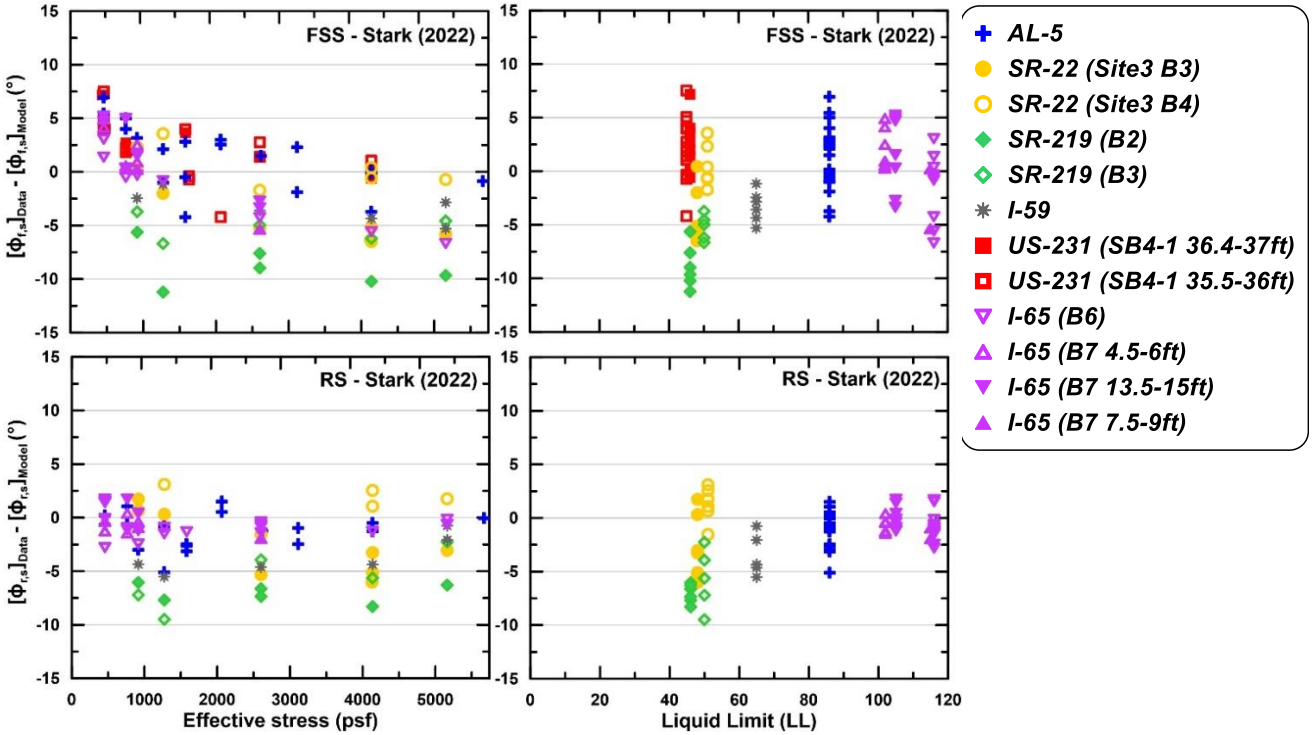

Figure 4-15. Residuals (data – model) for fully softened and residual secant friction angles predicted by the spreadsheet provided by Stark (2022).

The residual strength for US-231 was not fit well by any of the correlations due to the large curvature in the envelope (Figure 4-14). This unique behavior is believed to be a function on the mineralogy of this soil and similar soils (i.e., degraded illites from Ohio, Pennsylvania, West Virginia, Alabama) do not appear to have been included in previous databases used to develop these correlations. This study is believed to be the only one to perform ring shear tests on these soils, so there is some uncertainty in the strength characterization. Wu et al. (1987) examined stability of slopes with red Round Knob and Connesville shales in eastern Ohio and performed direct shear tests on samples with slickensides to obtain the residual strength. These shales have LLs between 30 and 48 and PIs between 10 and 22 (Wu et al. 1993), which covers the range observed at US-231. Wu et al. found that using a residual friction angle of 14 degrees provided a reasonable fit to their tests. This is lower than the 22 degrees determined by Okagbue (1986), but

Okagbue was focused on shallower slides and the friction angle is expected to increase at lower effective stresses. The results from the direct shear tests are compared with the ring shear results from this study in Figure 4-16. The tests are in very good agreement for stress levels between 2,000 psf and 4,000 psf showing a more linear envelope. Overall, these results give additional confidence in the evaluation of the measured results from US-231, which largely fall between the friction angles estimated in previous studies.

As the measured results from US-231 are in reasonable agreement with the tests from Wu et al. (1987), an effort was made to determine how the correlations from Stark (2022) might be modified to fit the US 231 data. The curvature of the envelope for US-231 is outside the bounds of the database examined by Stark and Idries (2021), so two curves were fit to provide bounds on the measured data. The first curve uses the LL of the site and the measured clay fraction (40.9%), while the second curve uses a LL of 90 to provide a lower bound on the data. Both curves are shown for residual and fully softened strengths in Figure 4-16. The fully softened curve using the true material properties provides a good fit to the measured data, while the curve using a LL of 90 underestimates the measured strengths. For the residual strengths, the two curves provide excellent bounds for the data from US-231 and the strength envelopes from Okagbue (1986) and Wu et al. (1987). Additional data is needed to determine if new correlations should be developed to fit soils similar to those found at US-231, but the residual strength bounds shown in Figure 4-16 should be reasonable to use for stability analyses in similar soils.

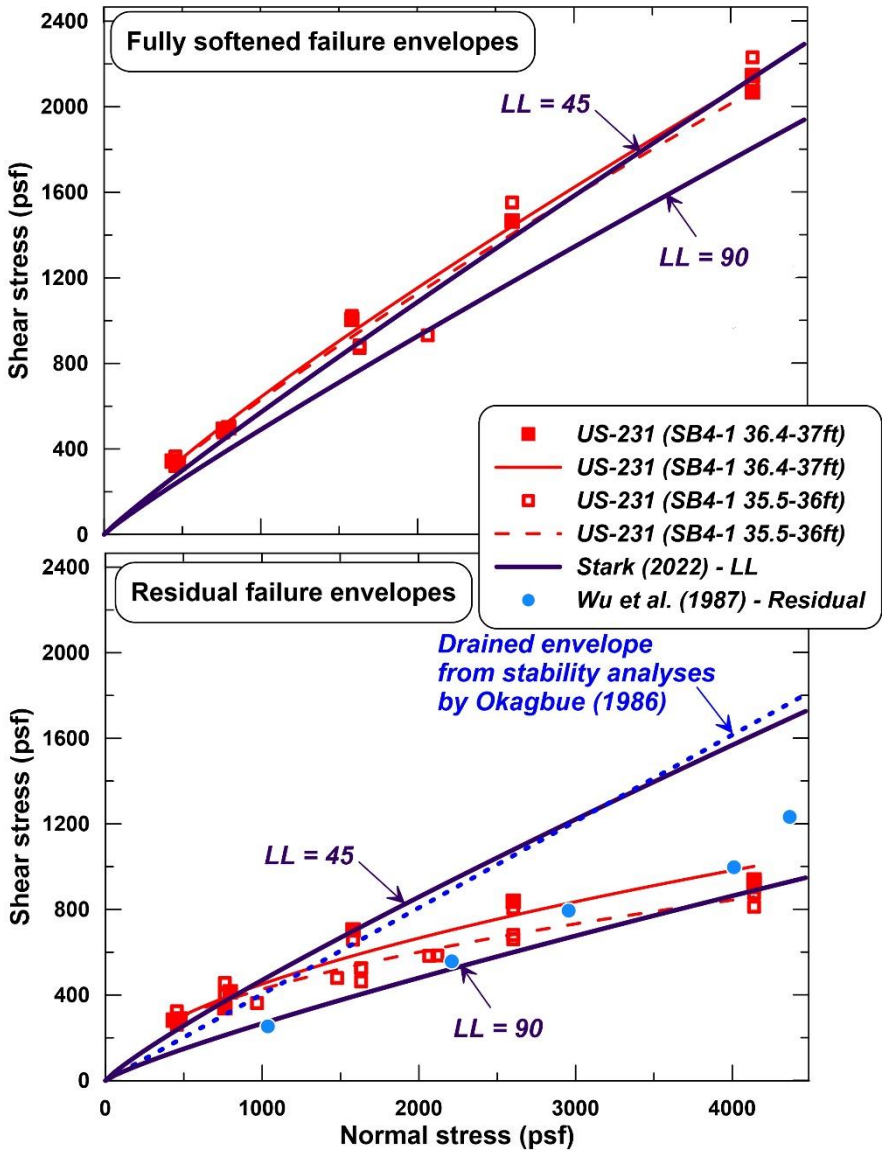

Figure 4-16. Comparison of fully softened and residual strength envelopes measured at US-231 with envelopes predicted by the spreadsheet provided by Stark (2022) and used by Okagbue (1986) for back analysis of a slope failure in similar soils. Direct shear results by Wu et al. (1987) from slickensides found within red shale deposits in western Ohio are shown for comparison.

CHAPTER 5: APPLICATION OF STRENGTH RESULTS TO SLOPE STABILITY ANALYSES

5.1 Introduction

The applicability of the FSS (Fully Softened Shear) and RS (Residual Strength) envelopes, developed in the preceding section with ring shear testing, was demonstrated through slope stability analyses conducted for two specific sites: SR-5 and US-231. These sites were chosen to represent distinct scenarios - SR-5, a location devoid of slope failures, and US-231, a site marked by a significant slope failure. The objective was to assess the ability of these strength envelopes to differentiate between these scenarios, crucial for their prospective application in future analyses. Additional analyses were carried out for I-65 by Kiernan (2021), incorporating both linear and nonlinear strength envelopes. The purpose was to emphasize situations where the consideration of nonlinear envelopes becomes pivotal. The evaluation commenced with an exploration of fully softened drained shear strength to ascertain the possibility of initial failure under drained conditions. Subsequently, peak undrained shear strengths were examined to investigate the likelihood of an initial undrained failure. The stability of the slope on an existing shear surface was then estimated through an examination of residual drained strengths.

The slope stability analyses were conducted utilizing limit equilibrium analyses in SLIDE2 (Rocscience 2021), considering both circular and noncircular surfaces. Critical circular surfaces were determined using an auto-refined search method, while critical noncircular surfaces were identified using an iterative Cuckoo search algorithm. The iterative Cuckoo search algorithm significantly enhanced slope stability analysis when integrated with SLIDE2 software providing detailed stability assessments based on input soil properties and slope geometry. The iterative

Cuckoo search algorithm located critical non-circular slip surfaces with initial number of surface vertices and number of surfaces to store Rocscience (2020). It was able to locate the critical failure surface higher success rate as well as accuracy and lower computation time than Simulated Annealing originally implemented to solve the exact same problem. This process allowed an additional optimization to the minimum safety factor surface generated by the Cuckoo Search and usually results in a lower safety factor. For further optimization of the critical failure surface, a refined surface with the lowest factor of safety given a slope geometry could be found.

The Factor of Safety (FS) values reported for these analyses were calculated employing Spencer's method. The safety of factor was calculated by limiting the equilibrium of the stability of slopes by calculating the factor of safety against sliding. The slope was analyzed by being divided into a series of slices, and the equilibrium was analyzed for each slice individually. Both force and moment equilibrium equations were used to determine the critical factor of safety by assuming a circular failure surface and calculate the shear forces and normal forces acting along this surface, accounting for both the driving forces (such as gravity) and resisting forces (such as shear strength of the soil). Nonlinear drained strength envelopes were depicted using the power curve option within SLIDE2 (Rocscience 2020). Linear envelopes were represented through the Mohr-Coulomb option, and undrained strengths were captured using the vertical stress ratio feature in SLIDE2. These detailed analyses aimed to shed light on the complexities of slope stability under varying conditions and envelope types.

5.2 Slope stability for SR-5 site

Slope stability analyses were performed to determine the likelihood of slope failure along the analyzed section of SR-5. The research site for this study is located west of Selma, AL in Perry

County (Figure 5-1). The highway in this area is generally flat with the surrounding land consisting of wooded areas and farms. Other areas of this highway (SR-5) with similar soils have experienced slope failures in the past, such as a failure that led to the placement of rockfill berm on an embankment approximately five miles south of the project site. Stallings (2016) observed cracking along the shoulders of the roadway within the study area that was not clearly attributed to swelling and some rutting and bulging was observed along the embankment face. The combination of cracking and bulging led to the hypothesis that slope movements might be occurring within the study area. Jackson (2016) measured moisture contents and suction values beneath the roadway and found that suction has been present during the duration of the study period (November 2016 – December 2019) and much of the embankment and foundation was saturated, but negative pore pressures were observed in the embankment.

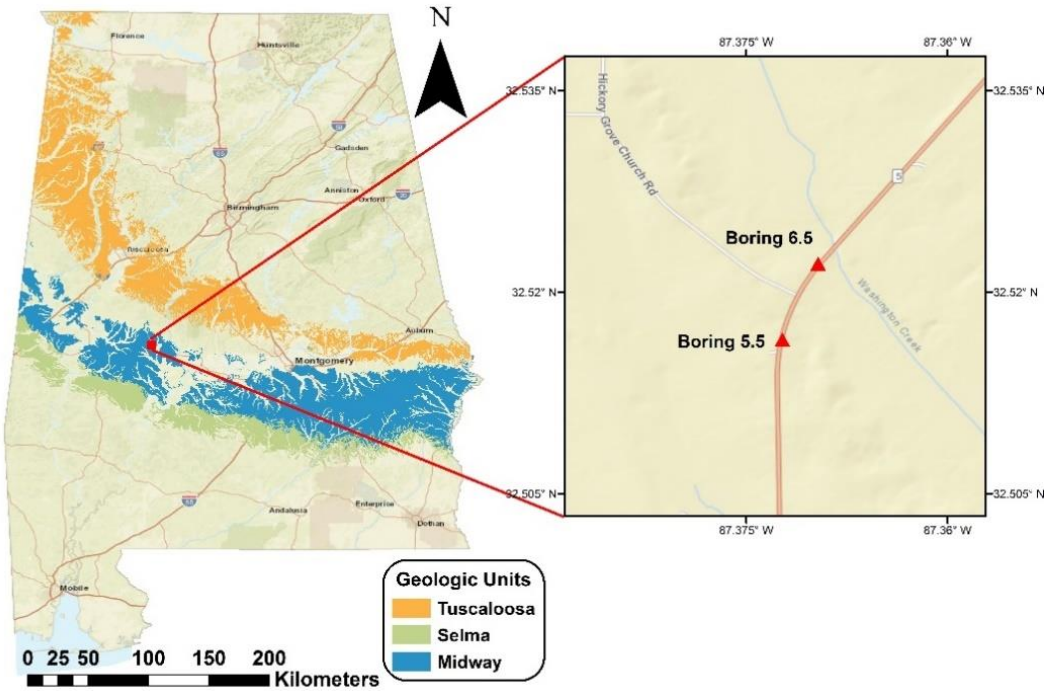

Figure 5-1. Locations of geologic units containing the high plasticity Prairie clays (after Szabo et al. 1988) and the location of the research site and borings examined in the current study.

Analyses were performed using the limit equilibrium slope stability software Slide published by Rocscience (Rocscience 2020). The cross-section near Boring 5.5 was used for the analyses (Figure 5-2) and the soil profiles were obtained from boring logs (Herman 2015, Stallings 2016). The embankment in this area is approximately 5 feet tall and the pavement is relatively thick (1 ft) due to many years of repaving to repair damage from swelling clays (Figure 5-2). The water table (indicated as the blue dashed line with triangles) was placed 2.3 ft lower than the embankment for these analyses based on in-situ measurements and field observations. The strength envelopes developed from the ring shear data (Figure 5-3 and Table 5-1) were used to represent the clay embankment and foundation. Strength data for foundation material was the same as embankment. The intact chalk layer (located approximately 6.5 ft below the embankment) was not included in the stability analyses, but no failure surfaces extended to more than 3.3 ft into the foundation. The properties for the pavement (γ = 145 pcf, ϕ = 34°, c = 7700 psf) were based on the lower bound of the triaxial test results presented by Christensen et al. (2000) and the densities of the embankment and the foundation were based on tests performed by Stallings (2016).

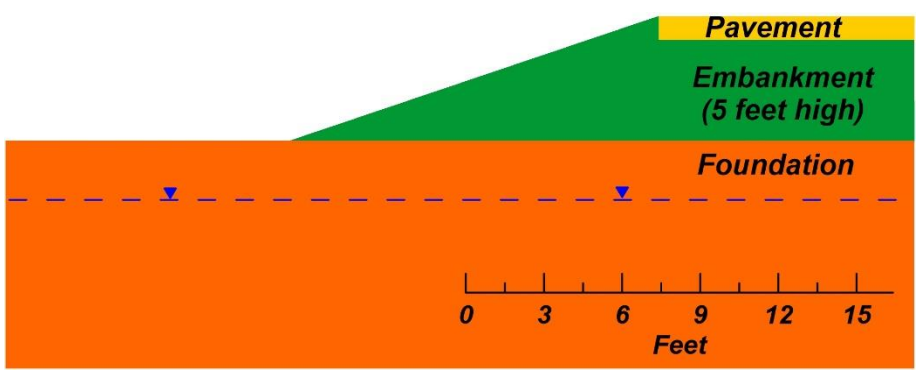

Figure 5-2. Cross-section of SR-5 at borehole B5.5. The dashed line shows the depth of the water table in the analysis.

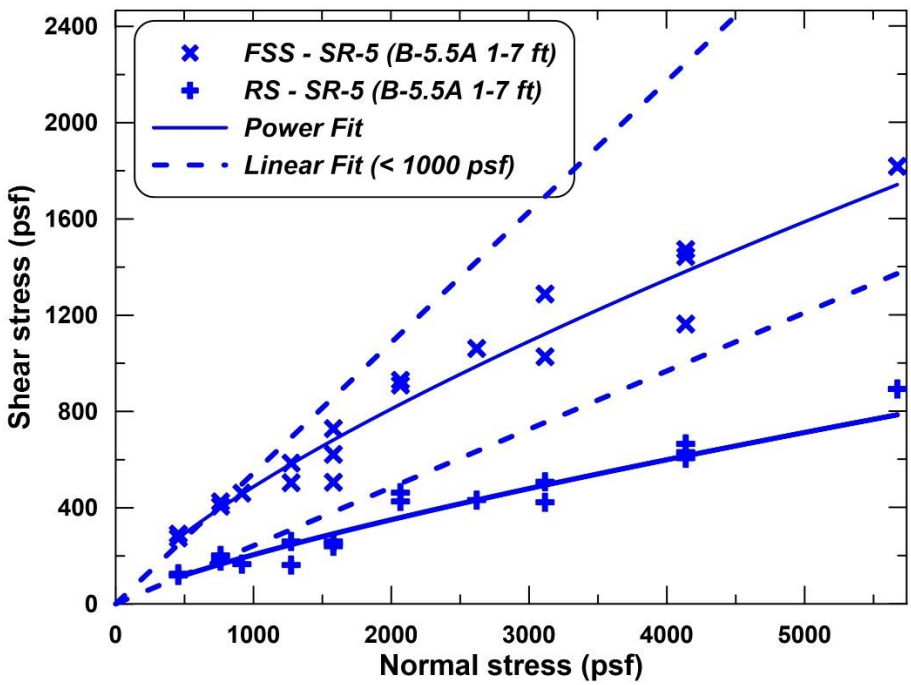

Figure 5-3. Fully softened (FSS) and residual strength (RS) envelopes for SR-5 at borehole B5.5 using both linear fits to data with a normal stress less than 1,000 psf and power fits.

Table 5-1. Saturated shear strength envelopes for SR-5.

Envelope Types	Strength Envelope (kPa)	R^2
Residual Strength – Linear Fit	$\tau = \sigma' \cdot \tan(13.6°)$	0.98
Residual Strength – Power Fit	$\tau = 0.173 \cdot P_a \left(\frac{\sigma'}{P_a}\right)^{0.75}$	0.88
Fully Softened Strength – Linear Fit	$\tau = \sigma' \cdot \tan(28.5°)$	0.99
Fully Softened Strength – Power Fit	$\tau = 0.407 \cdot P_a \left(\frac{\sigma'}{P_a}\right)^{0.79}$	0.93

The results of the slope stability analyses are shown in Table 5-2. The critical surface for both linear envelopes without suction is very shallow and approximates an infinite slope failure condition. This is not surprising as an infinite slope failure is often the critical case for dry frictional materials. The slope angle of the embankment is approximately 20 degrees and so the fully softened friction angle gives adequate stability, while the residual strength friction angle shows instability would be expected for an infinite slope failure. The analyses for the residual envelope

were re-run with a minimum slice depth of 1.6 ft to examine the stability against larger failures (Figure 5-4). These results still show a factor of safety below 1.0 indicating that larger failures may be expected if these residual strengths are mobilized, and the effects of suction are removed. The fully softened results, which would be used for first-time slides, indicate that adequate stability would be expected even without suction, so a failure would need to be initiated by some external loading or a significant change in the water table in order to mobilize the residual strengths.

Table 5-2. Summary of minimum factors of safety for the different strength envelopes.

	Factor of Safety			
	Fully Softened Strength - Linear fit (28.5°)	**Fully Softened Strength - Power fit**	**Residual Strength - Linear fit (13.6°)**	**Residual Strength - Power fit**
No suction	1.629	2.344	0.726	1.117
No suction – 1.6 ft minimum depth	1.819	2.344	0.810	1.117
With suction	3.320	-	1.480	-

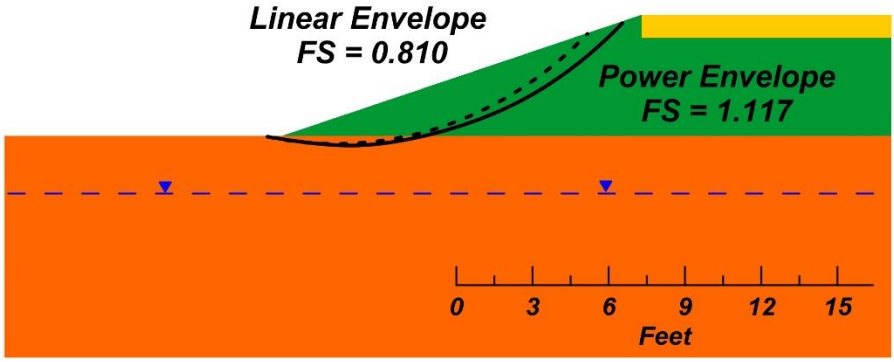

Figure 5-4. Critical failure surfaces for the linear and power fit residual strength envelopes. Similar surfaces were found for the fully softened strengths.

Using the power envelope increases the factors of safety for both strength cases compared with the linear fits. The critical failure surface using the power envelope is similar to the linear case with the minimum depth constraint (Figure 5-4). This difference in factor of safety is due to the higher strengths at very low stresses using the power fit compared with the linear fit. The two envelopes become equal at approximately 500 psf (Figure 5-3) and below this stress level the

power envelope gives higher strengths. The differences in the envelopes do not appear to be significant in Figure 5-3, but the effect on the minimum factor of safety is significant, even when considering a minimum depth constraint with the linear envelope. It is important for future studies to recognize that even seemingly small differences in these envelopes can have a significant effect on the results for shallow failures.

Xuan et al. (2021) also explored the effects of suction on the results of these analyses. The details of this analysis are described in the paper, but the results are shown in Table 5-2. Including suction with the linear envelope results in a large increase in the factor of safety as the critical failure surface is pushed farther into the foundation. The factors of safety for the linear envelope with suction are also larger than the results using power fit envelope. This demonstrates the importance of considering reasonable suction profiles when analyzing slopes located above the water table. While designers of new slopes may neglect suction values to avoid relying on them for stability, when analyzing existing slopes, it is important to consider suction conditions as they are likely to exist in the field. For this section of embankment, the stability results do not suggest large failures are likely to occur even if suction is lost.

The results show that under current conditions, both fully softened and residual strength envelopes would indicate stability (factors of safety larger than 1.0) except for the case of a linear residual strength envelope without suction. The linear residual strength envelope indicated that shallow failures would be expected to develop without the effects of suction, but the consideration of suction or the nonlinear envelope removes this concern. This study demonstrates that seemingly small differences in strength envelopes (Figure 5-3) can have a significant effect on the factor of safety for shallow failure surfaces. Neglecting both suction and curvature of the strength envelope could lead to a conclusion that this slope is at risk for failure. This conclusion is at odds with

observations at the site and could lead to unnecessary repairs being performed to address stability problems that are unlikely to occur. The consideration of suction or nonlinear strength envelopes indicates the slopes will remain stable even if residual strengths are mobilized.

5.3 Stability analyses for US-231 site

Stability analyses were also performed for a large landslide that occurred on US-231 near Lacey's Spring, AL on February 13, 2020 following a period of heavy rainfall. The section of highway is a heavily used corridor for Huntsville commuters and closures due to the slide added 30 to 60 minutes to commute times for local residents. This section of highway was likely constructed on an ancient landslide and had a history of movement. Following heavy rain in February 2019, ALDOT drilled five borings and installed inclinometers to monitor slope movement. The rate of movement increased following large storms in December 2019 and culminated in the failure of both north and southbound roadway lanes on February 13th (Figure 5-5). On February 14th, Auburn researchers and ALDOT personnel met on the site and seismic and resistivity tests (Figure 5-6) were performed the following week to better understand the stratigraphy and plan for a larger exploration program. The consulting firm Dan Brown and Associates was brought in to assist with the full investigation and design the repair (two bridges with large diameter drilled shaft foundation). The geophysical investigations are described by Montgomery et al. (2021) and the repair is described by Thompson and Dapp (2021).

Borings performed at the site generally show an upper layer of interbedded sand and clay or sandstone and clay, followed by an interbedded clay, mudstone and limestone. The majority of the site is located within the outcrop area of the Pennington Formation, which consists of medium-gray shale, containing interbedded limestone, dolomite, argillaceous sandstone, mudstone, and

minor shaly coal (Szabo et al. 1988). Interbedded mudstone and limestone were encountered in all borings at elevations ranging from about 1082 feet to 1087 feet. Above Pennington Formation bedrock, borings showed a mix of fill and colluvium, although it was difficult to identify a clear boundary between these. The inclinometers showed movements were primarily to the north – northwest and at elevations of about 1090-1086 feet in B-2 and about 1094-1088 feet in B-3.

Results from geophysical methods and borings were integrated to identify the stratigraphy at the site. The upper 30 feet of material under both roadways was identified as fill material and colluvium (alternating sandstone and clay), while a low resistivity, low velocity zone was found at depths of 30 – 40 feet below the road. Below this layer interbedded limestone and mudstone was observed. Based on these observations and the inclinometer data, the likely source of the slide plane was a plastic clay layer found between 30 and 40 feet. Subsequent investigations were able to confirm this layer as the critical zone and characterize the underlying rock for repair design.

Figure 5-5. View of the slide area along US-231 after removal of the pavement. The geophysical survey team can be seen along the SB shoulder on the left side of the figure.

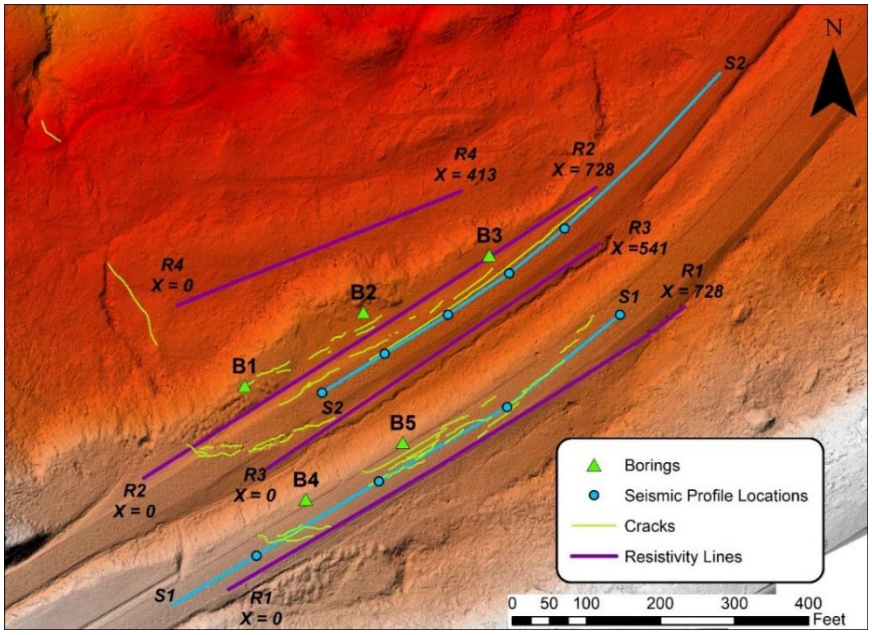

Figure 5-6. Map of the US-231 landslide showing approximate geophysical survey locations along with cracks mapped from UAV images and borings completed by ALDOT. A shaded relief map derived from UAV-based LiDAR collected after the landslide occurred is shown in the background.

Stability analyses were performed using a cross-section (Figure 5-7) through the original roadway near borings B2 and B-5 (Figure 5-6). The tested soil samples were collected from boring SB4-1, which was between B-2 and B-5. The roadway fill was a mix of sandstone and clay and was modeled with a friction angle of 35 degrees and a minor cohesion of 100 psf. The bedrock was considered to be strong and no failure surfaces intercepted the bedrock. The foundation was modeled using the residual strength envelopes shown in Figure 4-16. The power fit for the depth of 35.5 to 36 feet measured in this study was considered along with the two linear envelopes from Wu et al. (1987) and Okagbue (1986), which fit the data from this study at higher and lower stresses, respectively. It is believed that this landslide was due to reactivation of an existing slide plane, so residual strengths are the most accurate to use, but the power fit from the fully softened data was considered as well. The equations for these envelopes are shown in Table 5-3.

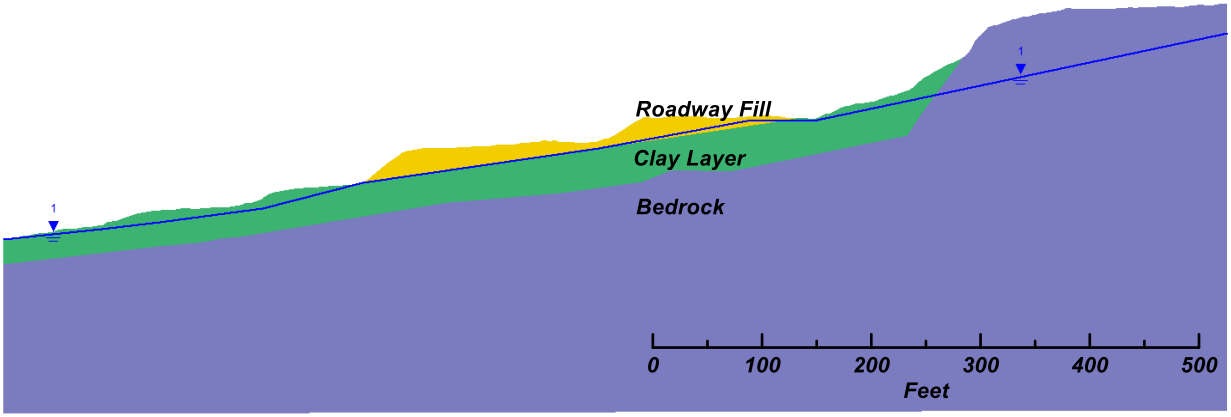

Figure 5-7. Analysis cross-section for US-231.

Table 5-3. Saturated Shear Strength Envelopes for US-231

Envelope Types	Strength Envelope (kPa)	R^2
Residual Strength – Wu et al. (1987)	$\tau = \sigma' \cdot tan(14°)$	N/A
Residual Strength – Power Fit	$\tau = 0.293 \cdot P_a \left(\frac{\sigma'}{P_a}\right)^{0.5}$	0.93
Residual Strength – Okagbue (1986)	$\tau = \sigma' \cdot tan(22°)$	N/A
Fully Softened Strength – Power Fit	$\tau = 0.56 \cdot P_a \left(\frac{\sigma'}{P_a}\right)^{0.89}$	0.98

Two water table levels were considered in the analyses. The first is shown in Figure 5-7 and represents the likely scenario at the time of failure when heavy rain had been occurring in the area and water was ponding on both the upslope and downslope sides of the roadway embankment. The second scenario considers a water table that is approximately 18 feet below the toe of slope as might be expected during drier weather or with adequate drainage. The factors of safety for these scenarios with the various strength envelopes are shown in Table 5-2Table 5-4. Summary of Minimum Factors of Safety for Southbound Failure for the Different Strength Envelopes.. For the FSS, all scenarios have adequate stability. This indicates that without a pre-existing shear plane, the road likely could have remained stable. Unfortunately, the topography suggests an ancient

landslide was present in this location and therefore residual strengths should be used. The linear secant envelope for low stress conditions (22 degrees) also shows adequate stability for all scenarios, but a shallow failure surface is present near the toe of the slope (Figure 5-8). This surface has factors of safety just at or above 1.0. When the linear envelope is lowered to the high stress condition (14 degrees), the factors of safety for the southbound lanes (where movements began) drop to below 1.0 for the higher water table and remain above 1.0 for the low water table. This result is consistent with observations, but the factors of safety for the toe circles drop to 0.62. This is not consistent with the observations at the site, as mature trees were present all along the toe of the slope and down the hill with no obvious signs of large failures away from the road.

Using the power envelope improves both observations, as the toe circle has a factor of safety significantly above one, while the stability of the southbound lanes is below 0.9 for high water levels and near 1.0 for low water tables. This result demonstrates that the slopes outside of the road area would be stable, while the southbound lanes would become unstable as the water table rose. The critical factor of safety for a circle intersecting the northbound lanes was 1.13 with the power envelope, which is similar to the 1.11 found using the lower secant envelope. This marginal stability indicates that failure would not initiate in the northbound lanes, but could be triggered once the buttressing effect of the southbound lanes was altered. This again is consistent with observations as large movements were first observed in the southbound lanes, followed by movement in the northbound lanes the following day.

Table 5-4. Summary of Minimum Factors of Safety for Southbound Failure for the Different Strength Envelopes.

	Factor of Safety			
	Fully Softened Strength - Linear fit (22°)	**Fully Softened Strength – Power fit**	**Residual Strength - Linear fit (14°)**	**Residual Strength - Power fit**
High GWT – Circular	1.20	1.57	0.80	0.89
Low GWT - Circular	1.56	1.89	1.06	1.01
High GWT - Noncircular	1.23	1.44	0.79	0.81
Low GWT - Noncircular	1.63	1.87	1.06	0.94

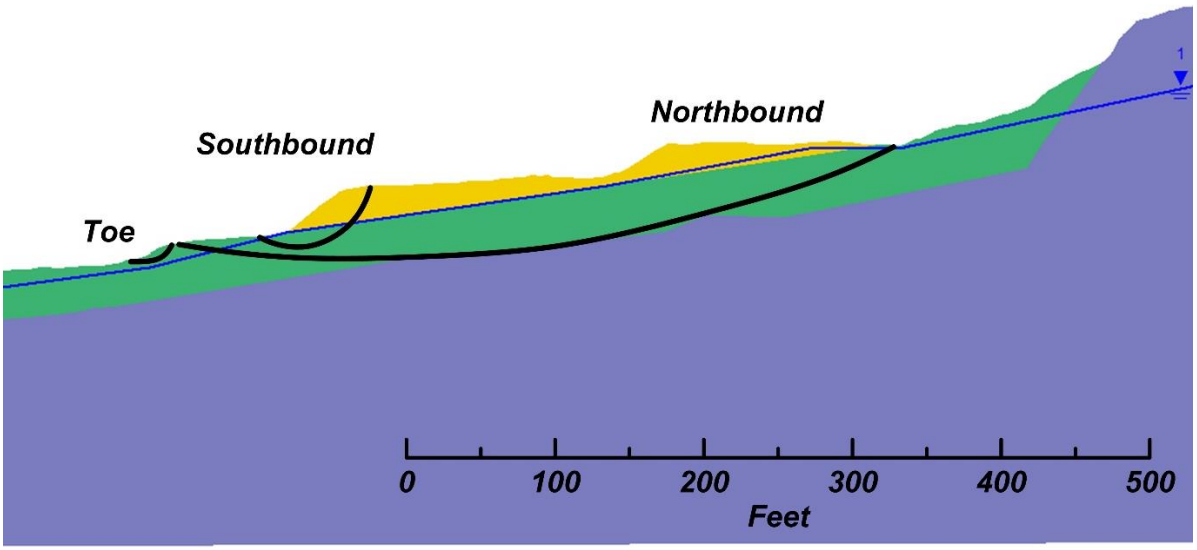

Figure 5-8. Key failure surfaces for US-231.

CHAPTER 6: CONCLUSION AND RECOMMENDATIONS

6.1 Summary and conclusions

Slope failures in clayey soils are a frequent concern in many parts of Alabama. Effectively addressing existing failures and ensuring stability in new slope designs necessitates a thorough understanding of soil strength. This understanding becomes particularly challenging in the case of high plasticity clays, given their tendency to lose strength under shearing forces. Initial slides are typically analyzed using fully softened strengths, accounting for potential strength reduction due to weathering and changes in moisture content. Subsequently, after mobilization, the strength can decrease to a residual value. While triaxial and direct shear testing can analyze fully softened strengths, tests capable of reaching large strains are required to measure residual strengths. Ring shear testing offers a solution by measuring soil strength changes over substantial displacements, covering both fully softened and residual strength. However, its practical application is limited due to the considerable time and effort involved in conducting the test. Previous researchers have developed correlations for both fully softened and residual strengths, but these correlations were often based on databases lacking representation from regions east of the Mississippi. Since the geologic history and mineralogy of soil significantly impact its strength, it is imperative to validate these correlations for their applicability in specific regions before implementation.

This study sought to address some of these gaps in the literature through an examination of the characterization and application of drained strengths for several clay deposits in Alabama. Clay samples gathered from various locations in west and north Alabama underwent comprehensive characterization, employing index tests, and X-ray diffraction (XRD). The primary

objective of was to provide a detailed understanding of the geotechnical properties of the soil in order to estimate the potential for strength loss and inform slope design and practices. By conducting a thorough laboratory testing and analysis of various soil parameters, including grain size distribution, moisture content, Atterberg limits, clay minerology identification, and shear strength, the study aims to estimate difference of soil strength before and after its failure, therefore, find the strength loss, and contribute guidance on the use of these strengths to the field of civil engineering and aid in ensuring the stability and safety of structures built atop this site.

Chapter 2 summarized the literature on the standard test methods of the index properties and the drained shear strengths, and the clay mineralogy structure evaluate the importance of the characterization shear strength on clays, and nonlinearity of the shear strength envelope to interpret the shear strength. Five fully softened shear strength correlations developed by Mesri and Shahien (2003), Stark and Hussain (2013), Eid and Rabie (2017), Stark and Fermandez (2020), and Stark (2022) and five residual strength correlations developed by Mesri and Shahien (2003), and Wright (2005)-Stark (2005), Stark and Hussain (2013), Eid et al. (2016), and Stark (2022) were identified and used in later chapters for comparing with the test results on similar type of soils.

Chapter 3 summarized the test procedures used in this study on each characterization properties, and the corresponding interpretation methods applied to the test results. Several methods were also described that were used to provide a statistical comparison of the lab results with the various correlations from Chapter 2 and to identify potential outliers in the data.

Scale effects matters while extrapolating laboratory results from small samples to represent the entire field site. The twelve collected samples may not fully capture the heterogeneity and spatial variability of the soils found in larger, in-situ conditions. Laboratory testing often involves samples that are more homogeneous and controlled compared to the natural variability

encountered in the field, which can lead to discrepancies between observed strengths in laboratory settings and actual conditions on-site. These differences highlight the need to consider scale effects when interpreting the findings and formulating recommendations. In summary, addressing these sampling limitations requires a comprehensive approach that includes an adequate number of samples, careful handling and preparation, consideration of temporal and spatial variability, and a thorough interpretation of results of the field.

Chapter 4 presented characterization results including the ring shear test to assess both fully softened and residual strengths at six sites in the state, where clay soils were suspected to be causing stability issues. Initially, clay samples underwent conventional index testing (including grain size and Atterberg limits), X-ray diffraction (XRD) for mineralogy determination to assess field applicability. The predominant clay mineral identified was illite, although samples from I-65 in Conecuh County and SR-5 in Perry County exhibited higher proportions of montmorillonite. Notably, clay samples from US-231 near Laceys Spring displayed intriguing characteristics; their Atterberg limits resembled those from SR-219 in Bibb County, but their resistivity results were akin to a sample from I-59 in Tuscaloosa County, which had significantly higher Liquid Limit (LL) and Plasticity Index (PI). XRD analysis suggested that the US-231 sample likely constituted degraded illite, a mineral also found in geologically similar regions in eastern Ohio, western Pennsylvania, and West Virginia. Although classified as low activity clay, degraded illites share properties with montmorillonites (Fisher et al., 1968).

The saturated residual and fully softened strengths of these clays were systematically measured across a wide stress spectrum for all sites using drained ring shear testing. Both linear and power envelopes exhibited comparable fits within a limited stress range. However, power envelopes demonstrated higher strengths at low stresses and lower strengths at higher stresses,

aligning more consistently with the complete stress range. Tests below 20 kPa stress were not conducted, leaving uncertainties about envelope accuracy at very shallow depths.

The strength results revealed that soils with higher plasticity, notably those along I-65 in Conecuh County and SR-5 in Perry County, exhibited the lowest strengths. Conversely, medium plasticity clays, as found along SR-22 in Chilton County, displayed the highest strengths among the examined soils. Notably, the tests from US-231 indicated the highest fully softened strength, but, the residual strength envelope exhibited a significant curve at higher stresses, leading to secant friction angles at or below 14 degrees. This unusual finding aligned with prior studies on the strength of red shales in Ohio and West Virginia and suggested that the tested soil from US-231 was likely a degraded illite, as confirmed by XRD and Atterberg limits results. While the developed strength envelopes aligned with existing correlations for soils sharing similar liquid limits, incorporating a margin of uncertainty (+5) degrees for the secant friction angle) is advisable.

Comparison with existing correlations for both fully softened and residual strengths, especially those proposed by Stark (2022), showed reasonable fits for most soils, considering an uncertainty band of +5 degrees for the secant friction angle. However, the residual strength for US-231 did not align well with any existing correlations. This indicated that the existing correlations might not be suitable for degraded illite soils like those at US-231. For similar soils (red weathered shale or mudstone with LLs between 30 and 48 and PIs between 10 and 22), preliminary estimates between 14 and 22 degrees for secant friction angles were considered reasonable, pending site-specific testing to confirm these values. The measured residual strengths from this study were similar to those measured by Wu et al. (1987) using direct shear tests on slickensides in red shale in western Ohio. Given the agreement between these two different studies using two different test methods (direct shear on slickensides and ring shear on remolded samples),

the measured strength envelopes are believed to be accurate, and the correlations do not seem to be capturing the true strength of these soils. A set of strength bounds was shown in Figure 4-16 that can reasonably be used for similar soils until additional test data is available to assess the need for new correlations.

Chapter 5 presented slope stability analyses conducted for two sites (SR-5 and US-231), while results for I-65 were presented in a prior study (Kiernan, 2021). These analyses utilized the measured strength envelopes and revealed consistency with observations, including no movement at SR-5, limited movements at I-65, and a significant failure at US-231. Nonlinear envelopes proved crucial for demonstrating adequate stability at SR-5 and predicting marginal stability at US-231 under low water levels, with destabilization occurring when the water table rose. Power envelopes accurately indicated low factor of safety for the southbound lanes at US-231 and captured the larger, marginally stable failure surface beyond the northbound lanes. Linear (secant) envelopes either overpredicted or underpredicted stability issues and circular failure surfaces failed to capture larger movements. Noncircular surfaces were vital for stability analysis at I-65 due to the presence of a shallow limestone interval serving as a sliding plane, although they were not significantly different from circular surfaces at US-231 or SR-5.

Measurement uncertainty significantly impacts the safety factor in slope stability assessments by introducing variability into input parameters such as soil strength and properties. The uncertainty of the measurements of soil properties can lead to an underestimation or overestimation of the true stability condition of the slope. High uncertainty of the soil strength measurements may result in the calculated factor of safety inadequately account for the worst-case scenarios, potentially leading to an unsafe design. To minimize the effects of these uncertainties and ensure the stability of slopes, a higher safety factor could be considered for slope stability

design, which provides a buffer against potential measurement errors and variability. This additional margin helps to account for the unknowns and ensures that the slope remains stable under a range of conditions, thereby mitigating the risk of slope failure.

The uncertainty in fully softened strength is kind of typically greater than in residual strength due to the transitional nature of the fully softened state, which is more sensitive to factors such as its normally consolidated loading conditions. Fully softened strength is measured where the soils are not yet stabilized, leading to higher variability compared to residual strength, which is estimated after the soil has settled into a stable, well-defined failure condition. Additionally, fully softened strength is influenced by conditions that may not be perfectly replicated in laboratory tests, further increasing uncertainty, while residual strength benefits from being a more stable and predictable measure of the soil to resist further deformation after significant shear displacement.

6.2 Discussion on practical benefits of research

The findings from the slope stability assessments underscore the significance of considering suction effects and curved failure envelopes when evaluating slopes involving high plasticity clays. For significant failures or sites with planar layering, noncircular surfaces warrant consideration. Previous studies have indicated curved fully softened and residual strength envelopes for such soils; however, the distinctions between these envelopes are often perceived as minor, and nonlinear envelope consideration is rare in practice. This study highlights that even subtle variations in strength envelopes significantly impact the factor of safety for shallow failure surfaces. Moreover, while suction's strengthening effect is widely recognized, it is frequently

overlooked in slope stability analyses. While neglecting suction might suffice for initial designs, realistic suction conditions should be incorporated for accurate back analysis.

The characterization results emphasize the effectiveness of Atterberg limits as a valuable tool for assessing the likely mineralogy of high and medium plasticity clays. The correlations between mineralogy and Atterberg limits, as illustrated in Figure 2-6, consistently aligned with the XRD outcomes. These correlations proved useful in identifying soils prone to strength loss, although sites underlain by degraded illites, like US-231 may be misleading as the residual strengths can be much lower than expected from the plasticity data alone. Incorporating knowledge from the geologic history of the deposit is key to identify deposits that may not follow typical trends.

This study confirmed that ring shear testing stands out as a reliable method for determining both fully softened and residual strengths. One of its key advantages is the ability to use disturbed samples, enabling testing on samples collected through various methods such as bulk sampling, SPT, or tube sampling. In situations where estimates of residual drained strength parameters are crucial for design, ring shear testing is strongly advised. However, for standard designs, where the time and effort required for preparing and testing a ring shear sample might not be cost-effective, the study suggests utilizing the fully softened and residual strength correlations proposed by Stark (2022). These relationships provided a reasonable fit to the data from all sites, except for the residual strength at US-231 (discussed in detail below), as long as an appropriate level of uncertainty in the estimates was considered. Incorporating an uncertainty range of +5 degrees for the secant friction angle seemed to provide reasonable boundaries, although this range could potentially be narrowed through further testing efforts.

The slope stability analyses underscored the consistency between the observed behavior and the results obtained from the measured strength envelopes, particularly when nonlinear strength envelopes were utilized. For US-231 and SR-5, employing the nonlinear power envelope significantly enhanced the agreement with observations. The envelope successfully accounted for the high secant friction angles at low stresses and the low secant friction angles at higher stresses. Most slope stability programs, including Slide and Slope/W (via the shear/normal function), incorporate power envelopes. In cases where power envelopes are unavailable, fitting secant friction angles at different stress levels and applying them to various regions of the model is necessary. While a single linear fit may suffice for sites lacking significant changes in effective stress, the power fit eliminates the need for such checks.

A pivotal finding of this study was the confirmation of stability issues linked to degraded illite clays within the Pennington formation. Similar soils have triggered landslides in Ohio, Pennsylvania, and West Virginia. Identifying these problematic soils involves screening for red or gray weathered shale or mudstone with Liquid Limits (LL) ranging between 30 and 48 and Plasticity Index (PI) between 10 and 22 in deposits featuring Mississippian or Pennsylvanian age rocks. The ring shear tests conducted in this study indicated unexpected curvature in the residual strength envelope for US-231 samples. This curvature resulted in remarkably low residual strengths, offering insights into the extensive failure witnessed at Lacey Spring. Existing correlations for residual strengths inadequately capture the strengths at this site. Therefore, if similar soils are encountered at future sites, a range of strengths should be taken into account to ensure accurate assessments.

6.3 Limitation

The samples collected of this study did not capture all the variabilities present of across the entire slope failure site as soil properties can vary significantly over different spatial scales. This sampling limitation can impact the sufficiency explanation of the site, accuracy and reliability of the results. Clay soils often exhibit considerable variability in strength across different locations due to factors such as changes in soil composition, moisture content, and compaction levels.

Sample size and depth are also another factor regarding the sampling limitation. Small or shallow samples may not capture the strength properties of deeper soil layers where significant strength loss could occur. This limitation underscores the importance of sampling at various depths to obtain a comprehensive understanding of the soil's strength profile. Scale effects present an additional challenge. Small-scale samples may not reflect larger-scale variations in strength loss, particularly in sites with considerable heterogeneity. A limited number of samples may not capture this spatial heterogeneity effectively, potentially leading to a misrepresentation of the soil's overall strength characteristics. Inadequate sampling density can result in an insufficient number of data points to accurately reflect the strength properties of the site, especially in areas with obvious localized variations. Without sufficient sampling, critical zones of strength loss or other significant soil features might be overlooked. This issue highlights the need for a well-designed sampling strategy that accounts for scale and variability. These factors can contribute to an incomplete characterization if not adequately measured or considered.

6.4 Future research

Future studies can conduct a detailed investigation into the spatial variability of soil properties to better understand and characterize strength loss. This should involve a comprehensive

sampling strategy that includes collecting samples from multiple, systematically chosen locations across different zones of the failure sites, particularly focusing on areas with observed variability in soil behavior or signs of instability. Utilizing advanced techniques such as geophysical surveys, remote sensing, and dense grid sampling can help capture the spatial distribution of clay soil properties more accurately. Incorporating data from these methods into a statistical analysis will provide a clearer picture of how strength varies across the failure sites and improve the reliability of slope stability assessment. Additionally, exploring seasonal or moisture-related changes in soil properties relating the suction effects can further explain factors contributing to strength loss and enhance the site's stability assessment.

A wider range of drained shear strength results on high plasticity clays in Alabama using torsional ring shear can be tested and add more test data to develop possible correlations with the characterization indexes and clarify the existing correlations between soil properties and how soil behave at lower and higher normal stress levels (the amount of nonlinearity) in the strength envelope. Understanding the effects of mineralogy on higher curvature in envelopes may help to provide recommendations on how to predict strength values in the field for high-plasticity clays in Alabama with less uncertainty.

Future analyses should integrate field observations with laboratory data and employ methods to account for these scale effects to ensure more accurate and reliable conclusions regarding soil strength and stability. In addition to index testing, tests such as electrical resistivity can be used to help identify soils with significant amounts of clay. Preliminary work presented by Montgomery et al. (2020) showed that using both resistivity values and plasticity data could help identify sites that may have a larger potential for strength loss, but this needs additional study.

This work has explored two case histories in Alabama using the torsional ring shear strength results, but additional sites should be examined and tested to clarify the effect of the parameters such as failure mechanism, soil properties and ground water level condition on the calculated factor of safety in the stability analysis.

REFERENCE

Advanced Geosciences Inc. (AGI), 2014, Earth Imager 2D Manual, Austin, TX.

ASTM C670. (2015). Standard Practice for Preparing Precision and Bias Statements for Test Methods for Construction Materials 1. ASTM International, West Conshohocken, PA.

ASTM D2216. (2019). Standard Test Methods for Laboratory Determination of Water (Moisture) Content of Soil and Rock by Mass.

ASTM D2435. (2011). Standard Test Methods for One-Dimensional Consolidation Properties of Soils Using Incremental Loading. ASTM International, West Conshohocken, PA.

ASTM D2487. (2020). Standard Practice for Classification of Soils for Engineering Purposes (Unified Soil Classification System). ASTM International, West Conshohocken, PA.

ASTM D4318. (2018). Standard Test Methods for Liquid Limit, Plastic Limit, and Plasticity Index of Soils. ASTM International, West Conshohocken, PA.

ASTM D6467. (2021). Standard Test Method for Torsional Ring Shear Test to Determine Drained Residual Shear Strength of Cohesive Soils. ASTM International, West Conshohocken, PA.

ASTM D7608. (2018). Standard Test Method for Torsional Ring Shear Test to Determine Drained Fully Softened Shear Strength and Nonlinear Strength Envelope of Cohesive Soils (Using Normally Consolidated Specimen) for Slopes with No Preexisting Shear Surfaces. ASTM International, West Conshohocken, PA.

ASTM D7928. (2017). Standard Test Method for Particle-Size Distribution (Gradation) of Fine-Grained Soils Using the Sedimentation (Hydrometer) Analysis. ASTM International,

West Conshohocken, PA.

ASTM G57. (2020). Standard Test Method for Measurement of Soil Resistivity Using the Wenner Four-Electrode Method. ASTM International, West Conshohocken, PA.

Baecher, G. B., & Christian, J. T. (2005). Reliability and statistics in geotechnical engineering. John Wiley & Sons.

Bhandary Netra P. and Yatabe R. (2007). Ring Shear Tests on Clays of Fracture Zone Landslides and Clay Mineralogical Aspects. In: Sassa Kyoji and Fukuoka H and WF and WG, editor. Progress in Landslide Science (Internet). Berlin, Heidelberg: Springer Berlin Heidelberg; 183–92.

Bromhead, E. N. (1979). A Simple Ring Shear Apparatus. *Ground Engineering*, *12*, 40–44.

Biscaye, Pierre E. (1965). Mineralogy and sedimentation of recent deep-sea clay in the Atlantic Ocean and adjacent seas and oceans. *Geological Society of America Bulletin*, 76, (7), 803-832.

Casagrande, A. (1948). Classification and identification of soils. *Transactions of the American Society of Civil Engineers*, 113(1), 901-930.

Chatterjee, Samprit, and Ali S. Hadi. (2015). Regression analysis by example. John Wiley & Sons.

Cohen, J. (2013). Statistical power analysis for the behavioral sciences. Routledge.

Cohen, J., & Cohen, P. (1983). Applied multiple regression/correlation analysis for the behavioral sciences (2nd ed.). Hillsdale, NJ: Lawrence Erlbaum Associates.

Commeau, Robert F., Leslie A. Reynolds, and C. Wylie Poag. (1985). Elemental X-ray mapping of agglutinated foraminifer tests: A nondestructive technique for determining compositional characteristics. *Micropaleontology*, 380-386.

Cullity, B.D. and Smoluchowski, R. (1957). Elements of X-ray Diffraction. *Physics Today*, 10(3), 50-50.

Crabb, G. I., and Atkinson, J. H. (1991). Determination of Soil Strength Parameters for the Analysis of Highway Slope Failures. *Proceedings of the Slope Stability Engineering Developments and Applications: Proceedings of the International Conference on Slope Stability Organized by the Institution of Civil Engineers, Isle of Wight*, 13–18.

Das, B. M., and Sivakugan, N. (2018). *Principles of Foundation Engineering*. Cengage learning.

Douglas, L.A. (1989). *Vermiculites. Minerals in soil environments*, 1, 635-674.

Duncan, J. M., Wright, S. G., and Brandon, T. L. (2014). *Soil Strength and Slope Stability*. John Wiley & Sons. Hoboken, N. J.

Dunkerley, D. L. (1976). A Study of Long-Term Slope Stability in the Sydney Basin, Australia. *Engineering Geology*, *10*(1), 1–12.

Folk, Robert L. (1974). The natural history of crystalline calcium carbonate; effect of magnesium content and salinity. *Journal of Sedimentary Research*, *44* (1), 40–53.

Gelman, A., Carlin, J. B., Stern, H. S., Dunson, D. B., Vehtari, A., & Rubin, D. B. (2013). Bayesian data analysis (3rd ed.). Boca Raton, FL: Chapman & Hall/CRC.

Eid, H. T., Rabie, K. H., and Wijewickreme, D. (2016). Drained Residual Shear Strength at Effective Normal Stresses Relevant to Soil Slope Stability Analyses. *Engineering Geology*, *204*, 94–107.

Eid, H. T., and Rabie, K. H. (2017). Fully Softened Shear Strength for Soil Slope Stability Analyses. *International Journal of Geomechanics*, *17*(1), 1–10.

Fredlund, D. G., Morgenstern, N. R., and Widger, R. A. (1978). Shear Strength of Unsaturated Soils. *Canadian Geotechnical Journal*, *15*(3), 313–321.

Fredlund, D. G., Rahardjo, H. (1993). *Soil Mechanics for Unsaturated Soils*. John Wiley & Sons. Hoboken, N. J.

Fredlund, D. G. (2006). Unsaturated Soil Mechanics in Engineering Practice. *Journal of Geotechnical and Geoenvironmental Engineering*, *132*(3), 286–321.

Gregersen, O. (1981). The Quick Clay Landslide in Rissa, Norway; The Sliding Process and Discussion of Failure Modes. *Proceedings International Conference on Soil Mechanics and Foundation Engineering*, *3*(10), 421–426.

Hahn, G. J. (1973). The coefficient of determination exposed. *Chemtech*, *3*(10), 609–612.

Hays, W. L. (1988). Statistics (5th ed.). New York, NY: Holt, Rinehart and Winston.

Helmy, A. K., E. A. Ferreiro, and S. G. De Bussetti. (1999). Surface area evaluation of montmorillonite. *Journal of colloid and interface science*, *210* (1), 167–171.

Hughes, Randall E., D. M. Moore, and H. D. Glass. (1994). Qualitative and quantitative analysis of clay minerals in soils. Quantitative methods in soil mineralogy: 330–359.

Kennedy, L. (2019). Drained Residual Strength of Expansive Soils Causing Pavement Distress Along Alabama Highway 5. M.S. Thesis, Auburn University, Auburn, AL.

Kibria, G., and Hossain, S. (2017). Electrical Resistivity of Compacted Clay Minerals. *Environmental Geotechnics*, *6*(1), 18–25.

Kiernan, M., Jackson, D., Montgomery, J., Anderson, J. B., McDonald, B. W., and Davis, K. C. (2021). Characterization of a Karst Site using Electrical Resistivity Tomography and Seismic Full Waveform Inversion. *Journal of Environmental and Engineering Geophysics*, *26*(1), 1–11.

Knights, M. J., Montgomery, J., and Carcamo, P. S. (2020). Development of a Slope Failure

Database for Alabama Highways. *Bulletin of Engineering Geology and the Environment*, *79*(1), 423–438.

Kiernan, M., Xuan, M., Montgomery, J., & Anderson, J. B. (2022). Integrated Characterization and Analysis of a Slow-Moving Landslide Using Geotechnical and Geophysical Methods. *Geosciences*, *12*(11), 404.

Holtz, R. D. and Kovacs, W. D. (1981). *An Introduction to Geotechnical Engineering*. Prentice Hall, Englewood Cliffs, NJ, USA.

Holtz, R. D., Kovacs, W. D., and Sheahan, T. C. (2011). *An Introduction to Geotechnical Engineering*. Pearson, Upper Saddle River, NJ.

Khan, M. S., Hossain, S., Ahmed, A., and Faysal, M. (2017). Investigation of a Shallow Slope Failure on Expansive Clay in Texas. *Engineering Geology*, *219*, 118–129.

Kiernan, M. (2021). *Site Characterization and Modeling Considerations for Slopes Involving Fine Grained Strain-softening Soils*. Ph.D. Dissertation, Auburn University, Auburn, AL.

Lade, P. V. (2010). The Mechanics of Surficial Failure in Soil Slopes. *Engineering Geology*, *114*(1–2).

Lambe, T. W., & Whitman, R. V. (1969). *Soil Mechanics*. John Willey & Sons. Inc., New York, 553.

Leong, E. C., and Abuel-Naga, H. (2018). Contribution of Osmotic Suction to Shear Strength of Unsaturated High Plasticity Silty Soil. *Geomechanics for Energy and the Environment*, *15*, 65–73.

Lupini, J. F., Skinner, A. E., and Vaughan, P. R. (1981). Drained Residual Strength of Cohesive Soils. *Geotechnique*, *31*(2), 181–213.

Mandel, John. (2012). The statistical analysis of experimental data. Courier Corporation.

Mesri, G., and Shahien, M. (2003). Residual Shear Strength Mobilized in First-Time Slope Failures. *Journal of Geotechnical and Geoenvironmental Engineering*, *129*(1), 12–31.

Mitchell, J. K., and Soga, K. (2005). *Fundamentals of Soil Behavior* (3rd ed.). John Wiley & Sons. New York.

Miller, S. J. (2006). The method of least squares. Mathematics Department Brown University, 8(1), 5–11.

Nagelkerke, N. J. (1991). *A note on a general definition of the coefficient of determination. biometrika*, *78*(3), 691–692.

Montgomery, J., Jackson, D., Kiernan, M., & Anderson, J. B. (2020). Use of geophysical methods for sinkhole exploration (No. 930-945). Auburn University. Highway Research Center.

Montgomery, J., Knights, M., Xuan, M., & Carcamo, P. (2019). Evaluation of Landslides along Alabama Highways (No. 930-931). Auburn University. Highway Research Center.

Poppe, L. J., Paskevich, V. F., Hathaway, J. C., and Blackwood, D. S. A Laboratory Manual for X-Ray Powder Diffraction. (2001). *U.S. Geological Survey Open-File Report 01-041*. Woods Hole, MA.

Rocscience (2020). Slide2 software. https://www.rocscience.com/.

Roy, S., and Bhalla, S. K. (2017). Role of geotechnical properties of soil on civil engineering structures. *Resources and Environment*, 7(4), 103–109.

Schmertmann, J. (1978). Guidelines for CPT: Performance and Design. *Report FHWA-TS-78-209*, Federal Highway Administration, 145.

Schoenemann, M. R., and Marvin Russell Pyles. (1984). Statistical description of shear strength in residual soils.

Skempton, A. W. (1964). Long-Term Stability of Clay Slopes. *Géotechnique*, *14*, 77–102.

Skempton, A.W. (1970). First-Time Slides in Over-Consolidated Clays. *Géotechnique*, *20*, 320–324.

Skempton, A. W. (1984). Slope Stability of Cuttings in Brown London Clay. *In Selected Papers on Soil Mechanics*. Thomas Telford Publishing, 241–250.

Skempton, A. W. (1985). Residual Strength of Clays in Landslides, Folded Strata and the Laboratory. *Géotechnique*, *35*, 3–18.

Spencer, E. (1967). A method of Analysis of The Stability of Embankments Assuming Parallel Interslice Forces. *Géotechnique*, 17(1), 11–26.

Stallings, E. G. (2016). Investigation of Pavement and Subgrade Distress at Alabama Highway 5. M.S. Thesis, Auburn University, Auburn, AL.

Stark, T. D., Choi, H., and McCone, S. (2005). Drained Shear Strength Parameters for Analysis of Landslides. *Journal of Geotechnical and Geoenvironmental Engineering*, *131*(5), 575–588.

Stark, T. D., and Eid, H. T. (1994). Drained Residual Strength of Cohesive Soils. *Journal of Geotechnical and Geoenvironmental Engineering*, *120*, 856–871.

Stark, T. D., and Eid, H. T. (1997). Slope Stability Analyses in Stiff Fissured Clays. *Journal of Geotechnical and Geoenvironmental Engineering*, *123*(4), 335–343.

Stark, T. D., and Fernandez, R. (2020). Fully Softened Shear Strength Measurement and Correlations. *Geotechnical Testing Journal*, *43*(5).

Stark, T. D., and Hussain, M. (2013). Empirical Correlations: Drained Shear Strength for Slope Stability Analyses. *Journal of Geotechnical and Geoenvironmental Engineering*, *139*(6), 853–862.

Stark, T. D., and Idries, A. (2021). Drained Residual Shear Strength Power Function Coefficients and b. *Geotechnical Testing Journal*, *44*(6).

Stark, T. D., and Vettel, J. J. (1992). Bromhead Ring Shear Test Procedure. *Geotechnical Testing Journal*, *15*(1), 24–32.

Stark, T.D. (2022) "Residual and Fully Softened Correlations Spreadsheet." Available from http://tstark.net/geotechnical-software. Last accessed on July 28, 2022.

Stephens, I., and Branch, A. (2013). Testing Procedure for Estimating Fully Softened Shear Strengths of Soils Using Reconstituted Material. Engineer Research and Development Center Vicksburg MS Geotechnical and Structures Lab: Vicksburg, MS.

Środoń, Jan. (2006). Identification and quantitative analysis of clay minerals. *Developments in clay science*, *1*, 765–787.

Søgaard SV, Pedersen T, Allesø M, Garnaes J, Rantanen J. (2014). Evaluation of ring shear testing as a characterization method for powder flow in small-scale powder processing equipment. *International journal of pharmaceutics*, *475*(1), 315–23.

Szabo, M. W. O., E.W., Copeland, C. W. Jr., Neathery, T. L. (1988). Geologic Map of Alabama, Geological Survey of Alabama Special Map 220, scale 1:250,000.

Terzaghi, K., Peck, R. B., and Mesri, G. (1996). *Soil Mechanics in Engineering Practice*. John Wiley & Sons.

Tiedemann, B. (1937). *Über die Schubfestigkeit bindiger Böden*; Preuß. Versuchsanst. f. Wasserbau u. Schiffbau.

Vandenberge DR, Duncan JM, Brandon TL (2013). Fully Softened Strength of Natural and Compacted Clays for Slope Stability. *Geotechnical Special Publication (Internet)*, 221–33.

Van Schouwenburg, J. C. H., and A. C. Schuffelen. (1936) "Potassium-exchange behaviour of an illite." *Netherlands Journal of Agricultural Science*, *11(*1), 13–22.

Weiss, Neil A., Carol A. Weiss, and Larry R. Griffey. (2012). *Introductory statistics*. London: pearson education.

Wright, S. G. (2005). Evaluation of Soil Shear Strengths for Slope and Retaining Wall Stability Analyses with Emphasis on High Plasticity Clays. *FHWA/TX-06/5-1874-01-1*. Federal Highway Administration: Washington, DC.

Wright, S. G., Zornberg, J. G., Aguettant, J. E. (2007). The Fully Softened Shear Strength of High Plasticity Clays. Center for Transportation Research, University of Texas at Austin, Austin, TX.

Wu, T. H., Randolph, B. W., & Huang, C. S. (1993). Stability of shale embankments. *Journal of geotechnical engineering*, *119*(1), 127-146.

Xuan, M., Montgomery, J., and Anderson, J. B. (2021). Examining the effects of suction and nonlinear strength envelopes on the stability of a high plasticity clay slope. *Geosciences*, *11*(11), 449.

Xuan, M., Montgomery, J., Anderson, B. J., & Kiernan, M. (2023). Characterizing strength loss in high plasticity clays along Alabama highways (No. 930-988). Auburn University. Highway Research Center.

APPENDIX A

Table A-1. Saturated residual and fully softened shear strengths nonlinear envelopes from ring shear tests performed on clay samples collected for this study over the full range of normal stresses.

Samples	Residual Strength Envelope	Fully Softened Strength Envelope
SR-5	$\tau_{RS} = 0.9572(\sigma'_v)^{0.7763}$ (R^2= 0.9482)	$\tau_{FSS} = 3.0407(\sigma'_v)^{0.7347}$ (R^2= 0.9541)
SR-22 (Site3 B3 12-13.5ft)	$\tau_{RS} = 4.7450(\sigma'_v)^{0.6647}$ (R^2= 0.9280)	$\tau_{FSS} = 3.0726(\sigma'_v)^{0.7507}$ (R^2= 0.9911)
SR-22 (Site3 B3 9-10.5ft)	$\tau_{RS} = 1.0856(\sigma'_v)^{0.8770}$ (R^2= 0.9829)	$\tau_{FSS} = 2.0153(\sigma'_v)^{0.8147}$ (R^2= 0.9904)
SR-219 (B2 38.5-39.9ft)	$\tau_{RS} = 1.0861(\sigma'_v)^{0.8263}$ (R^2= 0.9870)	$\tau_{FSS} = 1.0267(\sigma'_v)^{0.8613}$ (R^2= 0.9884)
SR-219 (B3 19-20.5ft)	$\tau_{RS} = 0.1480(\sigma'_v)^{1.0470}$ (R^2= 0.9640)	$\tau_{FSS} = 1.2062(\sigma'_v)^{0.8381}$ (R^2= 0.9902)
I-59	$\tau_{RS} = 0.3247(\sigma'_v)^{0.9296}$ (R^2= 0.9344)	$T_{FSS} = 2.6211(\sigma'_v)^{0.7397}$ (R^2= 0.9611)
US-231 (SB4-1 36.4-37ft)	$\tau_{RS} = 9.3575(\sigma'_v)^{0.5611}$ (R^2= 0.9490)	$\tau_{FSS} = 1.8866(\sigma'_v)^{0.8440}$ (R^2= 0.9975)
US-231 (SB4-1 35.5-36ft)	$\tau_{RS} = 14.392(\sigma'_v)^{0.4909}$ (R^2= 0.9299)	$T_{FSS} = 1.8968(\sigma'_v)^{0.8401}$ (R^2= 0.9813)
I-65 (B6 4.5-6ft)	$\tau_{RS} = 0.7872(\sigma'_v)^{0.7669}$ (R^2= 0.9828)	$\tau_{FSS} = 6.8279(\sigma'_v)^{0.0.5812}$ (R^2= 0.9899)
I-65 (B7 4.5-6ft)	$\tau_{RS} = 0.6564(\sigma'_v)^{0.8168}$ (R^2= 0.9436)	$\tau_{FSS} = 0.6564(\sigma'_v)^{0.8168}$ (R^2= 0.9274)
I-65 (B7 13.5-15ft)	$\tau_{RS} = 1.3890(\sigma'_v)^{0.7075}$ (R^2= 0.9807)	$\tau_{FSS} = 5.6803(\sigma'_v)^{0.6237}$ (R^2= 0.9878)
I-65 (B7 7.5-9ft)	$\tau_{RS} = 2.0516(\sigma'_v)^{0.6270}$ (R^2= 0.9998)	$\tau_{FSS} = 11.6400(\sigma'_v)^{0.5061}$ (R^2= 0.9999)